PHASE EQUILIBRIA INVESTIGATION OF BINARY, TERNARY, AND HIGHER ORDER SYSTEMS

Part I. The Phase Diagrams of the Systems Ti-Nb-C, Ti-Ta-C, and Ti-Mo-C

E. RUDY

FOREWORD

The research described in this technical report was carried out under USAF Contract F 33615-67-C-1513, Project 7350, Task 735001. The program was initiated on 1 April 1967 and was conducted at the Materials Research Laboratory, Aerojet-General Corporation, Sacramento, California. The contract was administered under the direction of the Air Force Materials Laboratory, WPAFB, with Captain P. J. Marchiando (MAMC) as Project Engineer, and Dr. E. Rudy (now at the Oregon Graduate Center, Portland, Ore.) serving as Principal Investigator. This report was released by the author January 1970.

This technical report has been reviewed and is approved.

W. G. RAMKE
Chief, Ceramics and Graphite Branch
Air Force Materials Laboratory

ABSTRACT

The ternary alloy systems Ti-Nb-C, Ti-Ta-C, and Ti-Mo-C were investigated by means of X-ray, melting point, DTA, and metallographic techniques and phase diagrams for all three systems from 1500° C through the melting range were established.

Titanium and niobium carbide form a continuous series of solid solutions, whereas Nb_2C (a= 3.127Å, c= 4.972Å) substitutes a maximum of 12.5 At.% Ti (a= 3.09Å, c= 4.92Å) at 2280° C. The binary (Ti,Nb) solution and the ternary monocarbide phase, $(Ti,Nb)C_{1-x}$ show a regular melting behavior. One non-variant, class II four phase reaction occurs in the system.

Titanium and tantalum monocarbide are miscible in all proportions and the solid solution shows a regular melting behavior. Ta_2C (a= 3.102Å, c= 4.940Å) substitutes up to 44 At.% Ti (a= 3.069Å, c=4.907Å)(2000° C, a=3.069Å, c=4.907Å), and is terminated by a three-phase equilibrium $(Ta,Ti)_2C + (Ta,Ti) + (Ta,Ti)C_{1-x}$ in the ternary. The order-disorder transition temperatures in the subcarbide are lowered from about 2150° C for the binary Ta_2C to about 1500° C at the ternary homogeneity limit. One class II non-variant ternary reaction occurs in the system, and the heterogeneous order-disorder transition of the hyperstoichiometric Ta_2C is terminated in a limiting tie line in the ternary.

The Ti-Mo-C system is characterized by complete solid solubility of the cubic monocarbides above 1960° C and a limited titanium exchange in Mo_2C (< 5 At.%) and the η-phase (< 10 At.%). The three isothermal ternary reactions occur in the investigated temperature range from 1500° C through melting. A ternary eutectic between metal, subcarbide, and monocarbide, at 2160° C, a class II reaction between melt η-MoC_{1-x}, Mo_2C, and $(Ti,Mo)C_{1-x}$ at 2500° C, and a pseudobinary eutectic between metal and monocarbide phase at 2240° C. The metal as well as the monocarbide solid solution shows a regular melting behavior.

TABLE OF CONTENTS

LIST OF ILLUSTRATIONS

LIST OF ILLUSTRATIONS (Cont'd)

LIST OF ILLUSTRATIONS (Cont'd)

LIST OF ILLUSTRATIONS (Cont'd)

LIST OF ILLUSTRATIONS (Cont'd)

LIST OF ILLUSTRATIONS (Cont'd)

LIST OF ILLUSTRATIONS (Cont'd)

LIST OF TABLES

I. INTRODUCTION AND SUMMARY

A. INTRODUCTION

Carbides and carbide alloys of the refractory transition metals form the basis of modern high performance tooling materials and wear resistant alloys. The refractoriness of this compound class also has prompted other applications, such as in coatings for fuel assemblies in high temperature reactors and as alloying additions in fuel material systems. Considerable effort has therefore been spent over the past decade to investigate the high temperature phase behavior in binary and ternary metal-carbon systems and as a result, the carbides probably belong to the best understood alloys in terms of their reaction behavior among the refractory hard materials. Nevertheless, data concerning the phase behavior in many of the ternary metal-carbon systems are still lacking or are unreliable as a result of inadequate experimental techniques used in the phase diagram studies. The current effort was undertaken to fill existing gaps in previous studies of the high temperature phase equilibrium characteristics of the Ti-Nb-C and Ti-Mo-C systems, and to revise the phase diagram data in the Ti-Ta-C system, which had been studied by us on a cursory basis in a preceding program.[1]

B. SUMMARY

1. The Ti-Nb-C System

An isometric view of the phase diagram Ti-Nb-C is shown in Figure 1, and a diagram depicting the flow of isothermal binary and ternary reactions in Figure 2. The melting troughs, the compositions of melts entering into isothermal reactions, as well as a projection of the liquidus isotherms are illustrated in Figure 3.

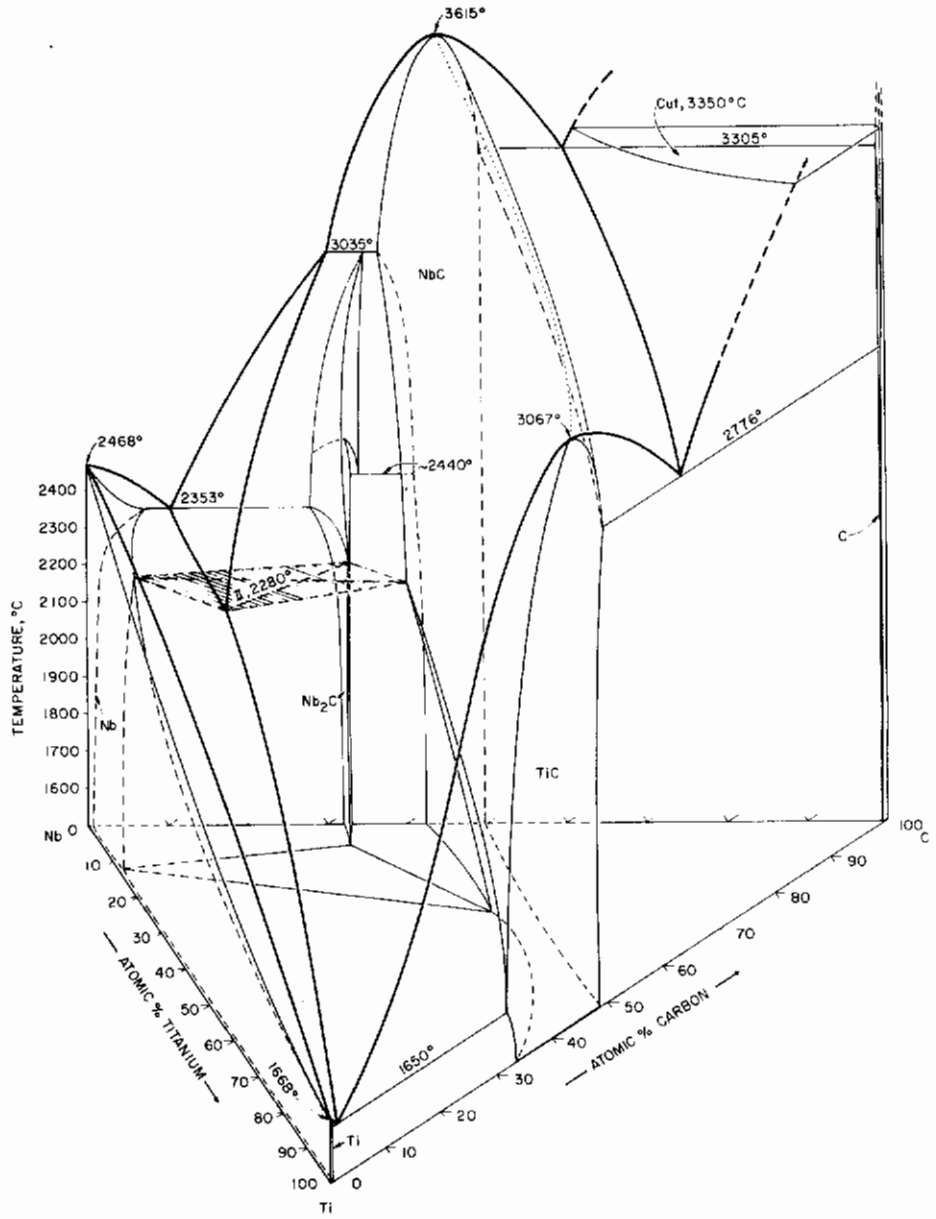

Figure 1. Isometric View of the Ti-Nb-C System.

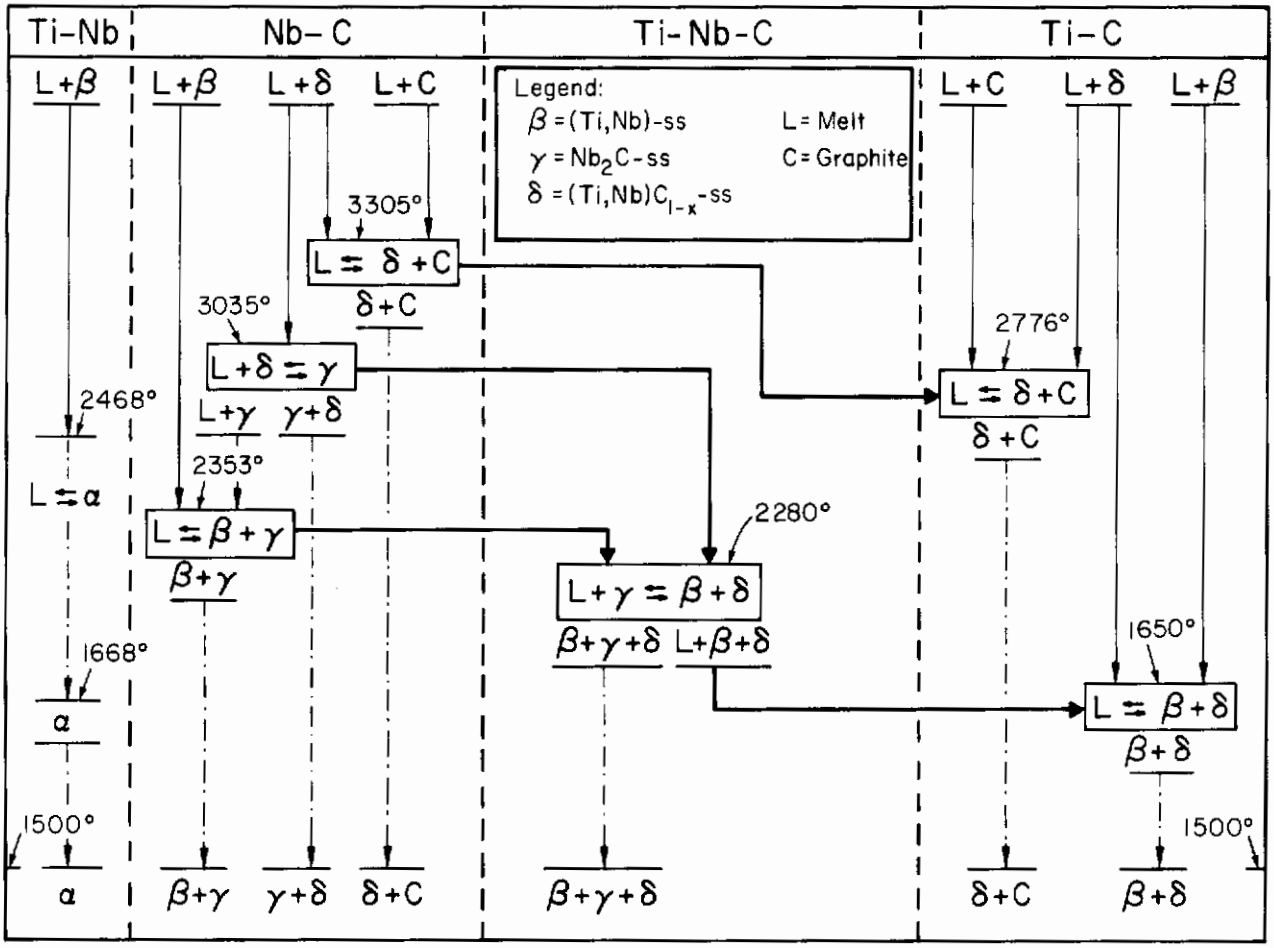

Figure 2. Reaction Diagram for Ti-Nb-C Alloys.

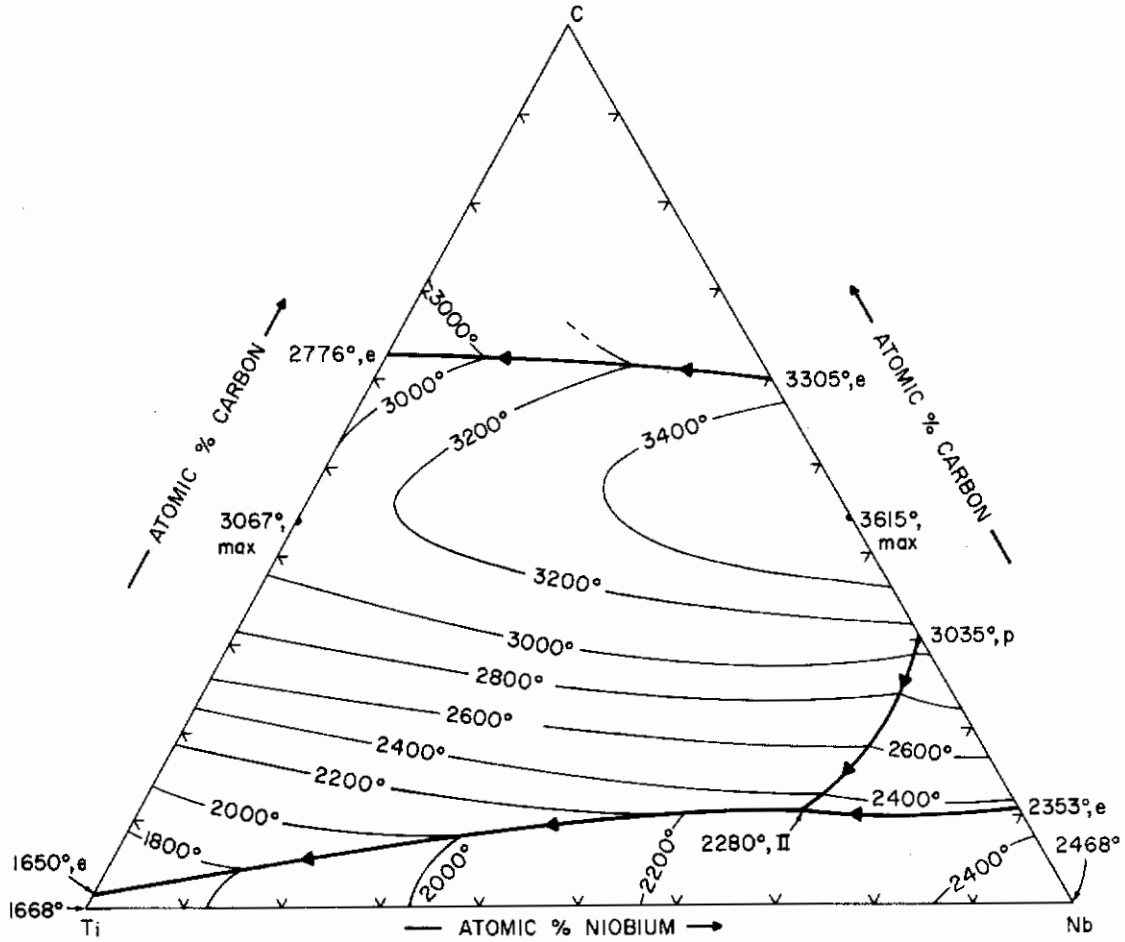

Figure 3. Liquidus Projections in the Ti-Nb-C System.

The solid state equilibria are characterized by a wide two-phase equilibrium between the metal and the monocarbide phase, complete solid state miscibility of TiC and NbC, and restricted solid solubility in Nb_2C (≤ 12.5 At.% Ti). The Nb_2C-phase is terminated by a three-phase equilibrium (Ti,Nb)-$(Ti,Nb)_2C$ + $(Ti,Nb)C_{1-x}$ in the ternary. The monocarbide phase shows a regular melting behavior and the boundary line monocarbide + graphite varies smoothly between the eutectic points of the edge systems TiC (2776°, 63 At.% C) and Nb-C (3305°, 60 At.% C). The eutectic trough in the metal-rich region of the system originates in the Ti-C binary at 1650° C

and merges at 2353° C (10.5 At.%) into the Nb-C system. A second melting trough originates at the liquidus vertex of the four-phase equilibrium.

$$L + Nb_2C\text{-ss} \xrightarrow[T \leq 2280^\circ C]{} (Ti,Nb)\text{-ss} + (Ti,Nb)C_{1-x}$$

at 2280° C and terminates at the peritectic point (3035°, 30 At.%) in the Nb-C binary. As a result of the low solid solubilities, the order-disorder transition temperatures in Nb_2C remain practically unaffected by titanium additions.

2. The Ti-Ta-C System

The isometric view of the phase diagram, Figure 4, is supplemented by a flow diagram of isothermal binary and ternary reactions, Figure 5, and a projection of the liquidus surface shown in Figure 6.

The cubic monocarbides in the boundary systems form a complete series of solid solution, while the ternary homogeneity range of Ta_2C (a= 3.102Å, c= 4.940Å) extends to 39 mole % Ti_2C at 1500° C, and to a maximum of 44 mole% (a= 3.069Å, c= 4.907Å) at 2000° C, the temperature of the four-phase reaction

$$L + (Ti,Ta)_2C \text{ (disord)} \rightleftharpoons (Ti,Ta) + (Ti,Ta)C_{1-x}$$

The carbon-deficient, Ti-rich, monocarbide solid solution forms an extended two-phase equilibrium with the metal phase. Other two-phase equilibria in the metal-rich region of the system are (Ti,Ta) + (Ti,Ta_2C), and $(Ti,Ta)_2C$ + $(Ti,Ta)C_{1-x}$.

The subcarbide order-disorder transition temperatures are lowered from ~2150° C for the binary Ta_2C, to about 1500° C at the

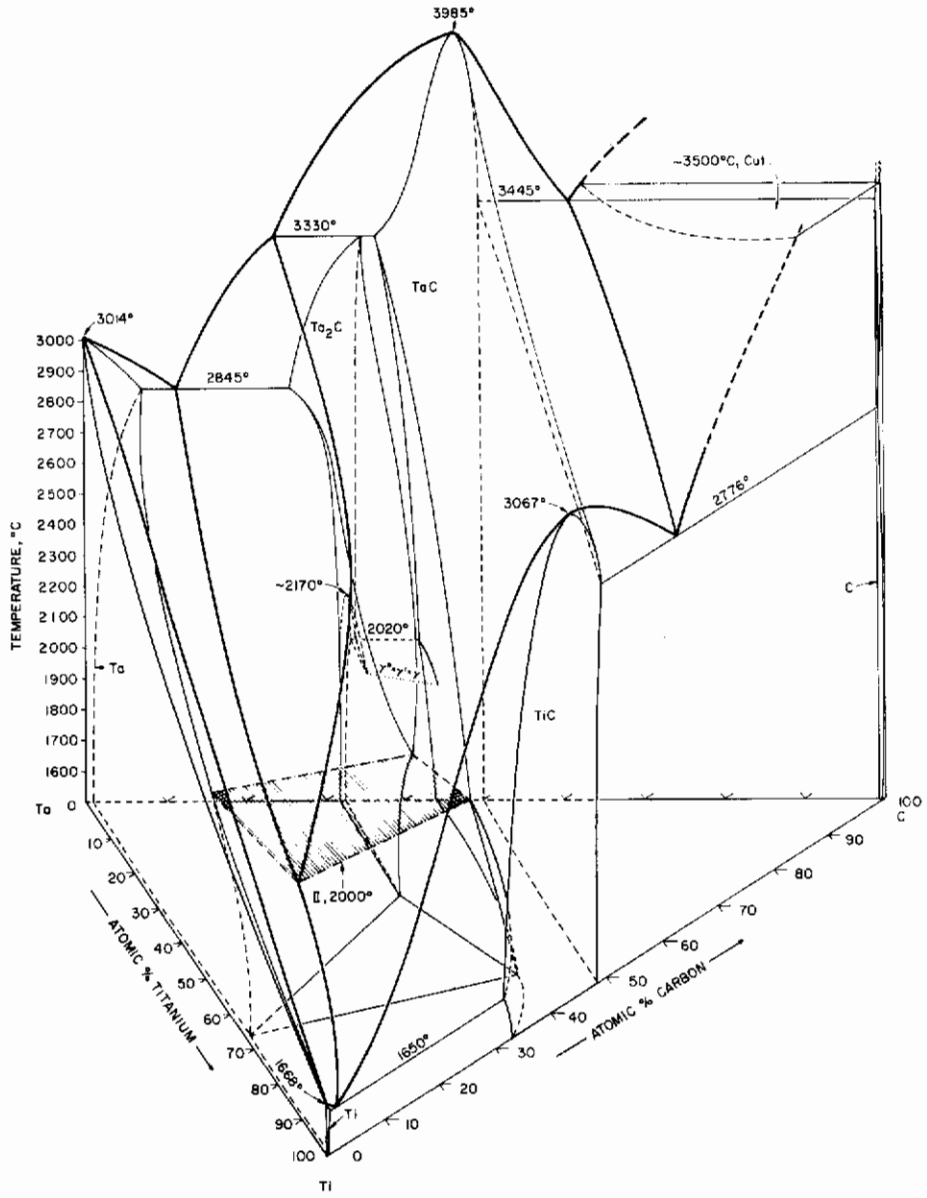

Figure 4. Isometric View of the Ti-Ta-C System.

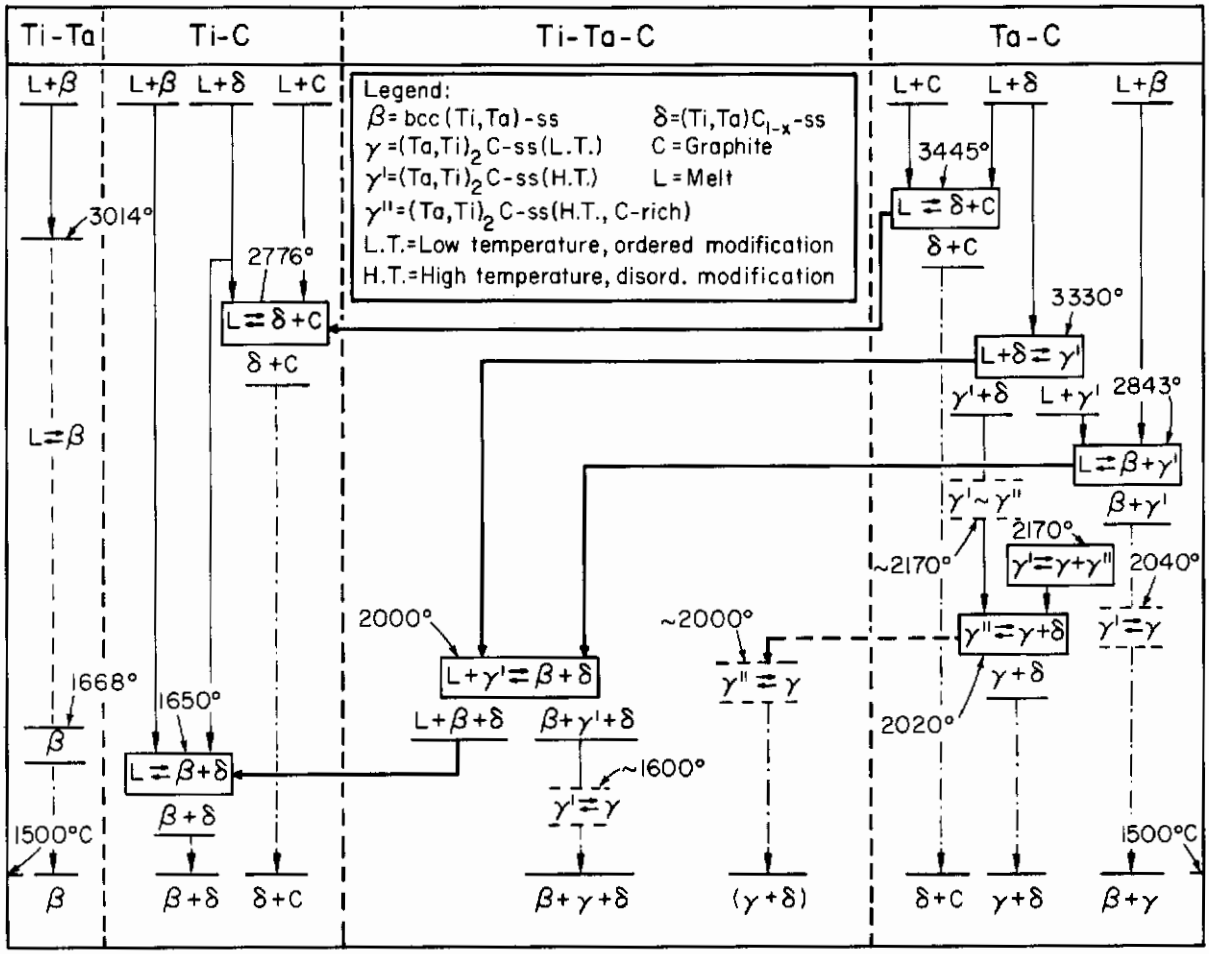

Figure 5. Reaction Diagram for Ti-Ta-C Alloys.

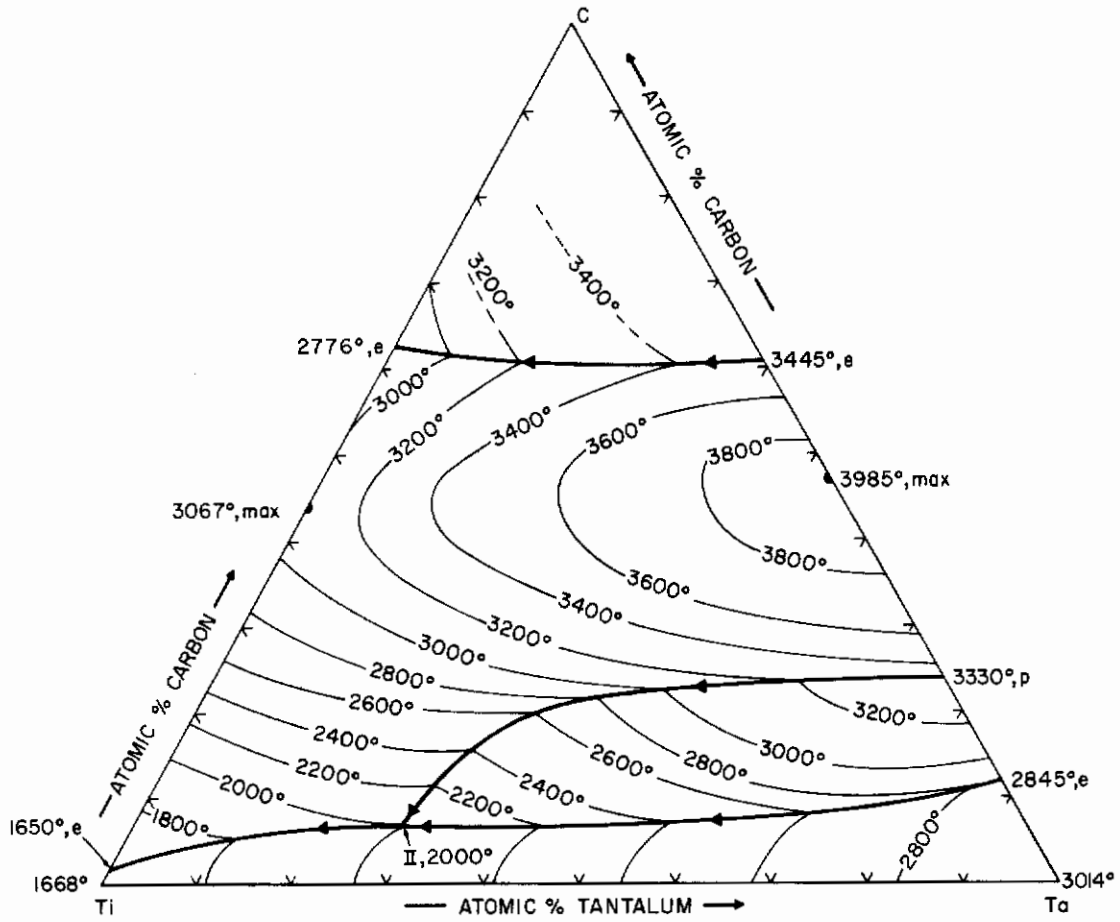

Figure 6. Liquidus Projections in the Ti-Ta-C System.

ternary homogeneity limit of the phase. The heterogeneous transformation of the hyperstoichiometric Ta_2C, which terminates in a pseudomonotectoid reaction in the binary, continues as a three phase equilibrium $(Ti,Ta)_2C$ (disord.) + + $(Ti,Ta)_2C$ (ord.)+ $(Ti,Ta)C_{1-x}$ into the ternary. This three-phase equilibrium is indicated to degenerate into a limiting tie at 11 At.% Ti and ~2000° C. At higher titanium contents the transformation is homogeneous.

The solution of the monocarbide shows a regular melting behavior, and the temperatures of the monocarbide + graphite eutectic trough vary smoothly between the MeC + C eutectic temperatures in the respective binaries, i.e. 2776° in the Ti-C and 3445° in the Ta-C system. The melting trough in the metal-rich region of the system originates at the binary β-Ti + TiC_{1-x} eutectic at 1650° C, and branches at 2000° C, the temperature of the class II four-phase reaction, into two arms, of which one terminates at the binary Ta + Ta_2C eutectic at 12 At.% and 2845° C and the other at the binary Ta_2C + TaC_{1-x} peritectic liquid at 3330° C and 24 At.% C.

3. The Ti-Mo-C System

An isometric view of the phase diagram is shown in Figure 7, while the isothermal reaction scheme and the liquidus projections of the system are depicted in Figures 8 and 9.

Three isothermal ternary reactions occur in the temperature range from 1500° C through melting. These are shown in the order of decreasing temperatures:

$$L + \eta\text{-}MoC_{1-x} \rightarrow Mo_2C\text{-ss} + (Ti,Mo)C_{1-x}\text{-ss} \quad \text{at } 2500^\circ C$$

$$L \rightarrow (Ti,Mo)\text{-ss} + (Ti,Mo)C_{1-x}\text{-ss} \quad \text{at } 2240^\circ C$$

$$L \rightleftarrows (Ti,Mo)\text{-ss} + Mo_2C\text{-ss} + (Ti,Mo)C_{1-x}\text{-ss} \quad \text{at } 2160^\circ C$$

Additional isothermal reactions are indicated to occur as a result of the ternary (eutectoid) decomposition of η-MoC_{1-x}, at temperatures around 1300° C, and the heterogeneous order-disorder transformation of the hyperstoichiometric Mo_2C, at about 1400° C.

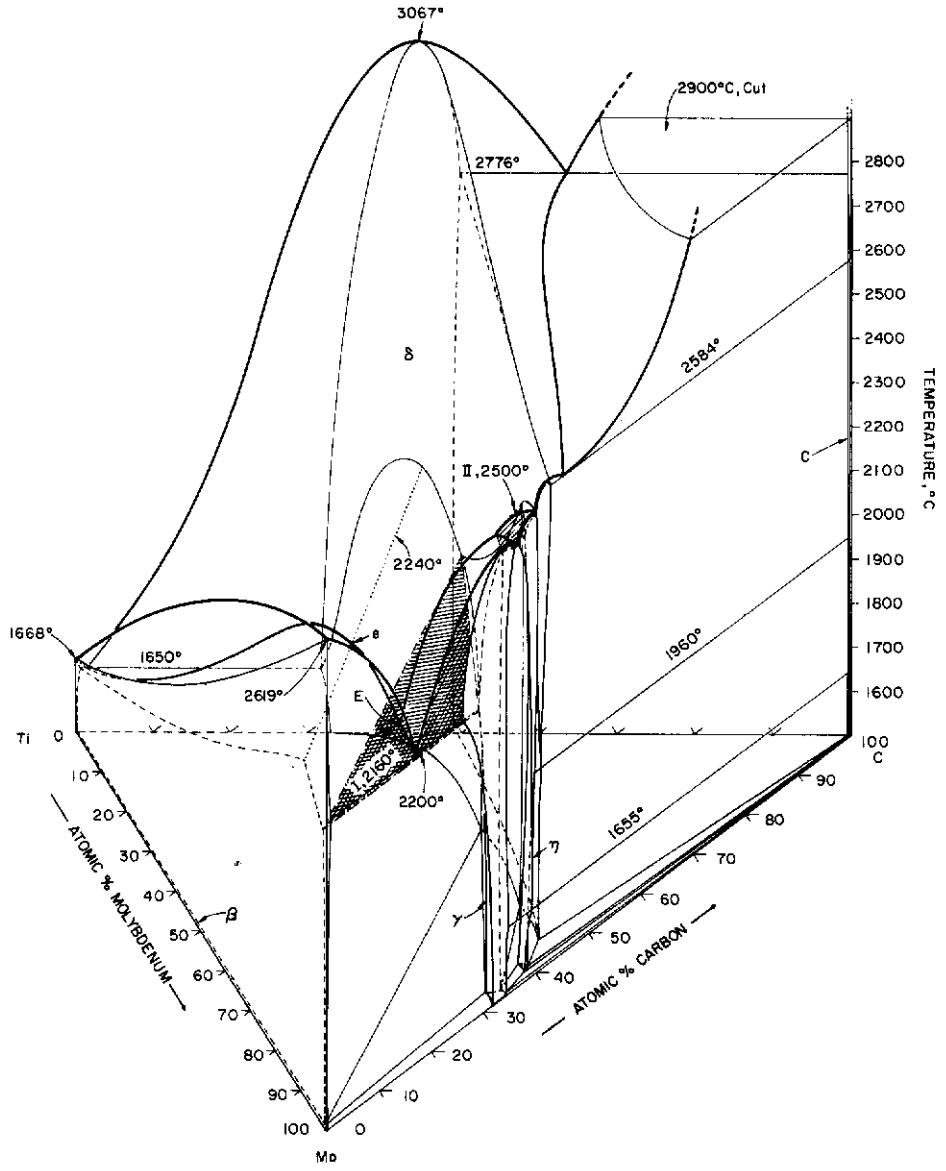

Figure 7. Isometric View of the Ti-Mo-C System.

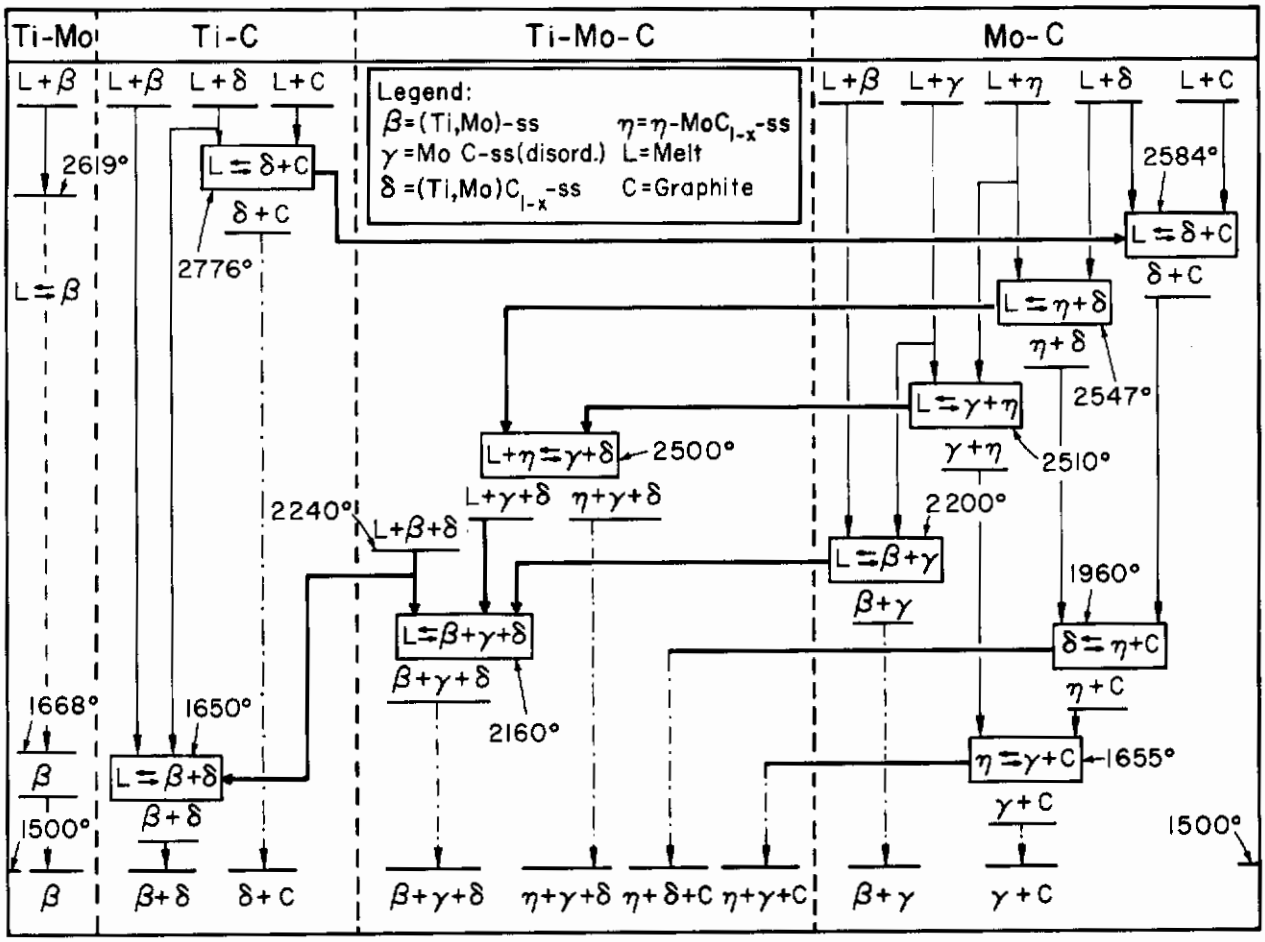

Figure 8. Reaction Diagram for the Ti-Mo-C System.

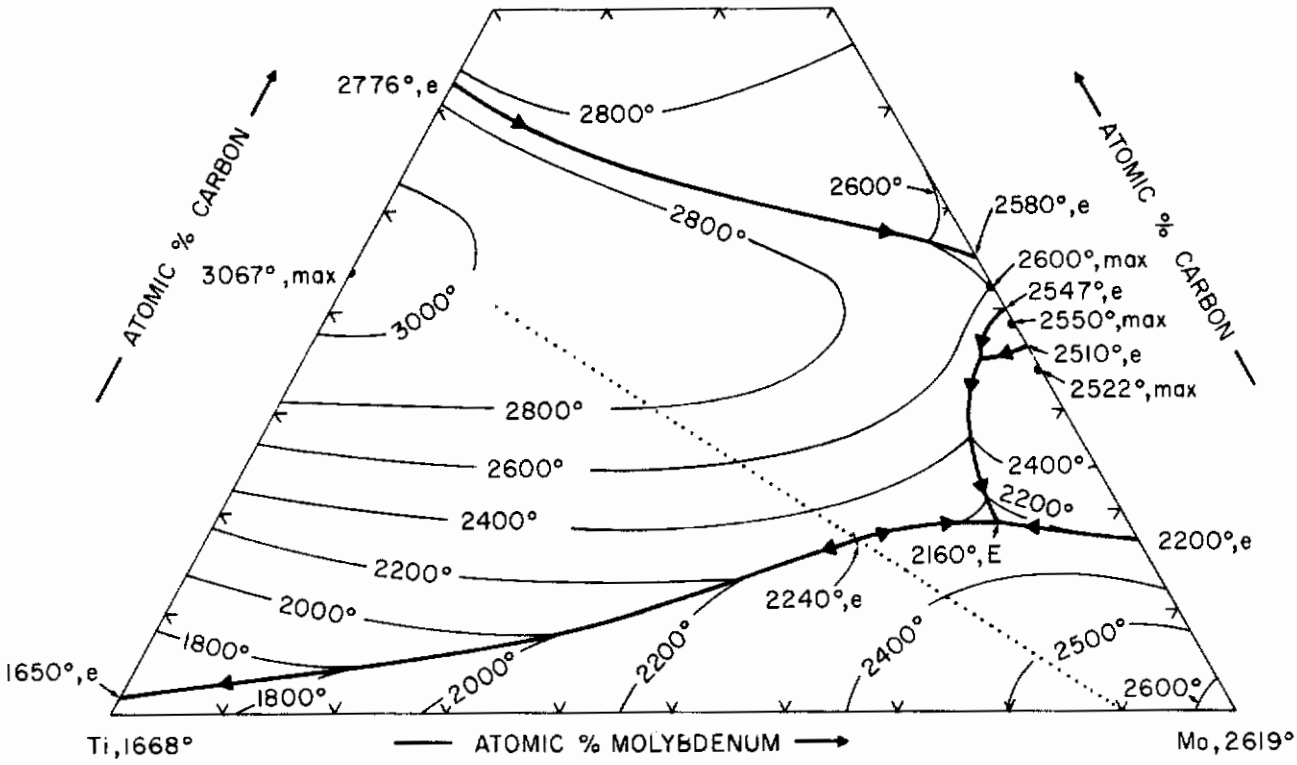

Figure 9. Liquidus Projections in the Ti-Mo-C System.

The solid state equilibria in the system are characterized by a wide composition range of coexistence between Ti-rich monocarbide alloys and the metal solid solution. Above 1960° C, the eutectoid decomposition temperature of the binary α-MoC_{1-x} phase, the cubic monocarbides form a complete series of solid solutions. Below 1960° C the maximum molybdenum exchange in TiC becomes temperature-dependent and decreases monotonically with decreasing temperatures reaching about 92 mole% MoC_{1-x} at 1500° C. The maximum titanium exchange in Mo_2C is less than 5 At.%, and in η-MoC_{1-x}

less than 10 At.%; the η-MoC_{1-x} phase, which decomposes in a eutectoid reaction at 1655°C in the Mo-C binary, appears to be stabilized to lower temperatures by titanium additions. The sublattice order-disorder transition temperature of 1430°C for the binary Mo_2C is lowered to ~1400°C by substitution of titanium.

II. REVIEW OF PREVIOUS WORK

A. BOUNDARY SYSTEMS

The principal phase diagram features of the three binary systems Ti-Nb, Ti-Ta, and Ti-Mo, are very similar[2,3,4]. Above the α-β transition temperature of titanium, complete miscibility in the solid state is observed in all three systems and the solid solutions show a regular melting behavior. Below the transition temperature of titanium (882°), the range of the β (bbc) solid solution becomes temperature dependent, extending to ~70 At.% Ti in all three systems at 600°C. The solid solubilities in the α-Ti phase are small.

The titanium-carbon system[5,6] (Figure 10) contains a refractory cubic monocarbide (Table 1), which forms eutectic equilibria with β-titanium and graphite. The lattice parameters of the monocarbide in alloys equilibrated near solidus temperatures show a maximum near 44 At.% C, which seems to disappear upon reannealing of the alloys at lower temperatures (Figure 11).

The investigations of the niobium-carbon system by C.K. Storms and N.H. Krikorian and by H. Kimura and Y. Sasaki[11] were recently supplemented by E. Rudy et al.[17,18]. The system, Figure 12, contains a very refractory monocarbide with a cubic, B1-type, of structure (Table 2) and a subcarbide, which exists in at least two different states of sublattice order at

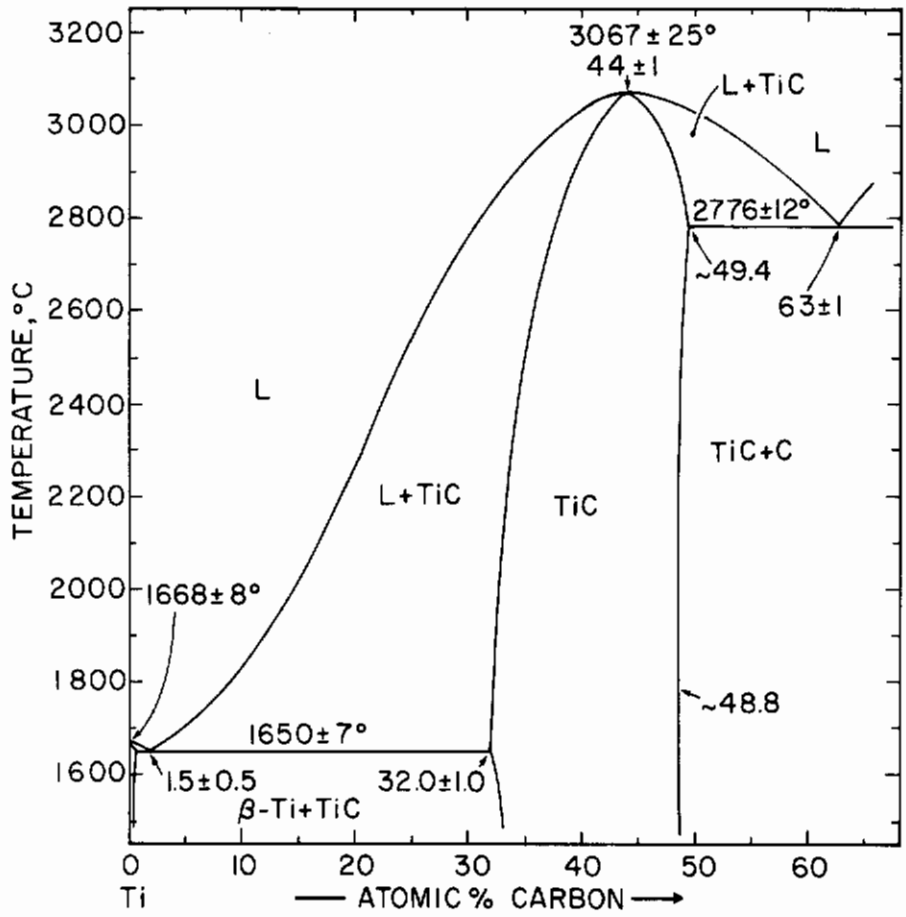

Figure 10. Phase Diagram of the Ti-C System (After E. Rudy et al.[5], 1965)

Table 1. Structure and Lattice Parameters of Titanium Carbides

Phase	Structure	Lattice Parameters	
TiC	fcc, B1-type	a= 4.3305 at $TiC_{0.86}$	(7)
		a= 4.299 at $TiC_{0.42}$ a= 4.330 at $TiC_{0.79}$ a= 4.327 at $TiC_{\sim 0.95}$	(8)
	fcc, O_h^7-Fd3m (32 to 40 At.% C, T< 1900° C)	a= 8.606 at $TiC_{\sim 0.5}$	(9)

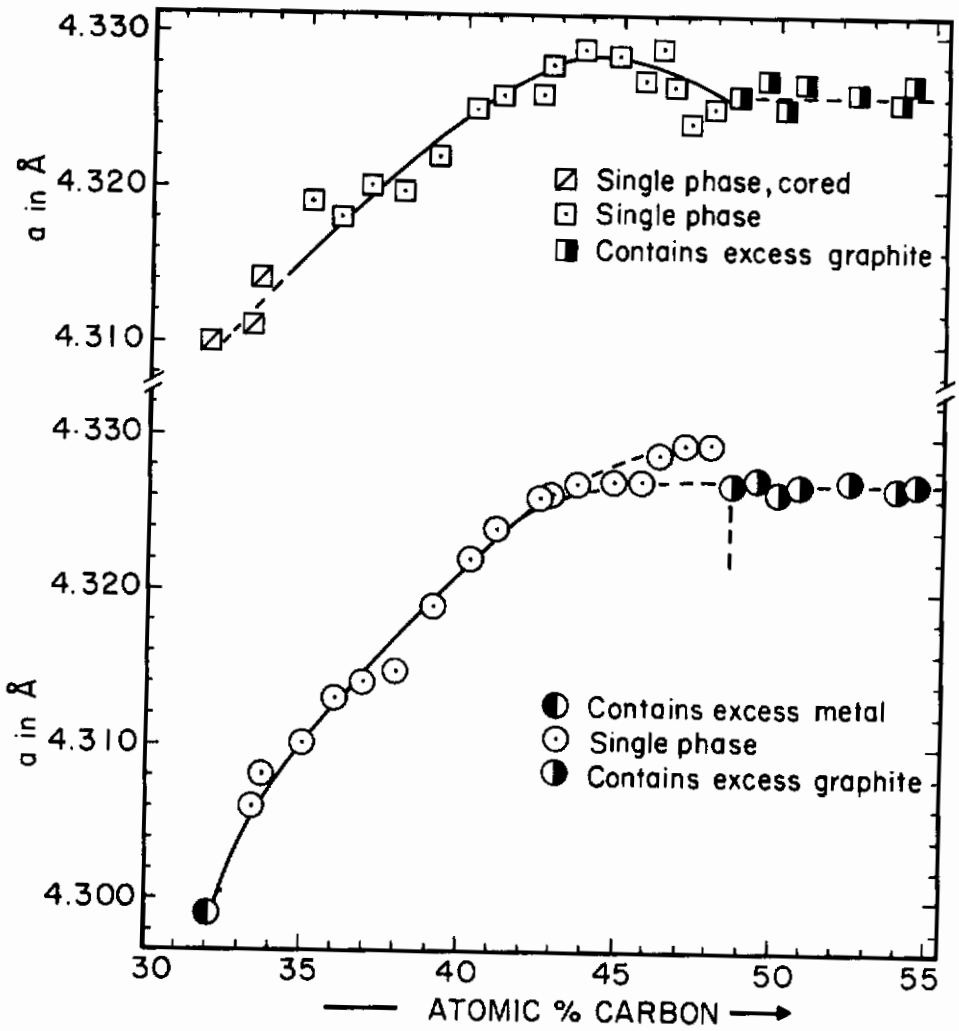

Figure 11. Lattice Parameters of the Carbon-Deficient Titanium Monocarbide.

Quenched from Solidus Temperatures

After Reannealing of Quenched Alloys at 1350° C.

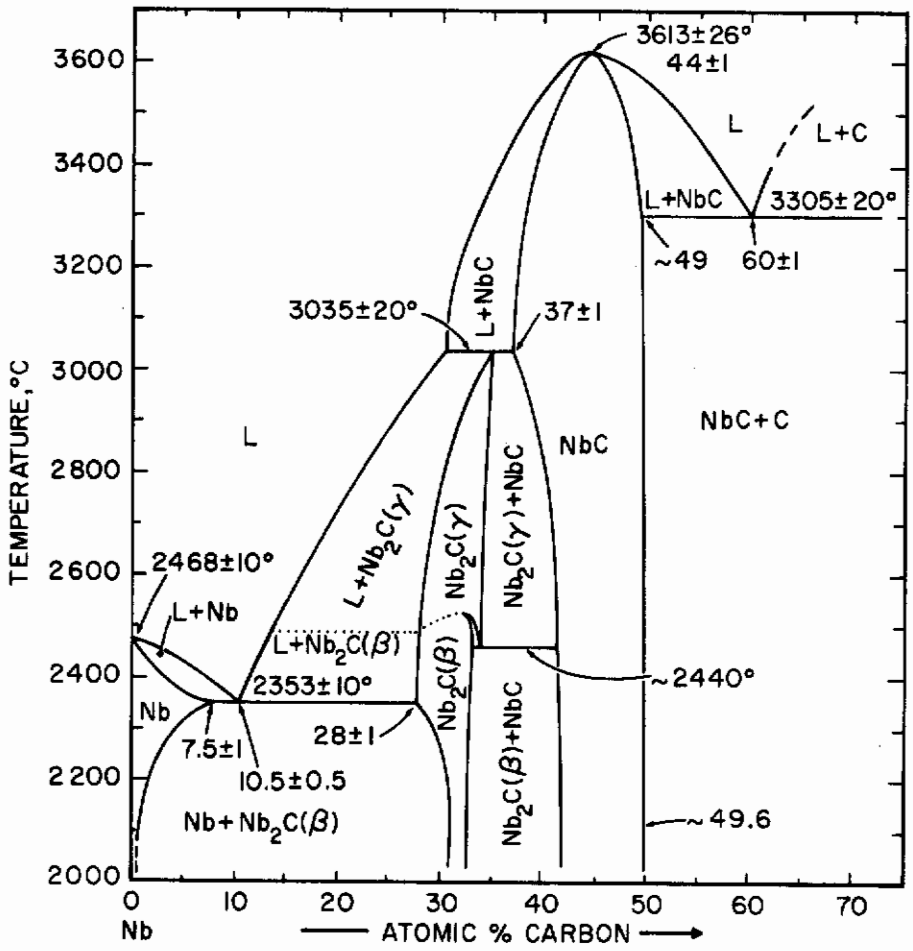

Figure 12. Phase Diagram of the Nb-C System.

(Additional Transformation of Nb_2C-Phase at 1230° C not Shown).

Table 2. Structure and Lattice Parameters of Niobium Carbides

Phase	Structure	Lattice Parameters, Å
Nb_2C	1. T<1230°C: Orthorh.	a=12.36; b=10.85$_5$; c=4.968 (13,18)*
		a=10.92; b=4.974; c=3.090 (19)**
	2. T>1230°C: Hex., ε-Fe_2N-Type	a=5.40$_7$; c=4.96$_0$ (17)***
	3. T>2500°C: Hex., L'3-Type	a=3.127; c=4.972 at 33 At.% C (10)
ζ-Nb_4C_3	Trig., $R\bar{3}m$-D_{3d}^5	a=3.14; c=30.10 at ~40 At.% C (20)
NbC	Cubic, B1-Type	a=4.431 at 41.5 At.% C a=4.469 at 49.6 At.% C (21)

The axes are related to the (distorted) hexagonal subcell approximately by:

(*) $a_{o.r.} \approx 4\, a_{hex}$; $b_{o.r.} \approx 2a_{hex} \cdot \sqrt{3}$; $c_{o.r.} = c_{hex}$.

(**) $a_{o.r.} \approx 2a_{hex} \cdot \sqrt{3}$; $b_{o.r.} = c_{hex}$; $c_{o.r.} \approx a_{hex}$.

(***) $a_{hex} = a_{hex.subcell}\sqrt{3}$; $c_{hex} = c_{hex.subcell}$

lower temperatures[12-18], and a disordered state (L'3-type) at high temperatures[12]. The melting point measurements by E. Rudy et al.[12] are in close confirmation of the data by H. Kimura and Y. Sasaki[11].

The Ta-C-system (Figure 13) contains an extremely refractory monocarbide and a peritectically melting hexagonal subcarbide. The ordered,

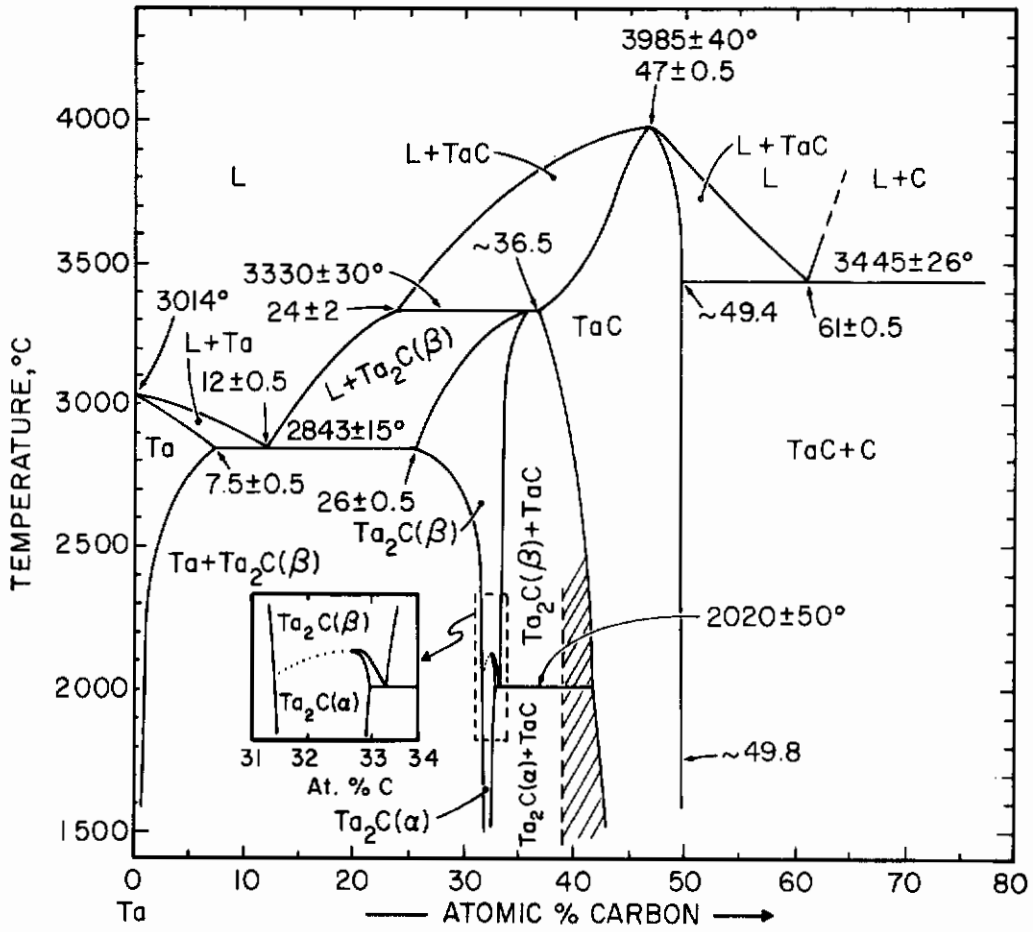

Figure 13. Phase Diagram of the Ta-C System.
(After E. Rudy....., slightly revised).

low temperature, modification of Ta_2C[22] transforms between 2100° C and 2200° C[23] into another modification, which is characterized by a disordered carbon sublattice. The ζ-phase, reported to occur near 40 At.% carbon[24] was indicated to be metastable[23]. Structural data as well as lattice parameters for the tantalum carbides are compiled in Table 3.

The complex phase relations in the Mo-C system, Figure 14, were only recently delineated in detail[25], although the intermediate phases had already been structurally characterized. Three intermediate phases,

Table 3. Structure and Lattice Parameters of Tantalum Carbides

Phase	Structure	Lattice Parameters, Å
Ta_2C	hex., C6-type (T<2000-2150°C Ordered)	a=3.103; c=4.938 at 33 At.% C (22) a=3.100; c=4.931 at 31.5 At.% C (23) a=3.102; c=4.940 at 33 At.% C (23)
	hex., L'3-type (T>2150°C, no long range order in carbon sublattice)	L'3-type cannot be retained by quenching; lattice parameters similar to L'3-type (see ref. 23)
ζ-Ta_4C_3	Trig., $R\bar{3}M$-D_3^5d	a=3.116; c=30.00 at ~40 At.% C (20)
TaC	fcc., B1-type	a=4.411 at 42.5 At.% C (24) a=4.4545 at ~50 At.% C (24)

Mo_2C, η-MoC_{1-x}, (Mo_3C_2), and α-MoC_{1-x}, occur in the system. The latter two are high temperature phases and can be retained only by severe quenching. The subcarbide Mo_2C exists in at least two states of sublattice order and shows a complex transition behavior: Substoichiometric (< 32.5 At.% C) alloys undergo a homogeneous (single-phased) order-disorder transition near 1400°C. Stoichiometric and hyperstoichiometric alloys, on the other hand, cannot exist in the ordered state; on cooling through the critical temperature range, they disproportionate into a hypostoichiometric alloy, which is ordered, and a hyperstoichiometric alloy, which is disordered and decomposes at somewhat lower temperatures in a eutectoid (pseudomonotectoid) reaction into the ordered modification and free graphite; the hexagonal close-packed metal host lattice undergoes a slight distortion in the transformation process. Structural details as well as lattice parameters for the molybdenum carbides are compiled in Table 4.

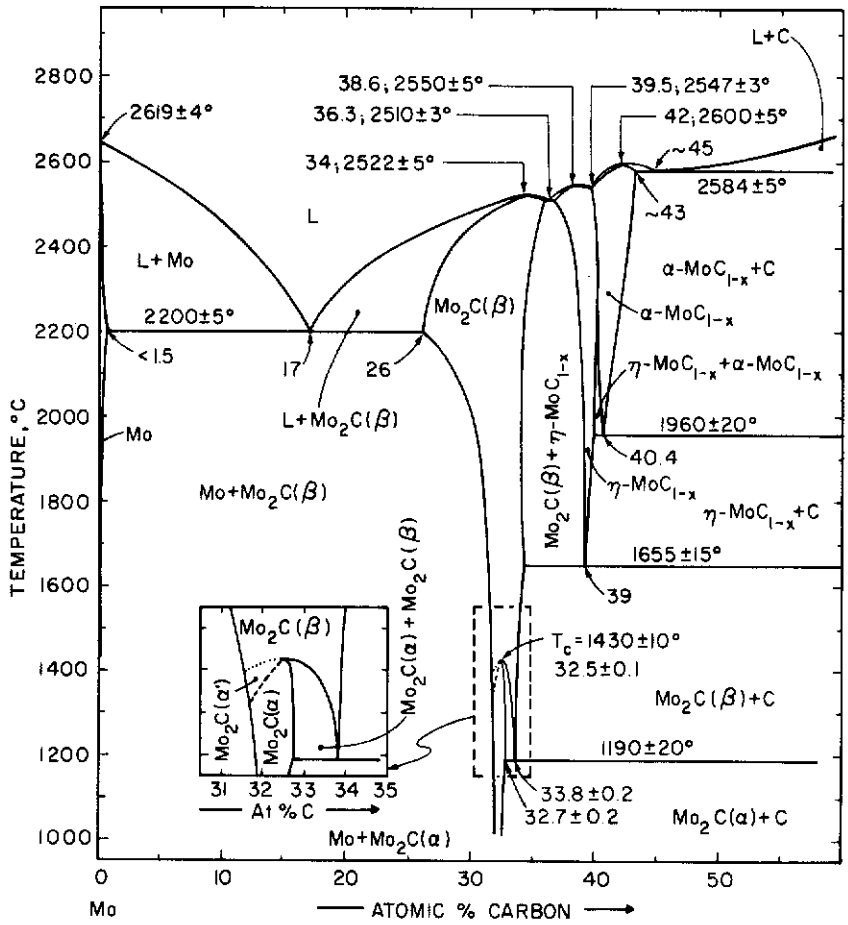

Figure 14. Phase Diagram of the Mo-C System (After E. Rudy et al., 1967).

Table 4. Structure and Lattice Parameters of Molybdenum Carbides.

Phase	Structure	Lattice Parameters, Å
Mo_2C	Orthorh., D_{2h}^{14}-Pbcn ($T < \sim 1400°C$, C-sublattice ordered)	a=4.724; b=6.004; c=5.19 (26)*
		a= 4.733; b=6.042; c=5.202 at 32.5 At.% C (25)*
	hex., L'3-type ($T > \sim 1400°C$), no long range order in carbon sublattice)	a= 2.990; c=4.730 at 30 At.% C
		a= 3.010; c=4.778 at 34.4 At.% C (25)
η-MoC_{1-x} (Mo_3C_2)	hex., D_{6h}^4	a= 3.006; c=14.64 (27)
		a= 3.010; c= 14.64 at 39 At.% C (25)
α-MoC_{1-x}	fcc., B1-type	a= 4.266 at 39.7 At.% C (25)
		a= 4.281 at 43 At.%

(*) The orthorhombic axes of the ordered structure of Mo_2C are related to the axes of the (slightly distorted) hexagonal subcell by:

$$a_{o.r.} = c_{hex};\ b_{o.r.} \simeq 2\,a_{hex};\ c_{o.r.} \simeq a_{hex}\sqrt{3}$$

B. Ti-Nb-C SYSTEM

An isothermal section of the system at 1600° C was established in 1964 by Stecher et al.[28] (Figure 15) and somewhat later one at 1500° C by Fedorov et al.[29], Figure 16. Both investigations show complete miscibility of the monocarbides[30] and a limited titanium exchange in Nb_2C.

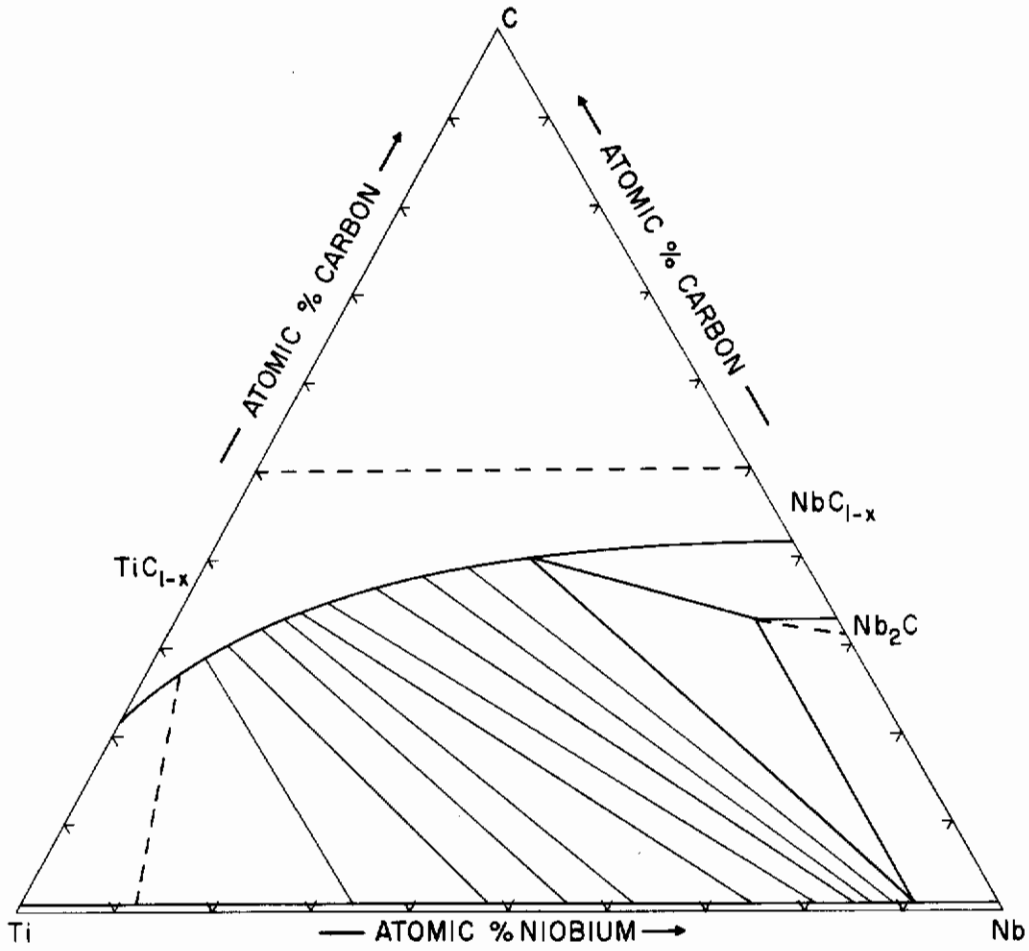

Figure 15. Isothermal Section of the Ti-Nb-C System at 1600°C.
(After P. Stecher et al., 1964)

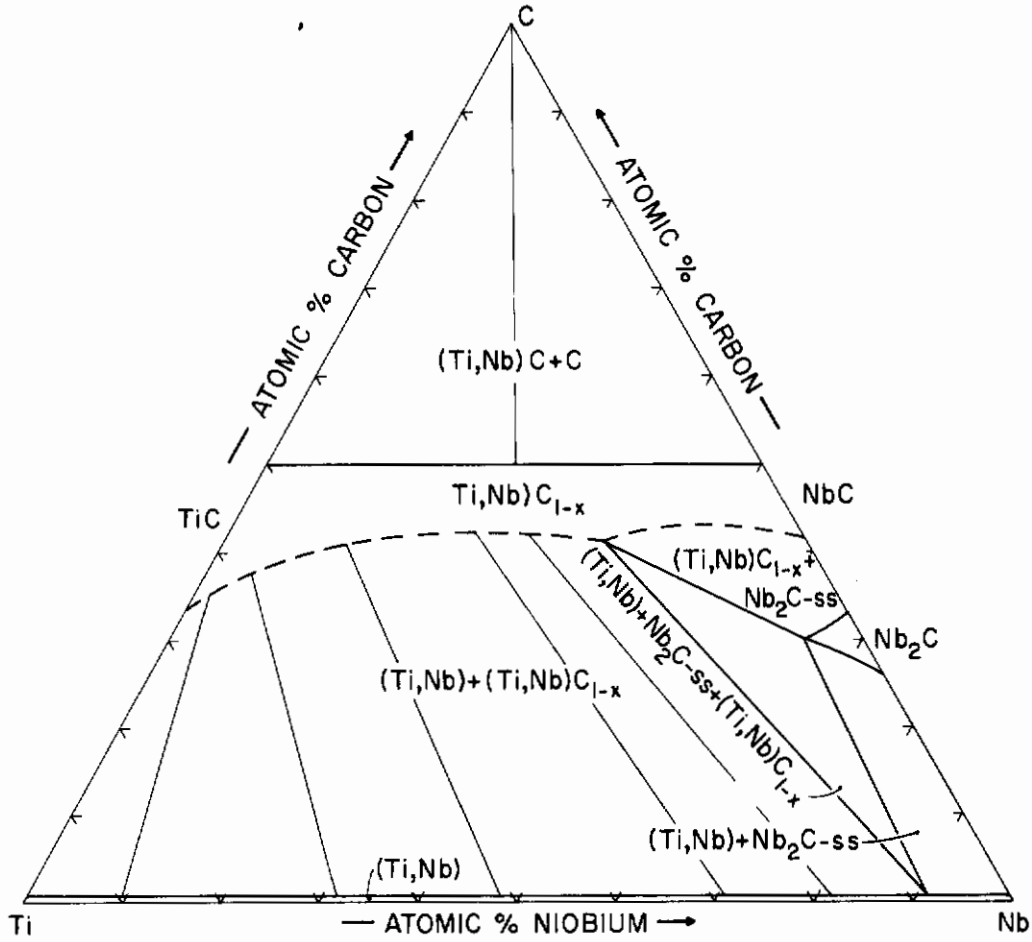

Figure 16. Isothermal Section of the Ti-Nb-C System at 1500° C.

(After Fedorov et al., 1965)

C. Ti-Ta-C SYSTEM

Isothermal sections of this phase diagram were established by McMullin and Norton[31] and an extended study of the entire system at temperatures above 1500° C was carried out in a preceding Air Force Program by Brukl and Harmon[1]. In view of the recent changes in the binary phase diagrams, the current effort was undertaken to supplement the old data and also to provide a more detailed analysis of the order-disorder transition in the ternary $(Ti,Ta)_2C$ solid solution.

D. Ti-Mo-C SYSTEM

The only investigation concerning the entire Ti-Mo-C system has been carried out by Albert and Norton[32] in 1956, after previous investigations had established extended solid solubility of molybdenum carbide in TiC[30]. The isothermal section of the system at 1710°C, Figure 17, shows the TiC solid solution to extend to approximately 87 mole% MoC at this temperature, while the Mo_2C-phase substitutes about 10 At.% titanium into the

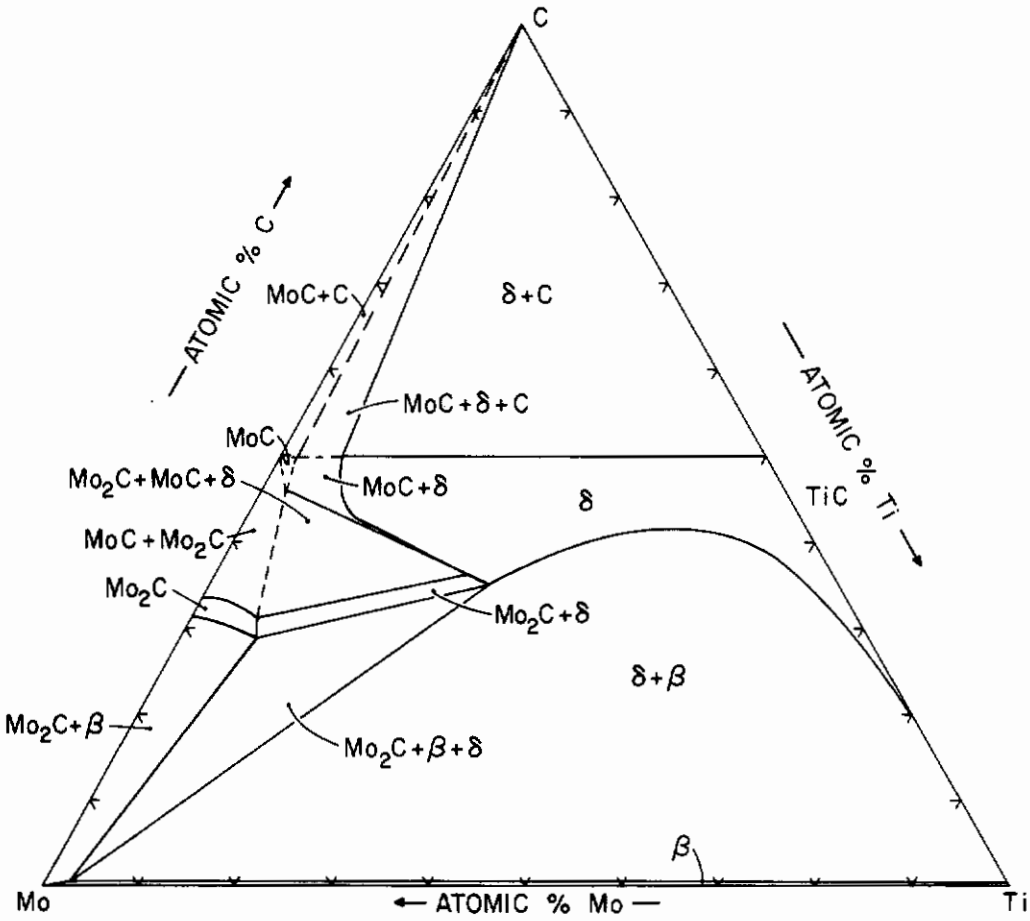

Figure 17. Isothermal Section of the Ti-Mo-C System at 1710°C.
(After H.J. Albert and J.T. Norton, 1956).

lattice. The three-phase equilibrium (Ti,Mo)-$(Ti,Mo)_2C$+ $(Ti,Mo)C_{1-x}$ which terminates the Mo_2C-phase in the ternary, borders a wide two-phase equilibrium between the metal and titanium monocarbide solid solution.

III. EXPERIMENTAL

A. STARTING MATERIALS

The elemental powders, as well as specially prepared, or purchased, master alloys consisting of TiC, Nb_2C, NbC, TaC, and Mo_2C, were used in fabricating the experimental alloys.

Titanium powder of 99.9% overall purity was purchased from Varlacoid chemical company. The main contaminants included 800 ppm oxygen and 1100 ppm carbon. Measured lattice parameters of a = 2.949Å and c= 4.687Å are in reasonable agreement with values of a= 2.950Å, and c= 4.6833Å reported in the literature for iodide titanium[33].

The impurities in the niobium powder (Wah Chang Corporation, Albany, Oregon, overall purity better than 99.8%) were as follows (in ppm): O-<420; N-<90; C-30; Ta-400; Zr-200; and the sum of other metallic impurities-<400. A lattice parameter of a= 3.306Å, obtained from an exposure with Cu-K_α radiation, is consistent with lattice spacings given in the literature.[33]

Tantalum (99.9% pure) powder was purchased from Wah Chang Corporation, Albany, Oregon, with impurities (in ppm) as follows: C-140, Nb-100; O-280, other contaminants <300. A lattice parameter of a= 3.303Å is in agreement with the lattice spacings for high purity tantalum given by Pearson.[33]

The molybdenum powder (Wah Chang Corporation, Glen Cove, New York) had the following impurities (in ppm) after an additional hydrogen reduction treatment at 1000 C: O-160; Si-<180; Nb-<180; N-<20, C-190; sum of Fe,Ni,Co-<110; and sum of other metallic impurities (Al,Cr,Cu,Mg, Mn,Pb,Sn,W,Ti)-<600. The lattice parameter was a= 3.1474 ± 0.0002 Å.

The spectrographic grade graphite powder (Union Carbide Corporation, Carbon Products Division, New York) had a total impurity content below 2 ppm.

The titanium monocarbide powder was purchased as 80 micron powder from Varlacoid Chemical Company. After a degassing treatment for 3 hrs at 2200° C under a vacuum of 5×10^{-6} Torr, the carbide had a total carbon content of 50.2 At.%, of which 1.1 At.% were present as elemental graphite. The combined content of oxygen and nitrogen, as determined by the gas-fusion technique, were 1300 ppm, and the sum of metallic impurities, determined by semiquantitative spectrographic methods, was below 700 ppm. A lattice parameter of a= 4.329Å was derived from an X-ray exposure with Cu-K_α radiation.

Tantalum monocarbide, purchased as 10 micron powder from Wah Chang Corporation, Albany, Oregon, was acid-leached to remove soluble constituents and high-vacuum degassed (2 hrs at 4×10^{-4} Torr at 2200° C) to eliminate volatile contaminants. The lattice parameter of the purified product was a= 4.4560 ± 0.003Å. The monocarbide had a total carbon content of 6.15$_6$ wt.%, of which 0.04 wt.% was present in elemental form. The following impurities (in ppm), were found in the processed material: Ti-<400; Nb-150; Y-200; O-<20; N-<10; H-not detected; Cr-<25; Co-40; Fe-<70; sum of B,Mg,Mu,Ni,Pb,Si, and Sn-<50.

Niobium monocarbide, Nb_2C, and Mo_2C were prepared by reacting the carefully blended and cold-compacted mixtures of the metal powders and graphite in a graphite-element furnace under a vacuum of approximately 2×10^{-5} Torr. The thermal treatments were 2 hrs at 1900° C for Nb_2C and NbC, and 2 hrs between 1600° and 1900° C for Mo_2C. The reaction lumps were crushed and ball-milled to a grain size smaller than 60 microns and cobalt pickup from the hard-metal-lined jars was removed by acid-leaching.

The Nb_2C powder had a total carbon content of 33.2 ± 0.2 At.%, and the X-ray powder pattern (Cu-K_α) revealed Nb_2C (a= 3.125Å, c=4.963Å) and traces of NbC. The oxygen content was smaller than 160 ppm. Total carbon in the monocarbide was 49.2 ± 0.2 At.%, and the powder also contained about 100 ppm oxygen. The lattice parameter, determined from a Cu-K_α exposure, was a= 4.470Å.

The Mo_2C powder contained 32.7 ± 0.2 At.% carbon, of which 0.2 At.% was present as elemental graphite. Other contaminants included (in ppm): O-70; N-<10; and Si-<100.

B. SAMPLE PREPARATION, MEASUREMENT OF MELTING TEMPERATURES AND DIFFERENTIAL THERMAL ANALYSIS

Most of the ternary samples were prepared by hot-pressing the hand-mixed powders of the ingredients in graphite dies for 2 to 5 minutes. The hot pressing temperatures varied, depending on the melting temperatures of the constituents present in the alloy, between about 1600 to 2800° C. After hot-pressing, the thin, carburized surface zones were removed by grinding, and the samples then subjected to further heat treatments. Equilibration temperatures for investigating the solid state sections of the system were 1500° (64 hrs) and 1800° C (11 hrs) for Ti-Nb-C and Ti-Ta-C alloys, and 1500° C

(109 hrs), 1800° C (11 hrs) and 2100° C (4 hrs) for the Ti-Mo-C system. Samples were heat-treated in a tungsten-mesh-element furnace, using either vacuum (5×10^{-6} Torr) or, above 2000° C, high purity helium at ambient pressure. The variation of certain equilibria, especially in the very high temperature range, was studied on alloys equilibrated in the Pirani-furnace or the DTA-apparatus and then radiation-cooled or quenched in tin. For metallographic purposes, a piece of each alloy was also arc melted under helium using a nonconsumable tungsten electrode arc furnace. For melting and DTA-experiments, binary metal alloy samples and ternary specimens located near the metal edge binaries were prepared by cold pressing the powdered ingredients and were used in the as-pressed state.

C. MELTING POINT DETERMINATION AND DIFFERENTIAL THERMAL ANALYSIS

The melting temperatures of approximately 390 alloys were measured by the method devised by Pirani and Alterthum. Design details of the apparatus used in this laboratory, as well as temperature calibration and correction data, were published elsewhere.[34] Measurements on metal-rich alloys were carried out under vacuum, while high melting alloy compositions (>~2300° C) were run under helium at approximately 2 atmospheres pressure, after the specimens were degassed between 1800 and 2200° C. Post-experimental analysis of the alloys indicated that the concentration shifts during melting were very nominal and the analyzed compositions agreed, as a rule, to within 1 At.% of the weighed-in compositions. Oxygen and nitrogen contamination of the melted alloys were normally lower than in the starting materials.

With tantalum carbide as well as annealed graphite as standards and graphite as container material, the thermal behavior of approximately

130 alloys was studied by DTA techniques. As a result of the limitations imposed by the container material, these measurements had to be restricted to temperatures below the monocarbide + graphite eutectics.

D. METALLOGRAPHIC, X-RAY, AND CHEMICAL ANALYSIS

For microscopic studies, the specimens were mounted in a mixture of diallylphthalate and lucite-coated copper powder, and preground on silicon carbide paper. The ground surfaces were polished using a slurry of Linde B alumina (0.3 microns) in a 5% chromic acid solution. The etching procedures varied with the alloy compositions and are listed in Table 5.

Carbon in the alloys was determined by combustion of the powdered specimens in oxygen and conductometric analysis of the resulting gas mixture. To determine free graphite, the powdered alloys were dissolved in a mixture of nitric and hydrofluoric acids, and the residual graphite was analyzed by combustion as described in the foregoing. The reproducibility of the results was usually within 0.02 wt.%.

Oxygen and nitrogen were hot-extracted in a gas-fusion analyzer and low level metallic impurities were determined spectrographically in a semiquantitative manner.

Powder diffraction patterns were prepared from all experimental alloys, and the film strips were evaluated with respect to number, structure, and lattice dimensions of the phases. The tie line distribution in the various two-phase fields and the location of the vertices of the three-phase equilibria were also determined by lattice parameter measurements.

Table 5. Etching Conditions for Ti-Nb(Ta,Mo)-C Alloys

System	Composition Range	Etching
Ti-Nb-C	Ti-Nb-$Nb_{0.70}C_{0.30}$-$Nb_{0.40}Ti_{0.30}C_{0.30}$-$Nb_{0.40}Ti_{0.25}C_{0.35}$-$Ti_{0.65}C_{0.35}$	Electroetched in 0.5% oxalic acid solution
	$Nb_{0.70}C_{0.30}$-$Nb_{0.40}Ti_{0.30}C_{0.30}$-$Nb_{0.40}Ti_{0.18}C_{0.42}$-$Nb_{0.58}C_{0.42}$	Electroetched in 0.5% oxalic acid followed by strong acid rinse to remove stains
	$Ti_{0.5}C_{0.35}$-$Ti_{0.50}C_{0.50}$-$Nb_{0.50}C_{0.50}$-$Nb_{0.58}C_{0.42}$-$Nb_{0.40}Ti_{0.18}C_{0.42}$-$Nb_{0.40}Ti_{0.30}C_{0.30}$	Dip-etched in 20% Murakami's followed by acid rinse.
	$Ti_{0.50}C_{0.50}$-$Nb_{0.50}$-C	Examined in as-polished state
Ti-Ta-C	Ti-$Ti_{0.80}C_{0.20}$-$Ta_{0.80}C_{0.20}$-Ta	Electroetched in 2% NaOH
	$Ti_{0.80}C_{0.20}$-$Ti_{0.45}C_{0.55}$-$Ta_{0.45}C_{0.55}$-$Ta_{0.80}C_{0.20}$	Etched in mixture of aqua regia and HF
	$Ti_{0.45}C_{0.55}$-$Ta_{0.45}C_{0.55}$-C	Examined in as-polished state
Ti-Mo-C	$Ti_{0.50}Mo_{0.50}$-$Ti_{0.50}C_{0.50}$-Mo	Swab-etched in 20% Murakami's.
	Ti-$Ti_{0.5}M_{0.5}$-$Ti_{0.10}Mo_{0.50}C_{0.40}$-$Ti_{0.60}C_{0.40}$	Electroetched in 0.5% oxalic acid solution
	$Ti_{0.60}C_{0.40}$-$Ti_{0.10}Mo_{0.50}C_{0.40}$-$Ti_{0.25}Mo_{0.25}C_{0.50}$-$Ti_{0.50}C_{0.50}$	Dip-etched in 40% solution of 6 parts HNO_3, 2 parts HCl and 2 parts HF
	$Ti_{0.50}C_{0.50}$-$Ti_{0.25}C_{0.25}C_{0.50}$-$Ti_{0.10}Mo_{0.50}C_{0.40}$-$Mo_{0.50}C_{0.50}$-C	Examined in as-polished

IV. RESULTS

A. BOUNDARY SYSTEMS

Melting point and lattice parameter measurements on the three binary metal systems, Ti-Nb, Ti-Ta, and Ti-Mo, substantially confirmed previous investigations[1-4, 35-37] (Figures 18-23). Slightly revised phase diagrams of these systems, are shown in Figures 24, 25, and 26.

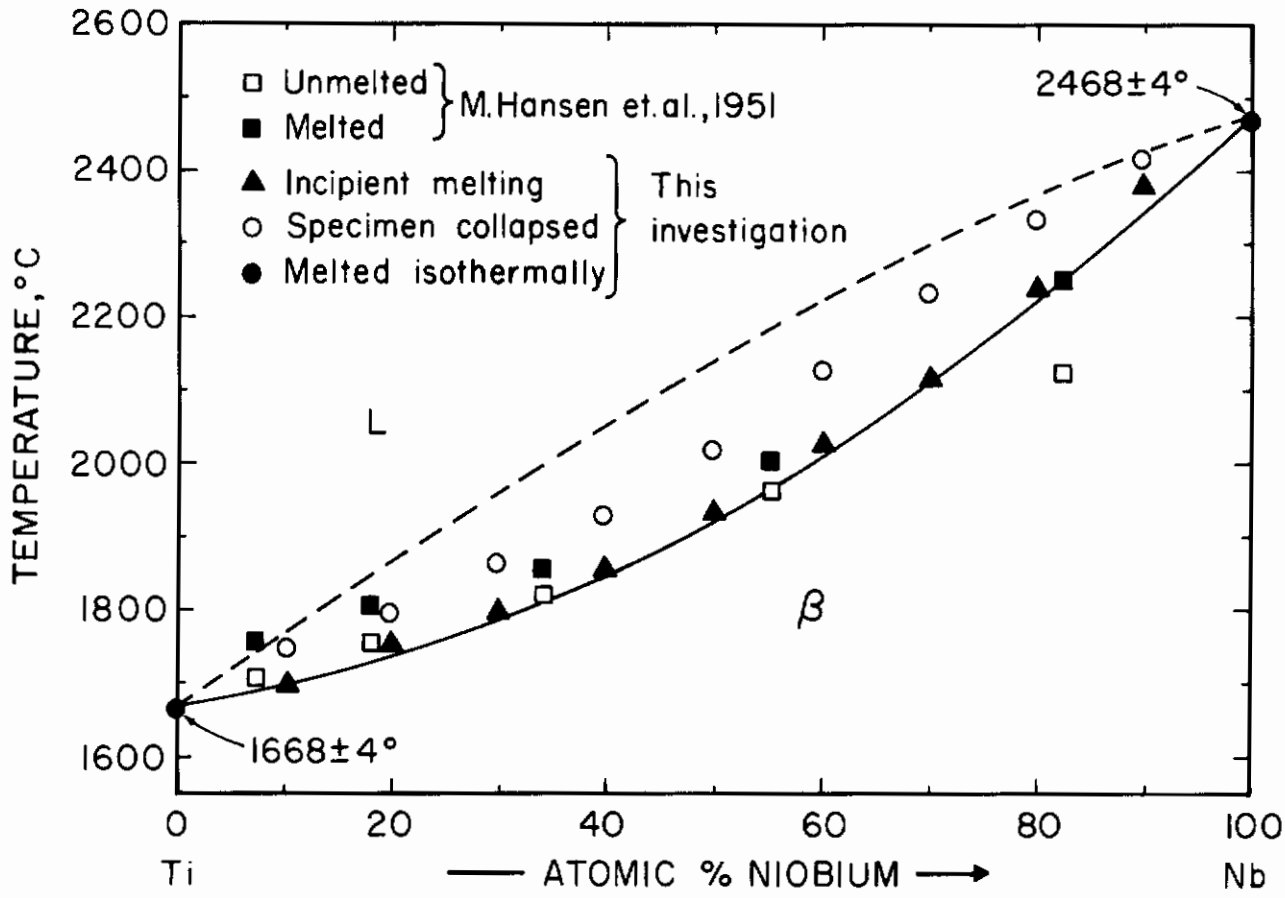

Figure 18. Melting Temperatures of Ti-Nb Alloys
(Temperature error figures based on reproducibility)

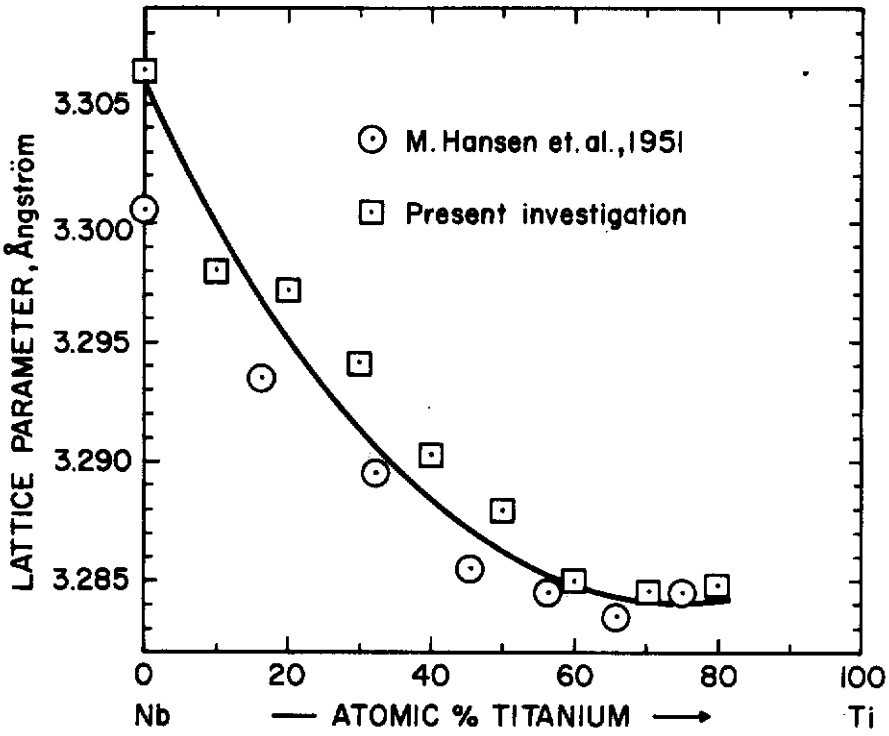

Figure 19. Lattice Parameters of the Cubic (Ti,Nb)-Solid Solution.

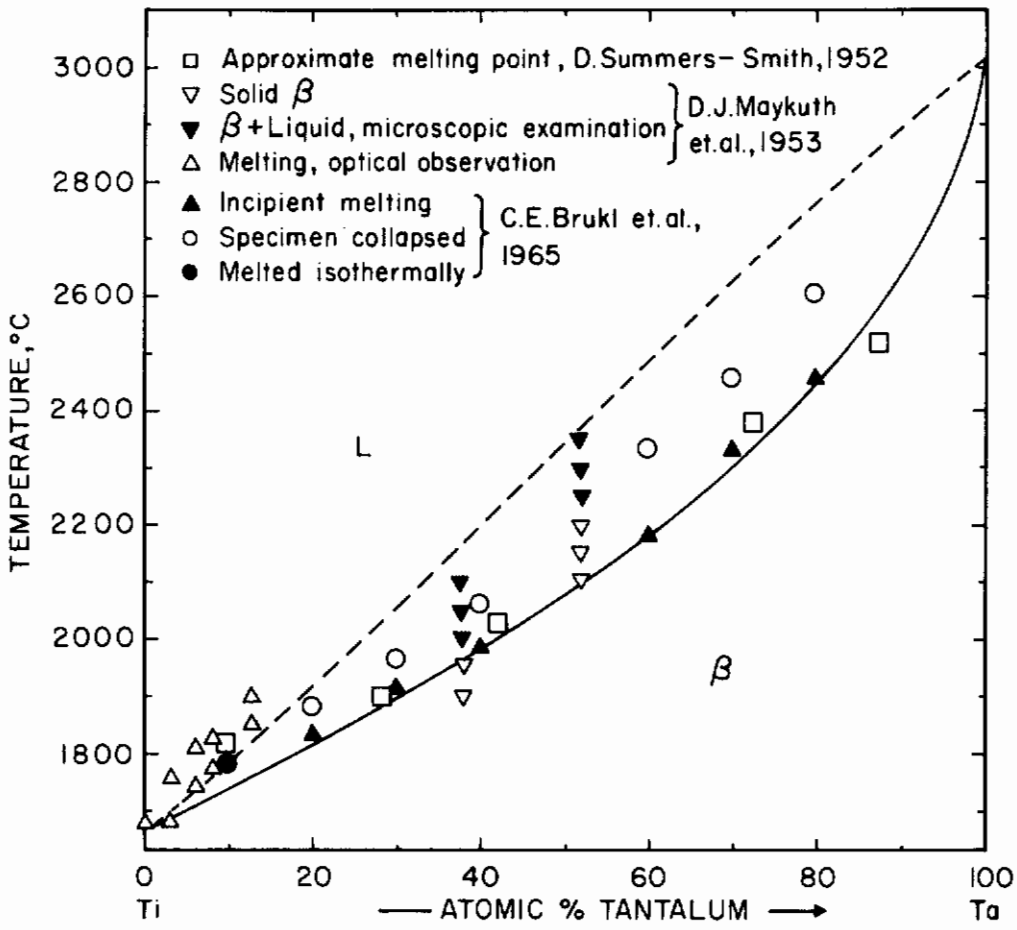

Figure 20. Melting Temperatures of Ti-Ta Alloys

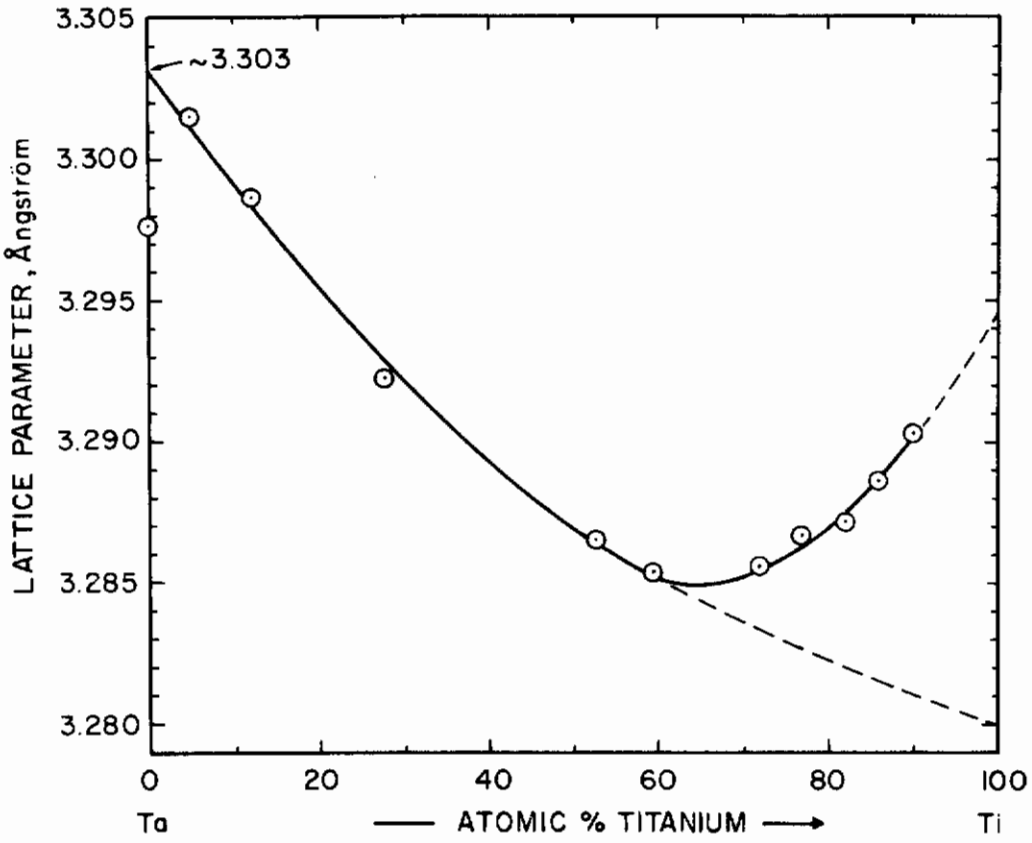

Figure 21. Lattice Parameters of the Cubic (Ti-Ta)-Solid Solution.

(After D. Summers-Smith, 1952. Alloys Quenched, Respectively, from 850 and 650°C).

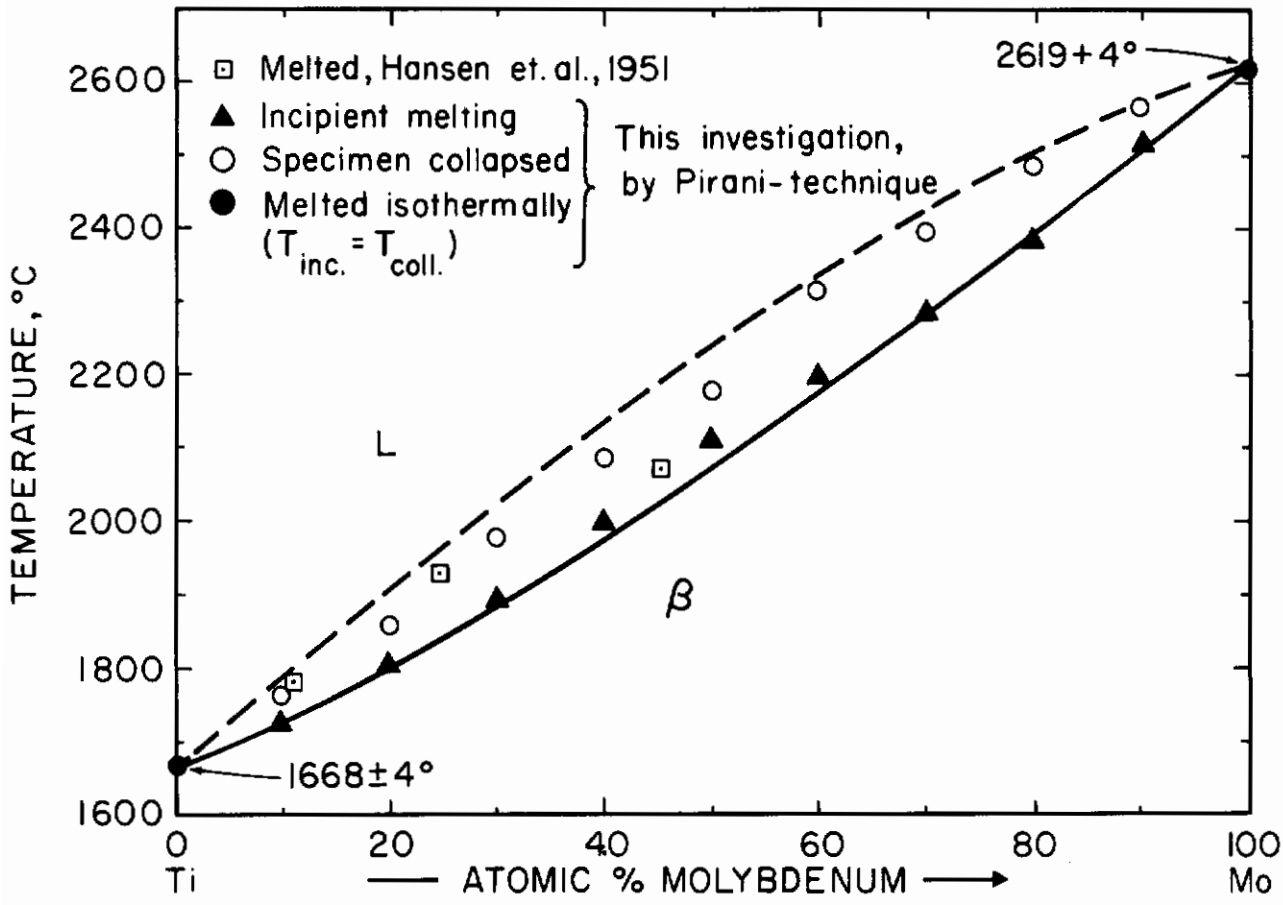

Figure 22. Melting Temperatures of Ti-Mo Alloys.

(Temperature Error Figures Based on Reproducibility)

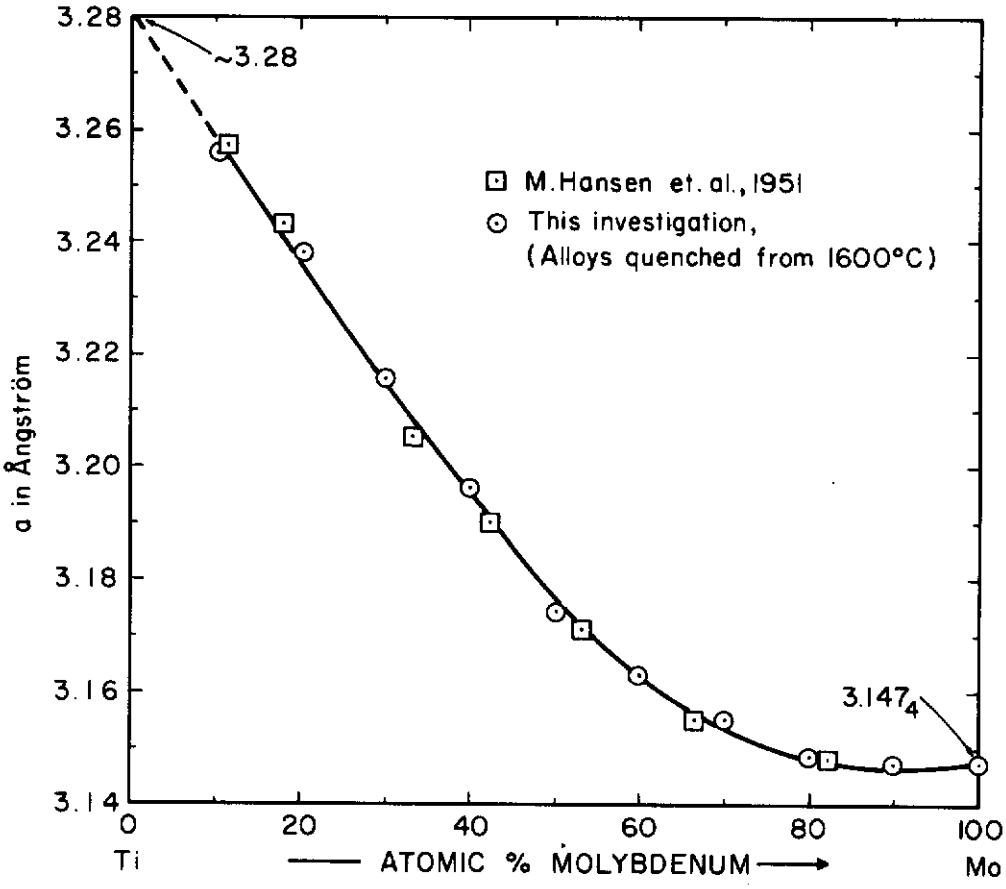

Figure 23. Lattice Parameters of the Cubic (Ti, Mo)-Solid Solution.

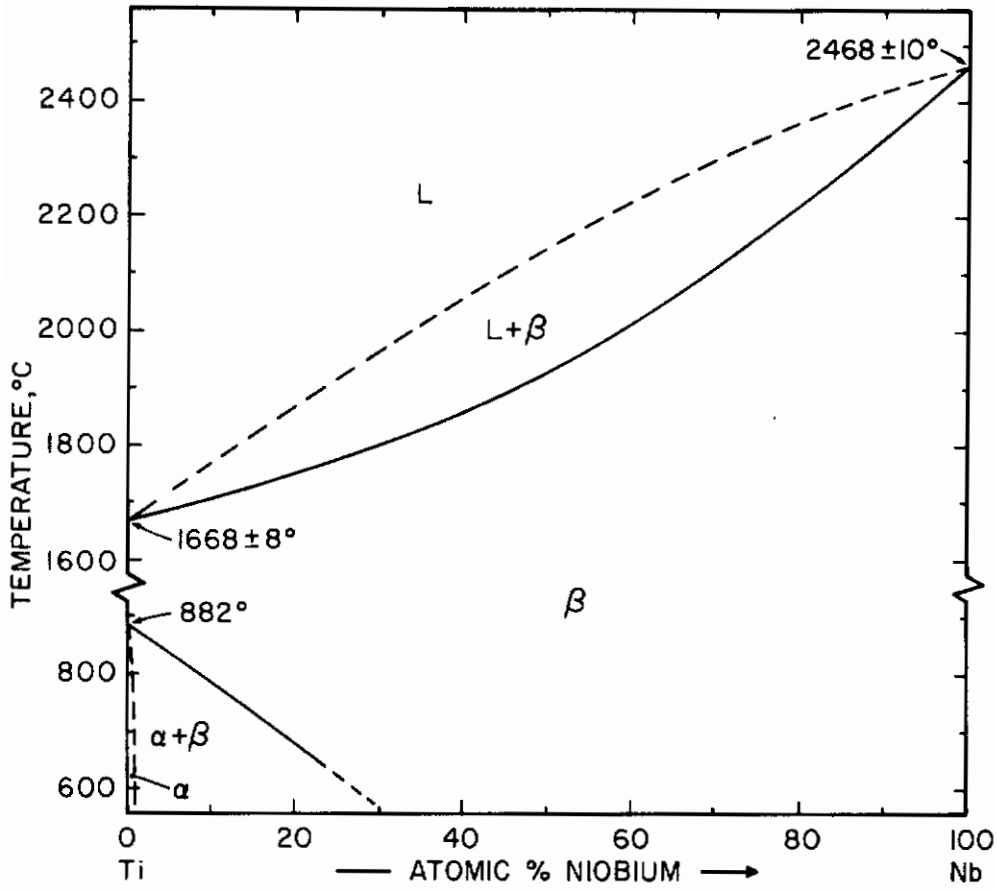

Figure 24. Phase Diagram of the Ti-Nb System

(Temperature Error Figures Based on Estimated Overall Uncertainties)

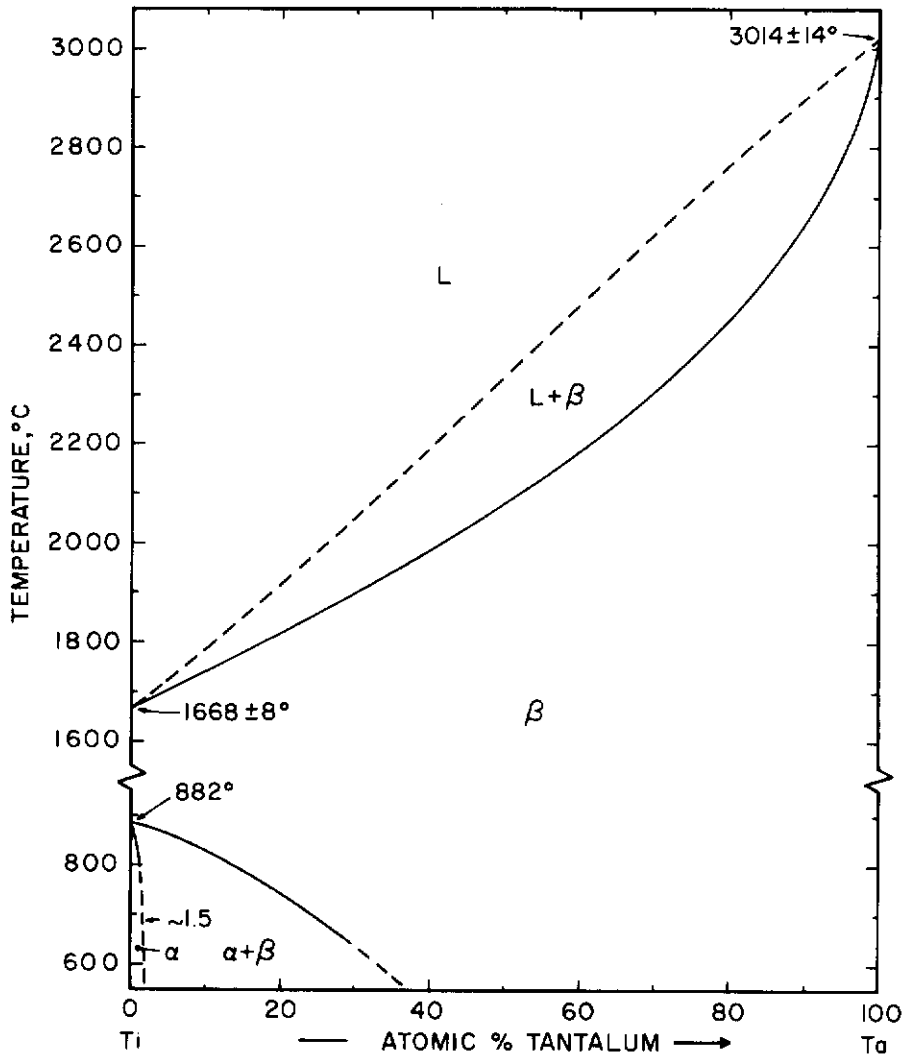

Figure 25. Phase Diagram of the Ti-Ta-System.

(Temperature Error Figures Based on Estimated Overall Uncertainties)

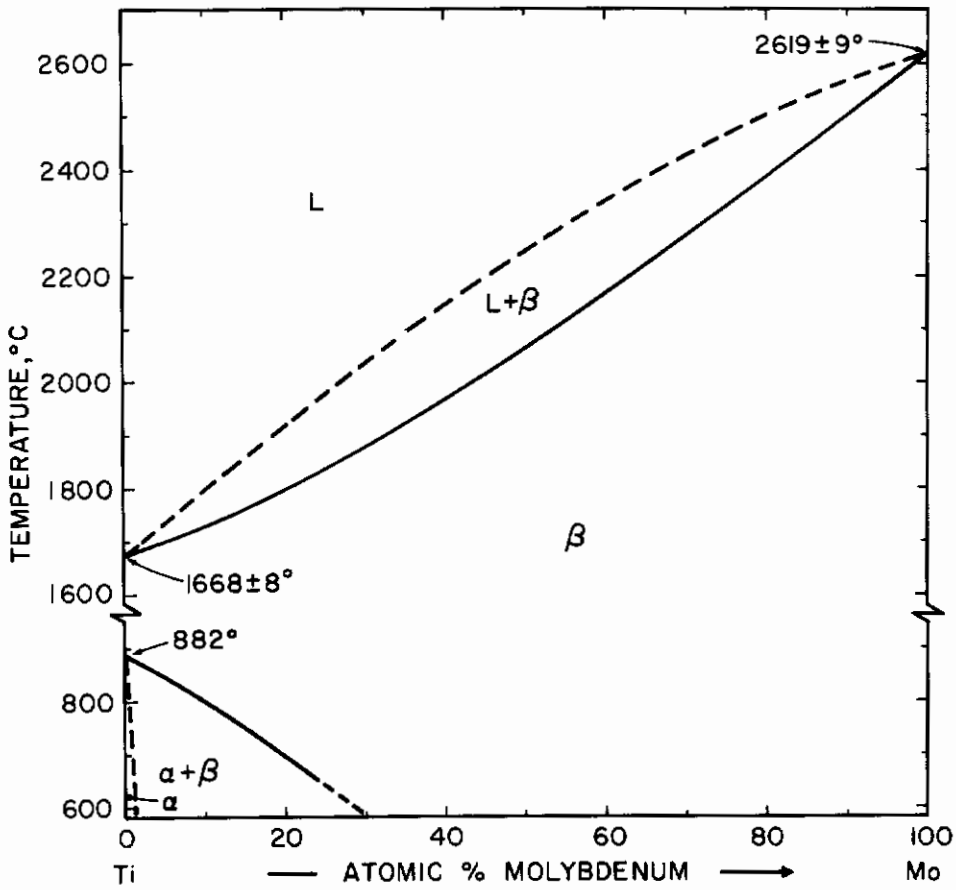

Figure 26. Phase Diagram of the Ti-Mo System

(Temperature Error Figures Based on Estimated Overall Uncertainties)

B. Ti-Nb-C SYSTEM

The qualitative phase evaluation of the sample series equilibrated at 1500° C and 1800° C (Figure 27) led to similar conclusions concerning the phase distribution, except that in the higher temperature section liquid appears near the Ti-C boundary. The average parameters of the Nb_2C-phase in three-phased, (Ti,Nb) + $(Ti,N)_2C$ + $(Ti,Nb)C_{1-x}$ alloys was a= 3.100Å, c= 4.972Å (pure Nb_2C: a= 3.127Å, c= 4.972Å), indicating some titanium solubility. The tie line distribution in the two-phase field, determined by lattice parameter-concentration graphs such as shown in Figure 28, indicate

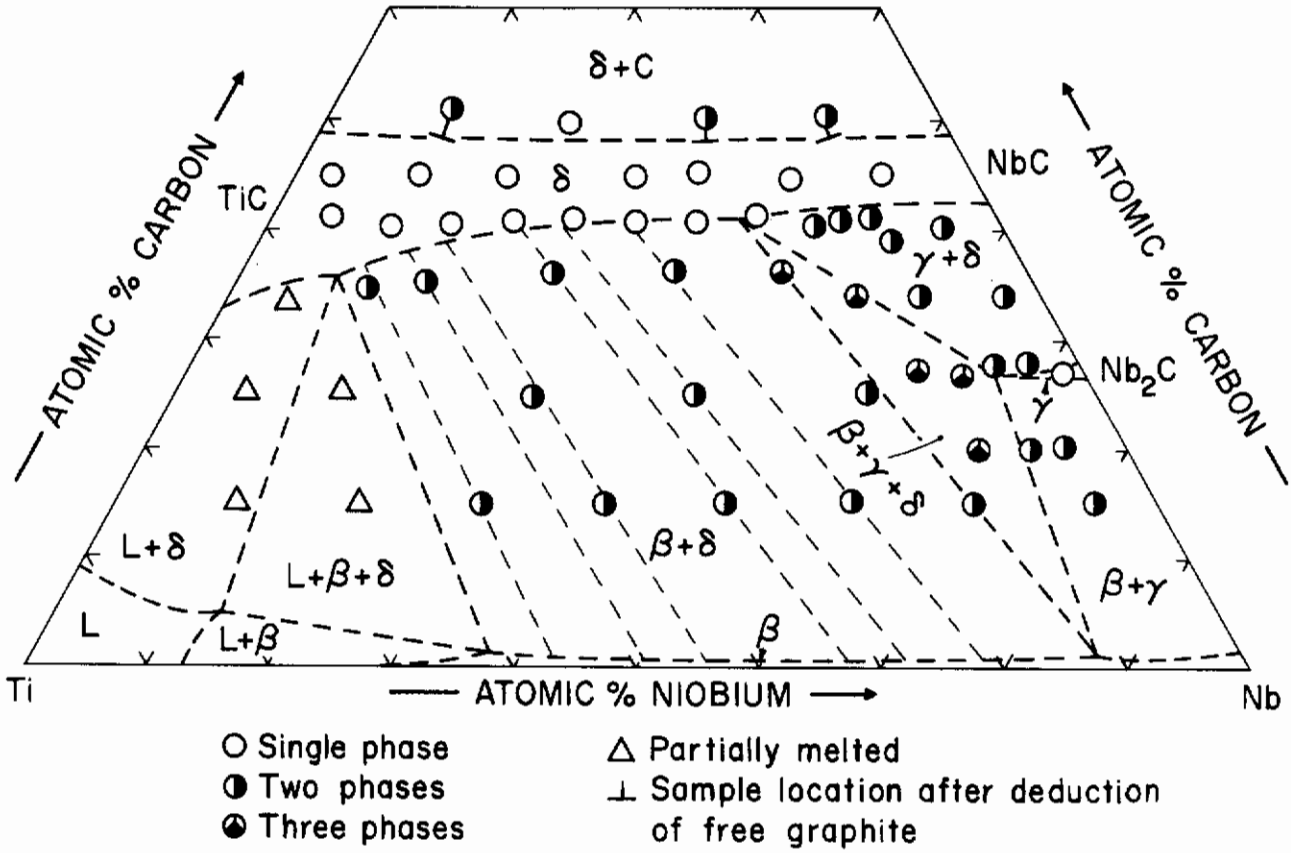

Figure 27. Qualitative Phase Evaluation of Ti-Nb-C Alloys Equilibrated at 1800° C.

(Sample Locations Shown are Based on Chemical Analysis After the Heat Treatment)

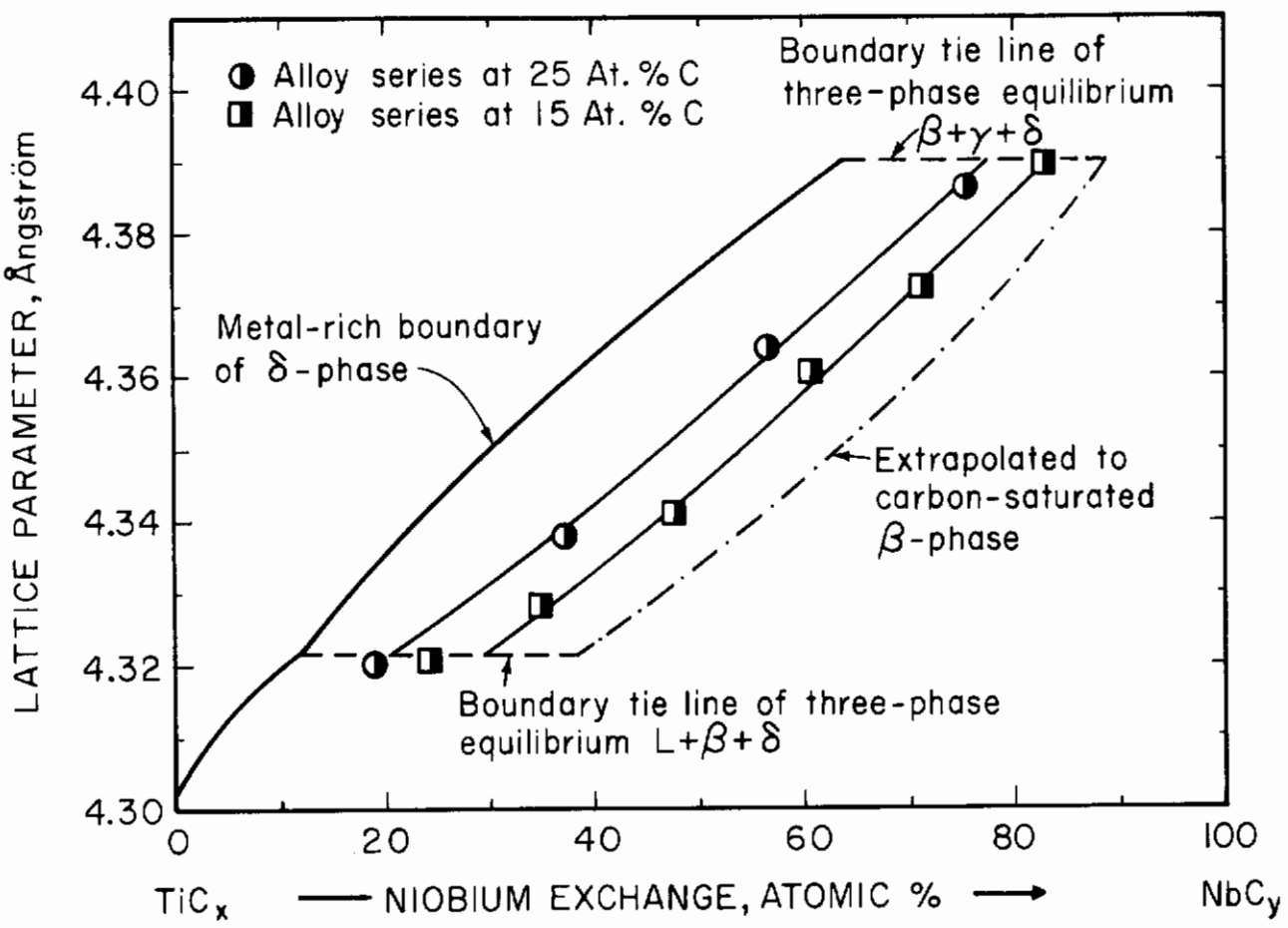

Figure 28. Determination of the Tie Line Distribution in the Two-Phase Field β + δ by the Lattice Parameters of the Monocarbide Phase in Two-Phased, Metal + Monocarbide, Alloys.

(Samples Equilibrated at 1800° C).

a relative enrichment of titanium for the carbide phase. Lattice Parameter measurements on the monocarbide phase at a number of carbon defect concentrations (Figures 29, 30, 31 and 32) show a near-linear dependence of the unit cell dimensions on the metal-exchange.

The solidus temperatures at the metal-rich eutectic trough (Figure 33) vary smoothly between the metal + carbide eutectic temperatures in the binary Ti-C and Nb-C systems. Solidification of the alloys at the

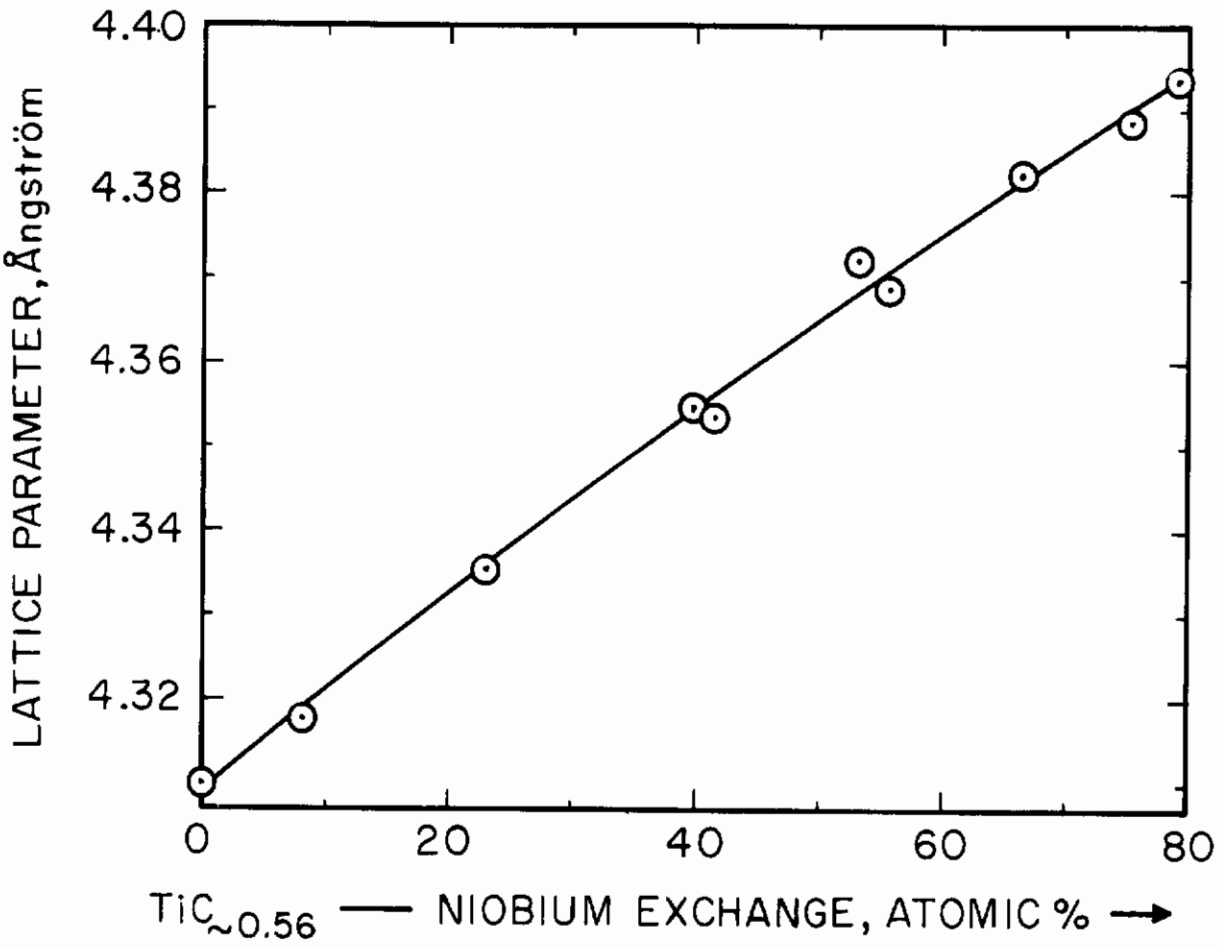

Figure 29. Lattice Parameters of the Monocarbide Phase Containing Between 35 and 38 At.% Carbon.

(Samples Quenched after Equilibration at 2400°C).

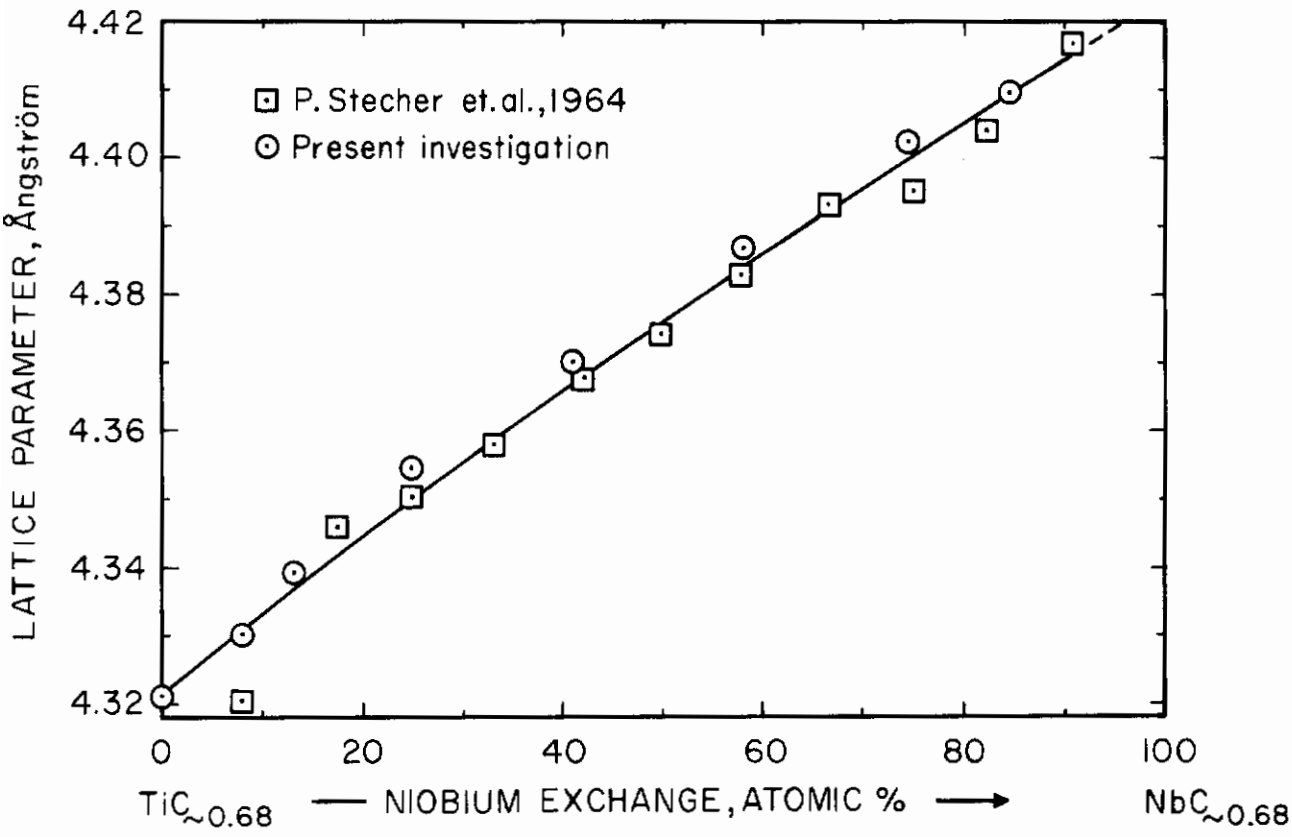

Figure 30. Lattice Parameters of the Carbon-Deficient Monocarbide Solution at 40 to 41 At.% Carbon.

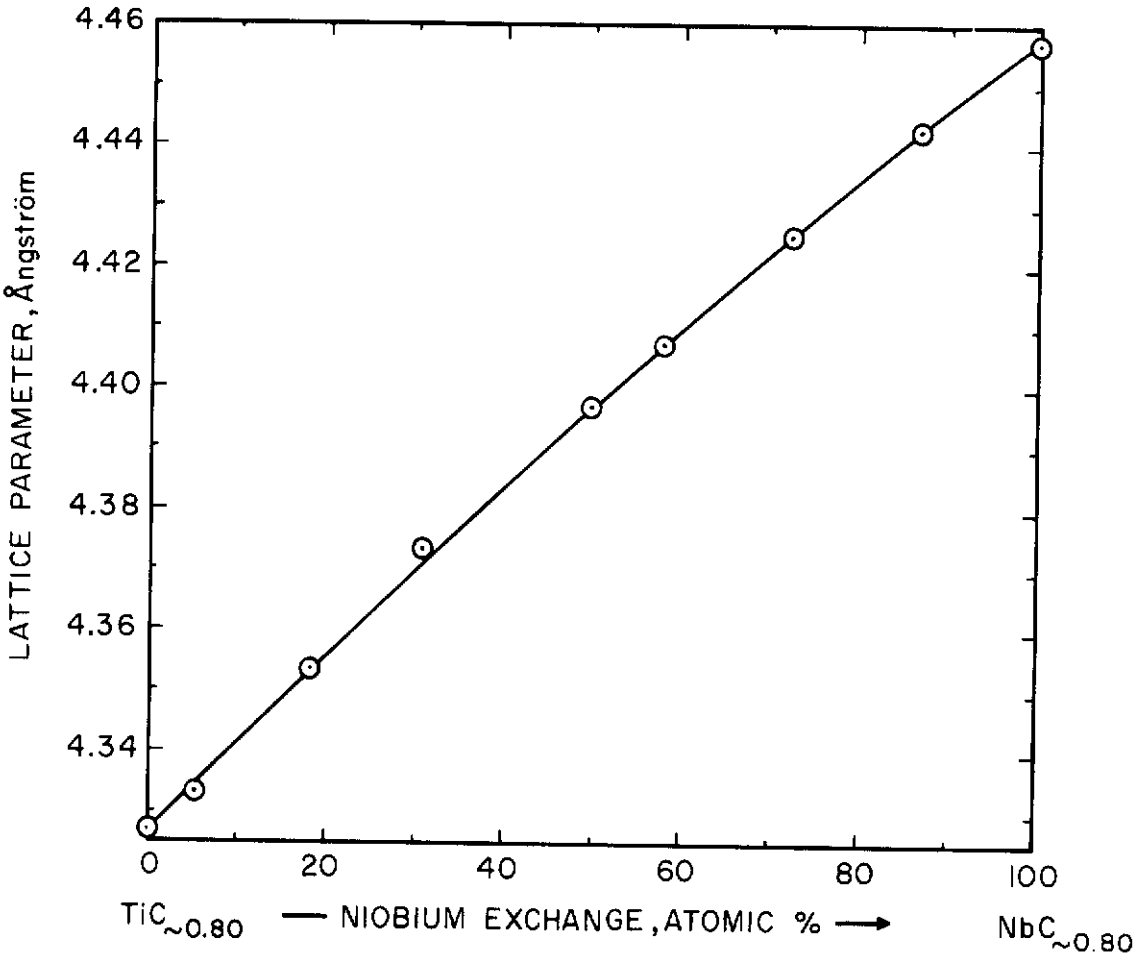

Figure 31. Lattice Parameters of the Monocarbide Solution at 44 to 45 At. % C.

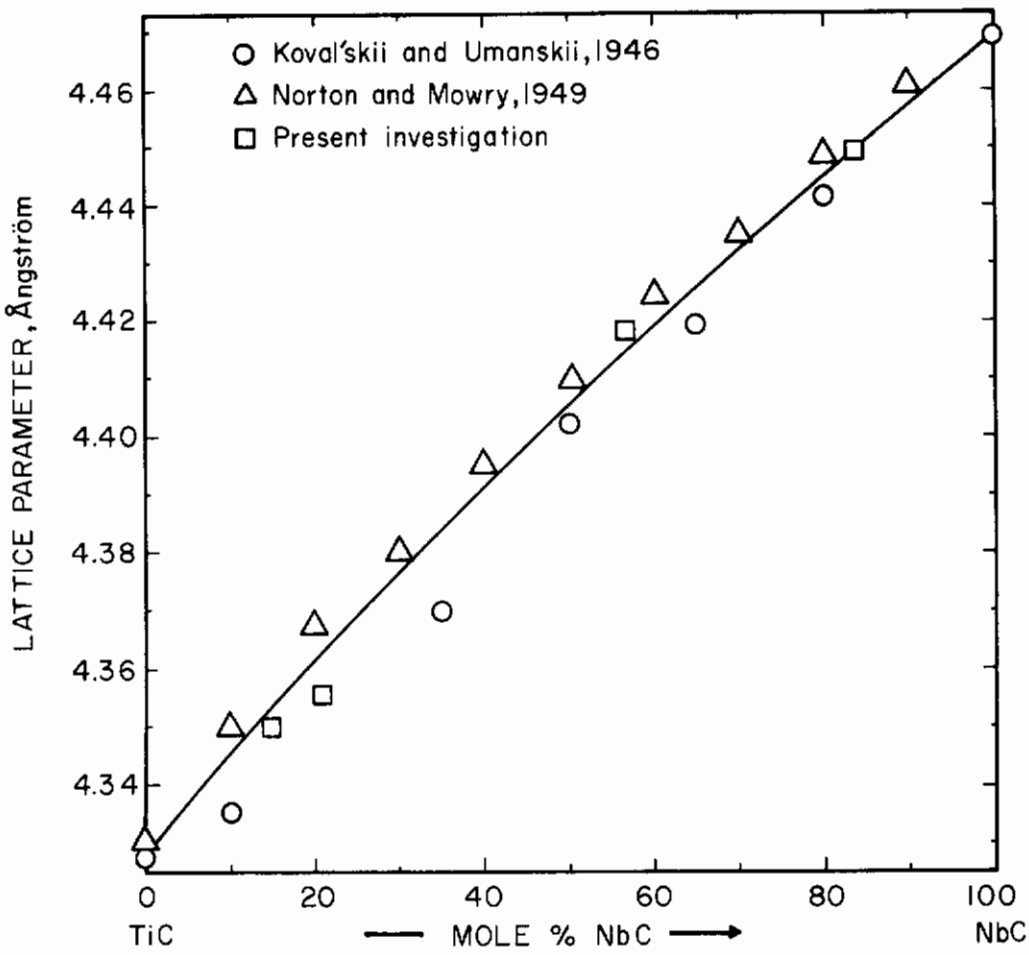

Figure 32. Lattice Parameters for the Carbon-Saturated Monocarbide Phase.

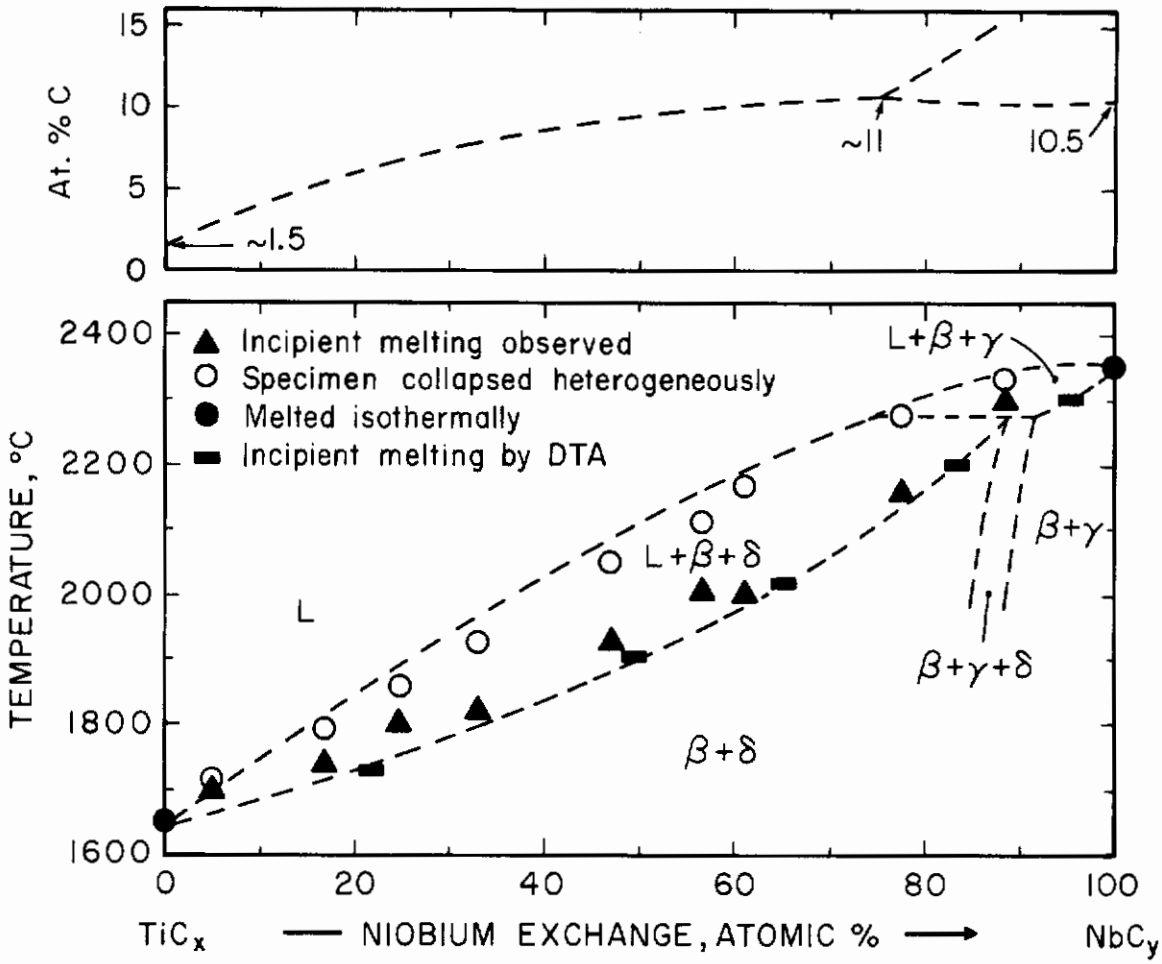

Figure 33. Measured Melting Temperatures of Alloys Located Along the Metal-Rich Eutectic Trough.

(Top: Metallographically Estimated Location of Eutectic Trough)

boundary line occurs two-phased and, as a consequence, the resulting structures remain, even at high quenching rates, coarse and bear little resemblance to eutectics (Figures 34 and 35).

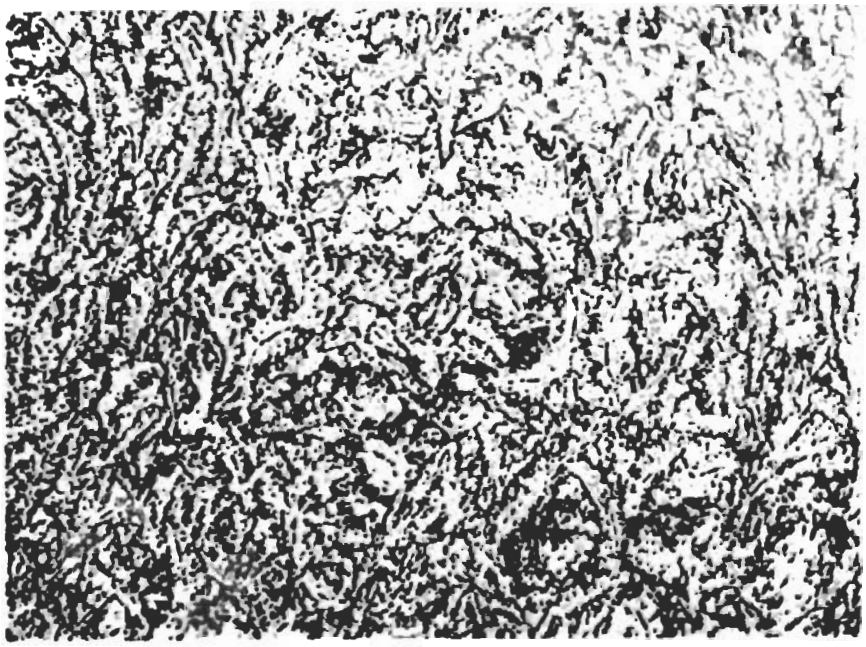

Figure 34. Ti-Nb-C (40-51-9 At.%), Melted and Quenched X760
Bivariantly Solidified Eutectic at the Boundary Line
(Ti,Nb) + (Ti,Nb)C_{1-x}.

The temperature-dependent, metal-rich phase boundary of the monocarbide phase was delineated by a combination of metallographic and X-ray techniques on high temperature equilibrated and quenched alloys. DTA-techniques also proved very useful, mainly because even small amounts of melt formed could be reliably detected. (Figure 36); incipient melting of extremely two-phased melting alloys was usually not detected in the Pirani furnace until temperatures considerably above the solidus were reached.

The solidus envelope of the monocarbide solid solution (Figure 37), at a given metal exchange, indicates an increase in the carbon contents of the ternary alloys with the highest solidus temperatures; thus, while both

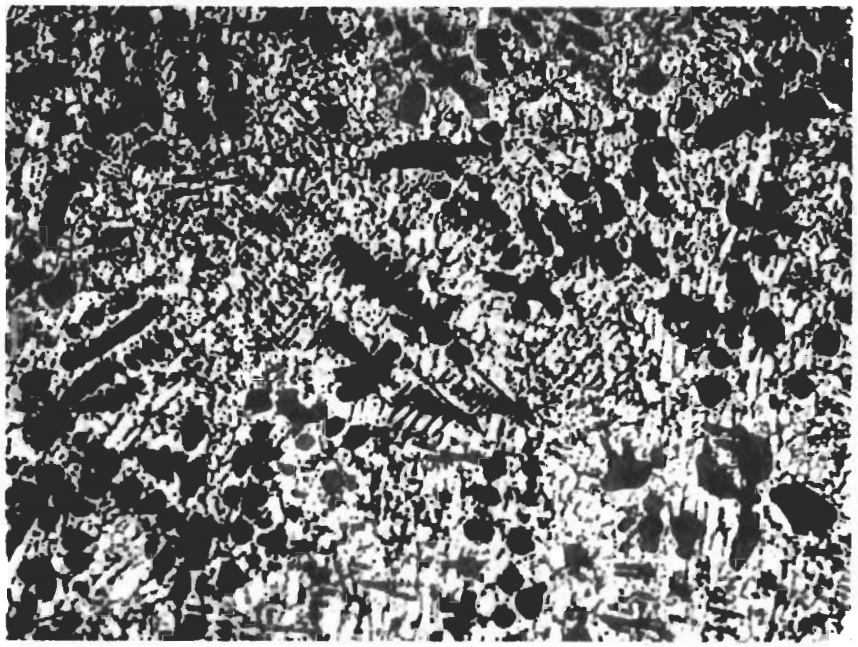

Figure 35. Ti-Nb-C (30-56-14 At.%), Melted and Quenched X680
Primary Monocarbide (Dark Grains) in a Matrix of
(Ti,Nb) + $(Ti,Nb)C_{1-x}$ Eutectic-Like Structure.

binary carbides melt congruently at a carbon content of 44 At.% C, the maximum solidus temperature at a metal-exchange of 50 At.% are observed near 48 At.% C (Figure 38).

Metal precipitation from the substoichiometric (< 38 At.% C) and titanium rich (> 50 At.% Ti) monocarbide solution is comparatively slow and cooling rates exceeding 30° C per second in the critical temperature range from 2300° to 1500° C were, as a rule, found to be sufficient to retain the alloys single-phased to room temperature. Precipitation of metal, and of Nb_2C-phase, in alloys located near the Nb_2C boundary, however, occurs extremely fast, and consequently the high temperature equilibrium states in these alloys difficult to retain (Figure 39). The high temperature phase boundaries and the (temperature dependent) vertex of the three-phase equilibrium (Nb, Ti) + Nb_2C-ss + $(Nb, Ti)C_{1-x}$-ss at the monocarbide phase were therefore located primarily by metallographic inspection of quenched alloys.

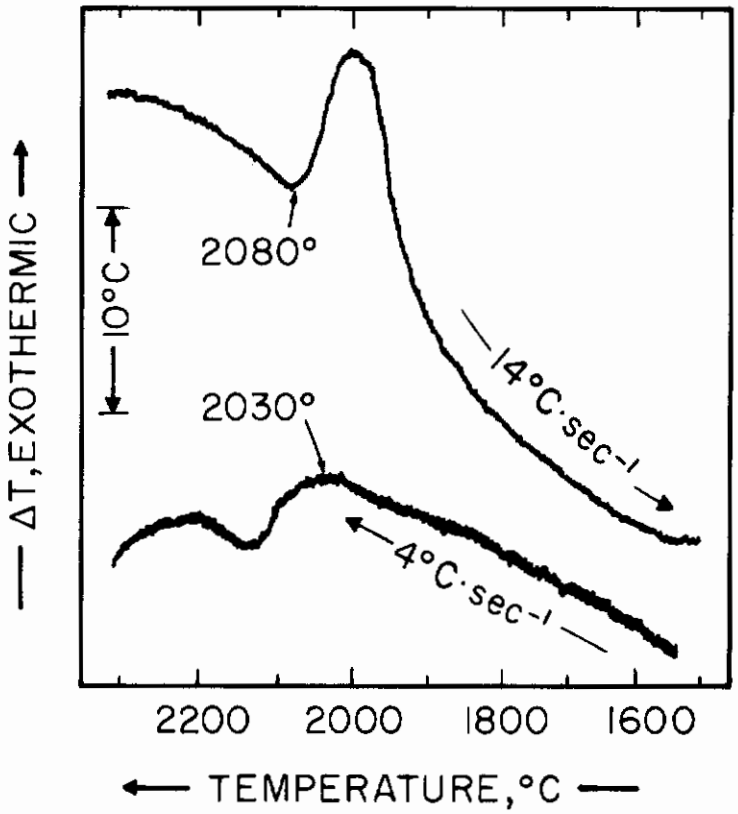

Figure 36. DTA-Thermogram of a Ti-Nb-C (28-47-25 At.%) Alloy Showing Bivariant Melting and Solidification of Metal-Rich Eutectic Alloys.

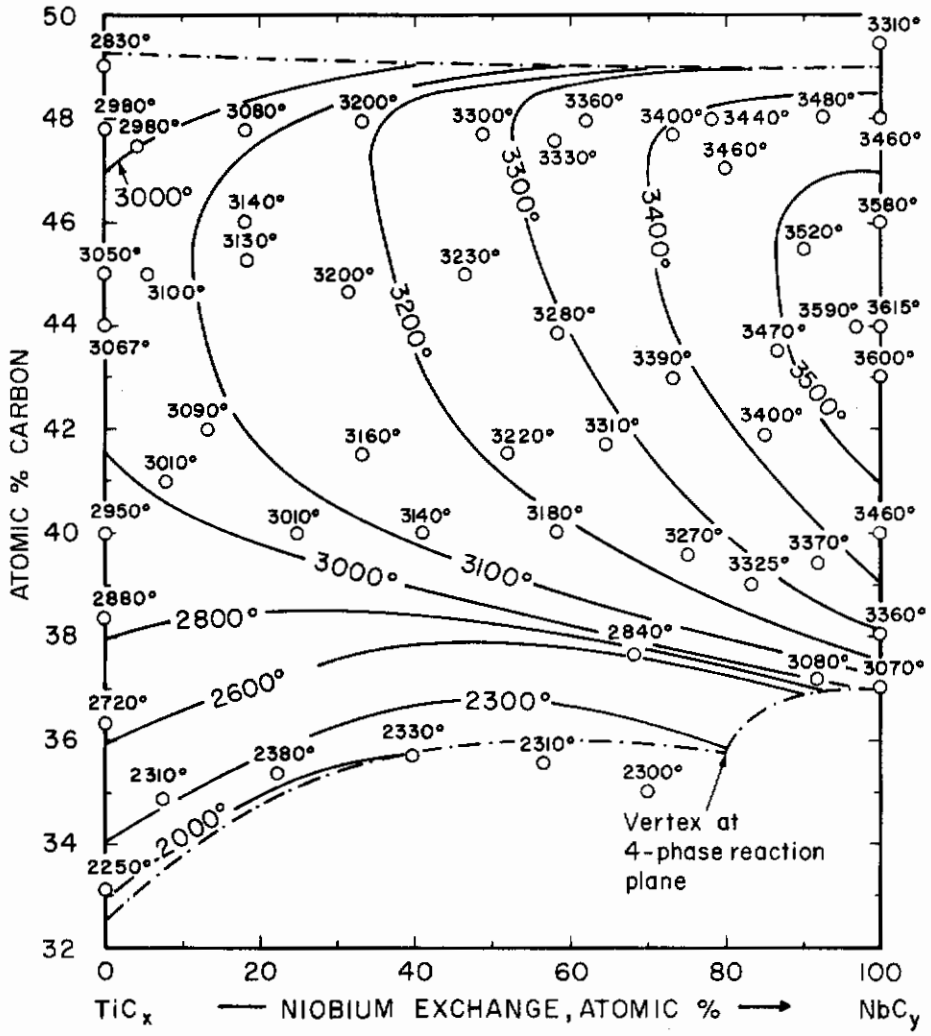

Figure 37. Solidus Temperatures of the Monocarbide $(Ti,Nb)C_{1-x}$, Solid Solution.

Note large scatter of the data for the extremely heterogeneously melting alloys near the metal-rich phase boundary.

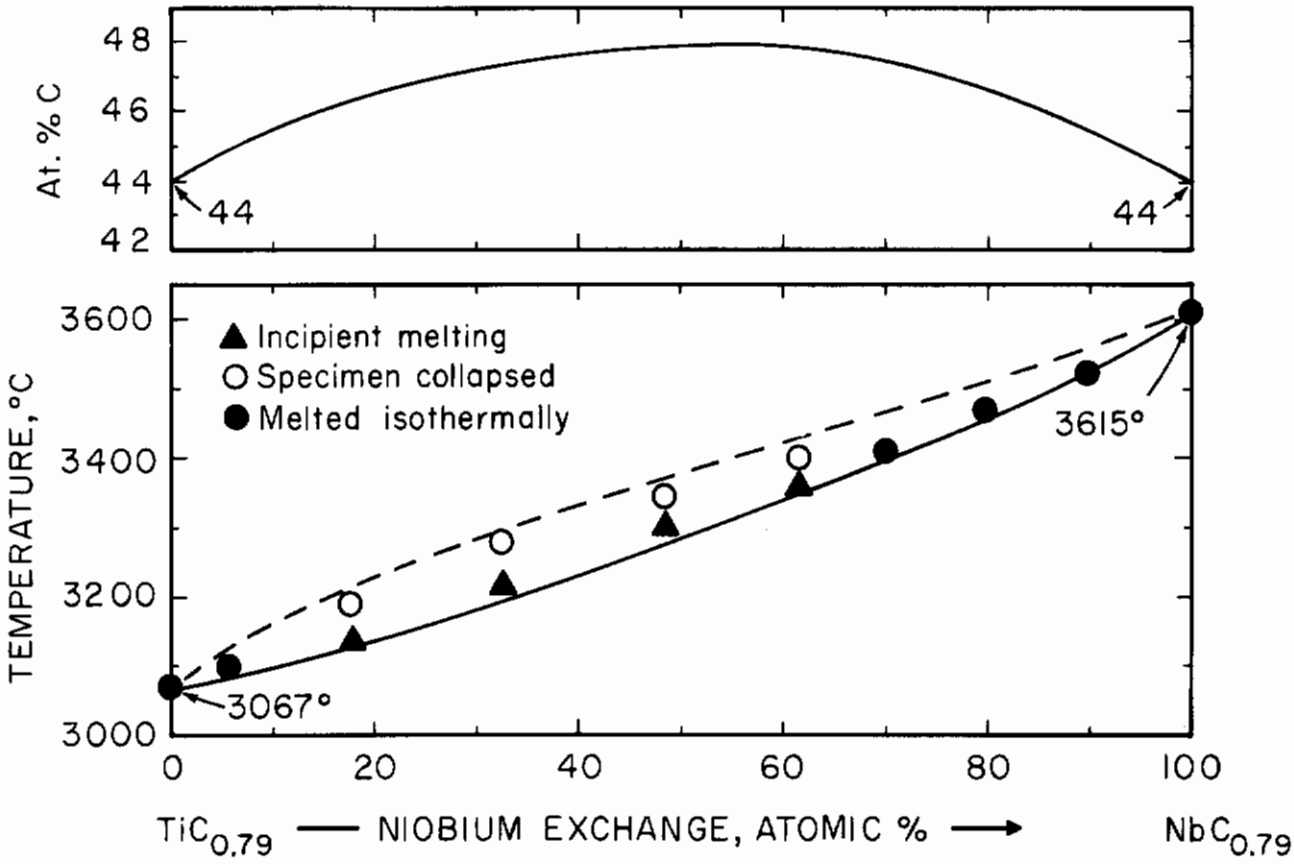

Figure 38. Maximum Solidus Temperatures of the $(Ti,Nb)C_{1-x}$ Solid Solution.

(Top: Locus of Compositions Corresponding to the Maximum Solidus Temperatures).

Figure 39. Ti-Nb-C (13-53-34 At.%), Equilibrated at 2600° C and Rapidly Cooled. X400

Monocarbide with Excess Metal at Grain Boundaries. Note Intragranular Localized Precipitation of Subcarbide During Cooling.

X-Ray: Monocarbide and Small Amounts of Metal and Subcarbide Phase.

The average parameters of the Nb_2C-phase in ternary alloys quenched equilibrated at, and quenched from, 2280° C, the temperature of the four-phase reaction plane

$$L + Nb_2C\text{-ss} \rightleftarrows (Ti,Nb)\text{-ss} + (Ti,Nb)C_{1-x}\text{-ss}$$

were a= 3.086Å and c=4.921Å; Metallographic examination of the alloys indicated this parameter to correspond to a titanium exchange of about 12.5 At.%.

Ternary monocarbide alloys usually were heavily cored, and the X-ray diffraction patterns correspondingly diffuse when cooled rapidly from melting temperatures, but a one- to two-minute equilibration at slightly sub-solidus temperatures proved, as a rule, sufficient, to reestablish homogeneity (Figure 40). The melting temperatures of alloys located along the monocarbide + graphite boundary line (Figure 41), established by direct melting point measurements and, independently by DTA (Figure 42) were found to vary smoothly between those of the binary monocarbide + graphite eutectics. The bivariant solidification along the boundary line as well as the rapid recrystallization of the monocarbide + graphite aggregates resulted in fairly coarse-grained structures (Figure 43). In view of the rather non-characteristic microstructures, the accuracy of the boundary line shown in Figure 41 in terms of the carbon content, is therefore estimated not to be better than ± 2 At.%.

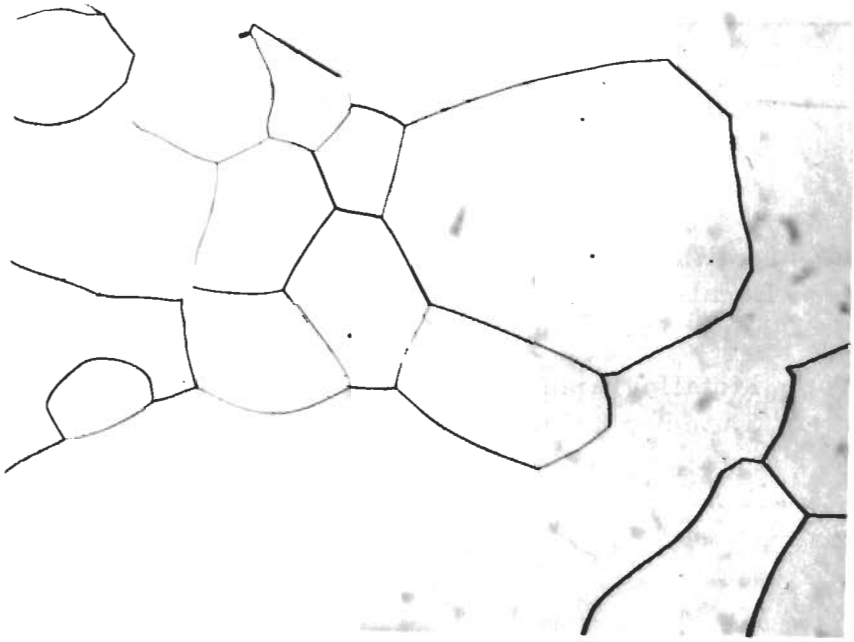

Figure 40. Ti-Nb-C (5-47-48 At.%), Melted, Reequilibrated for 1 Minute at 3300°C, and Cooled. X190

Homogeneous Monocarbide Alloy.

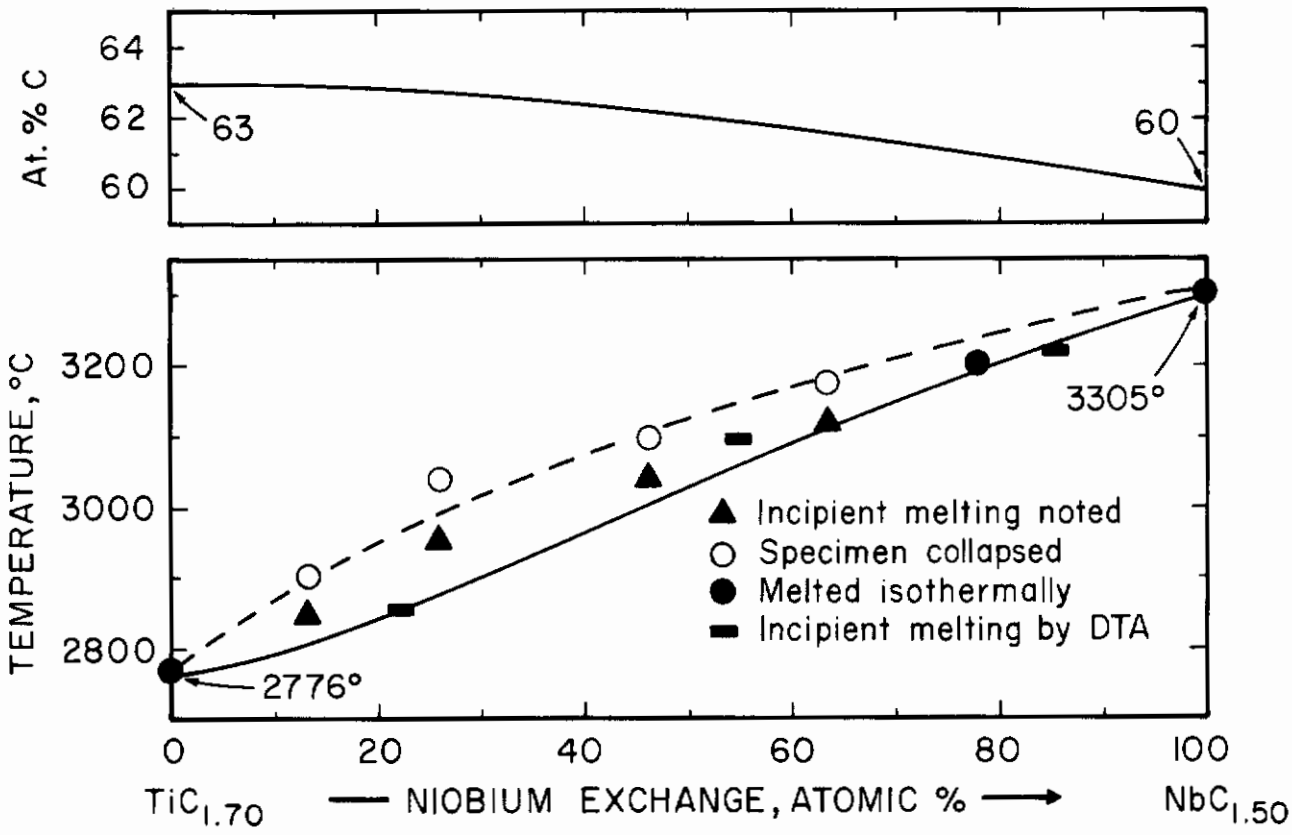

Figure 41. Melting Temperatures of Ti-Nb-C Alloys Located Along the Monocarbide + Graphite Eutectic Trough.

Top: Metallographically Estimated Location of Eutectic Trough.

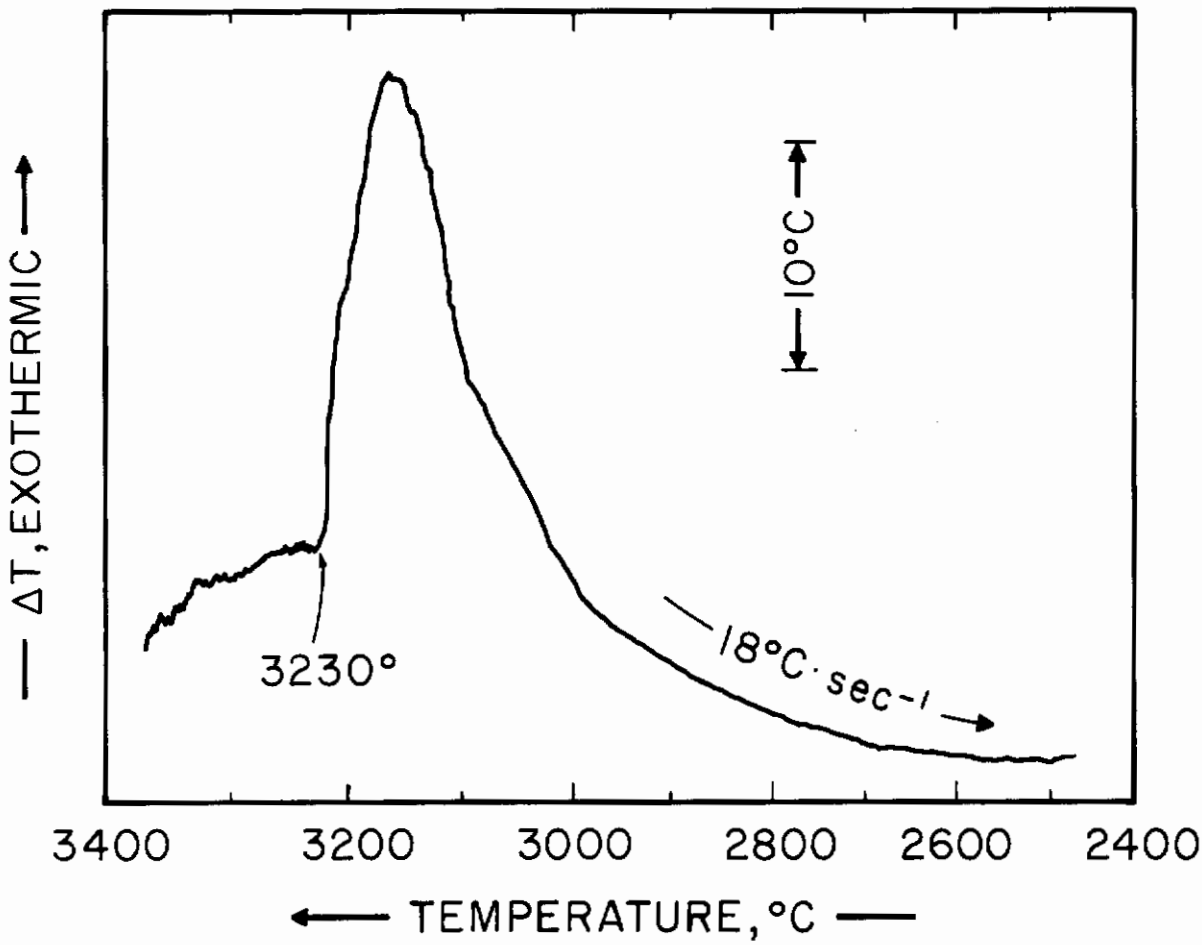

Figure 42. Solidification of the Bivariant (Nb, Ti)C + C Eutectic in a Ti-Nb-C (7-38-55 At.%) Alloy.

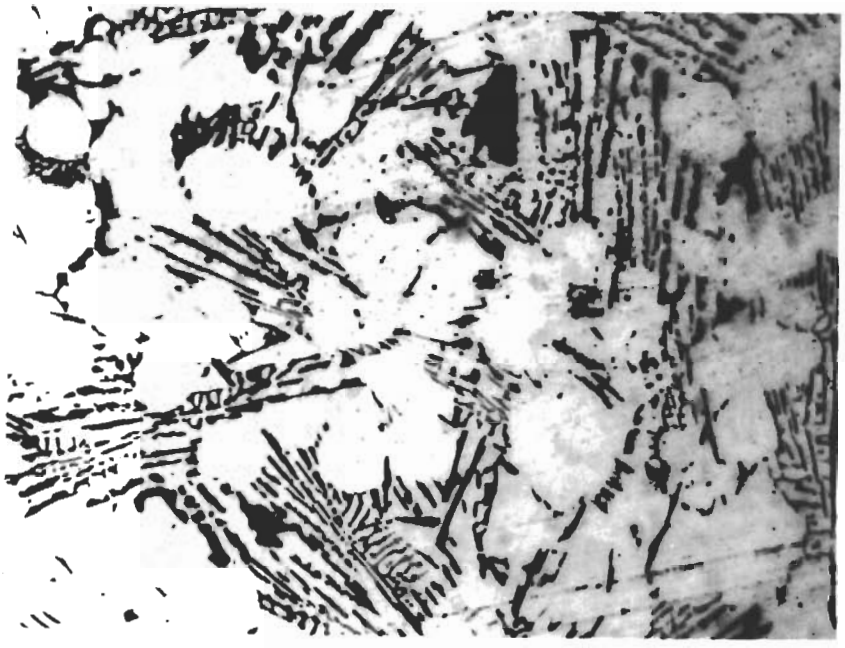

Figure 43. Ti-Nb-C (9-35-56 At.%), Melted and Rapidly Cooled. X375

Primary Monocarbide in a Partially Recrystallized (Ti,Nb)C + C Bivariant Eutectic.

The experimental data gained through isothermal phase, melting point, and DTA studies have been combined to yield the phase diagram shown in Figure 1. To facilitate use of the phase diagram data, a number of isothermal reactions were prepared from the available information and are presented in Figures 44 through 49; the isotherms are supplemented by two concentration sections, $Ti_{0.5}Nb_{0.5}$-C and $TiC_{0.5}$-$NbC_{0.5}$, which are shown in Figures 50 and 51.

C. Ti-Ta-C SYSTEM

The gross features of the phase diagram of the system below 2000° C, determined by a reevaluation of the samples used in the previous work[1] as well as by additional specimens agree reasonably well with the previous findings (Figures 52 through 55).

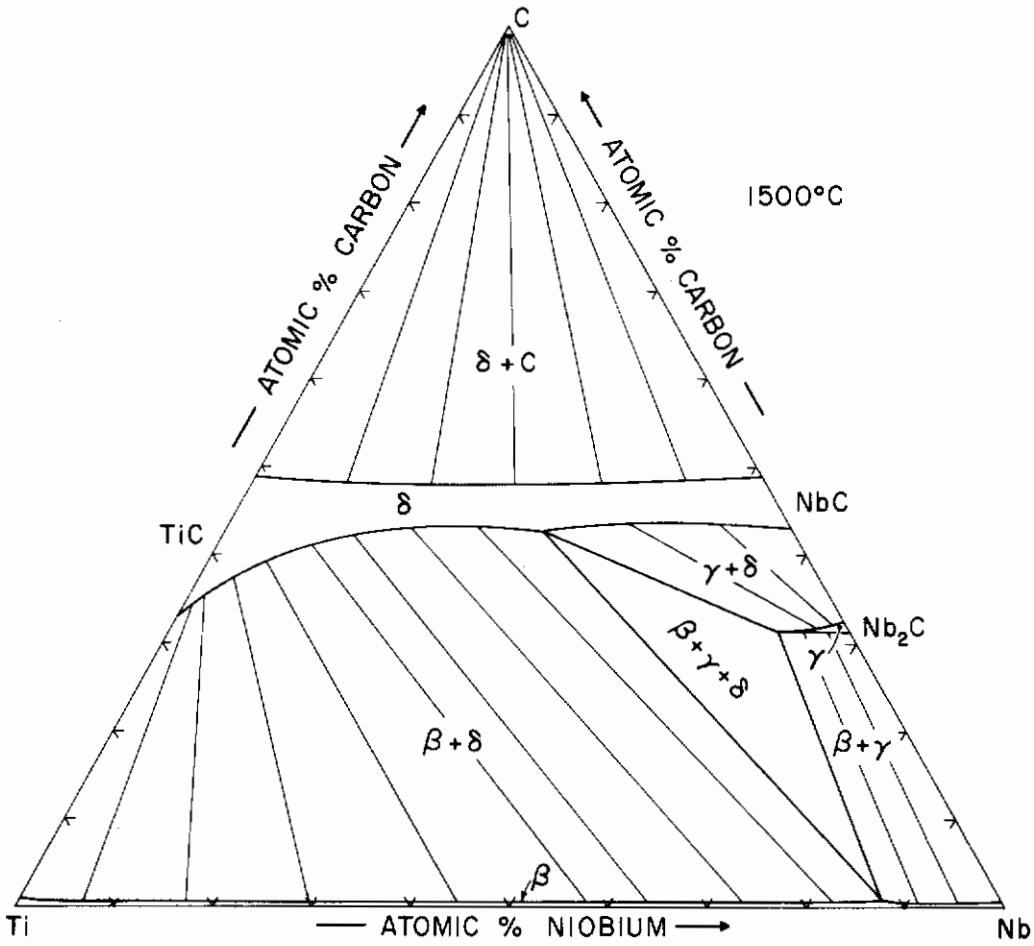

Figure 44. Isothermal Section of the Ti-Nb-C System at 1500° C.

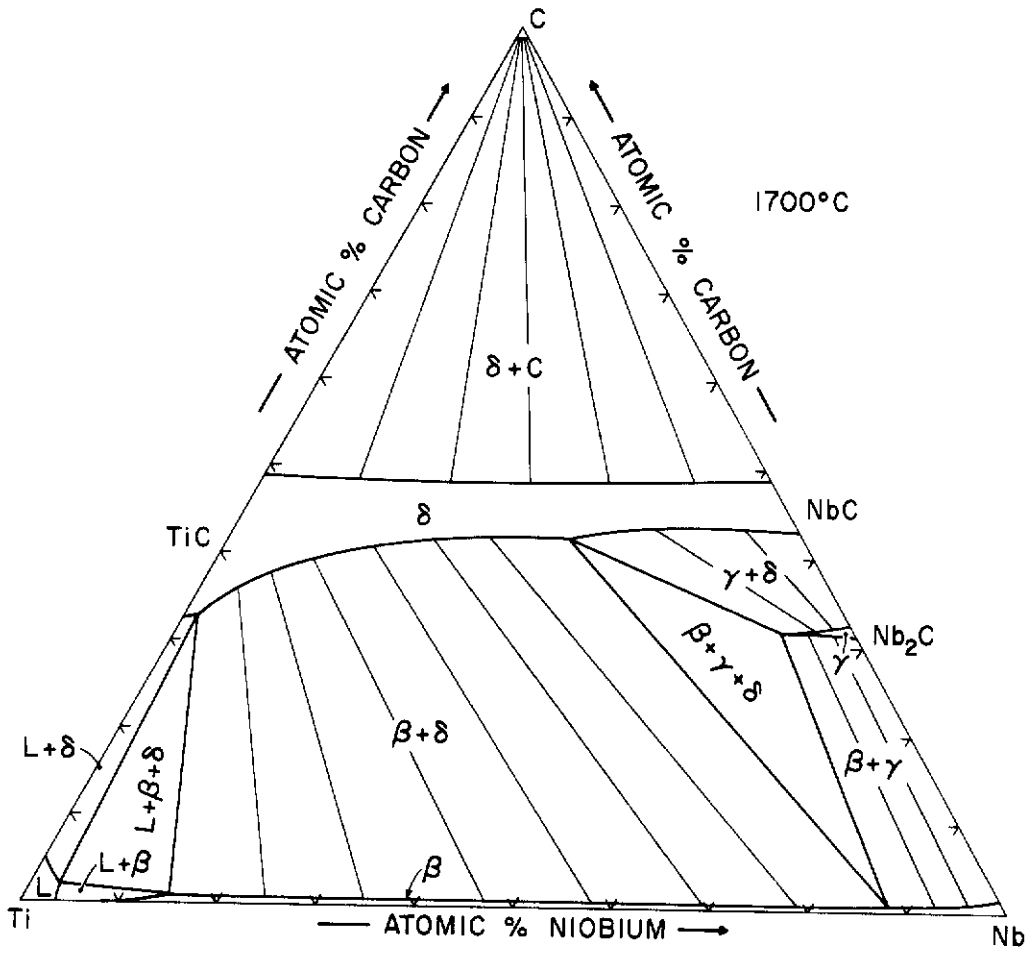

Figure 45. Isothermal Section of the Ti-Nb-C System at 1700°C.

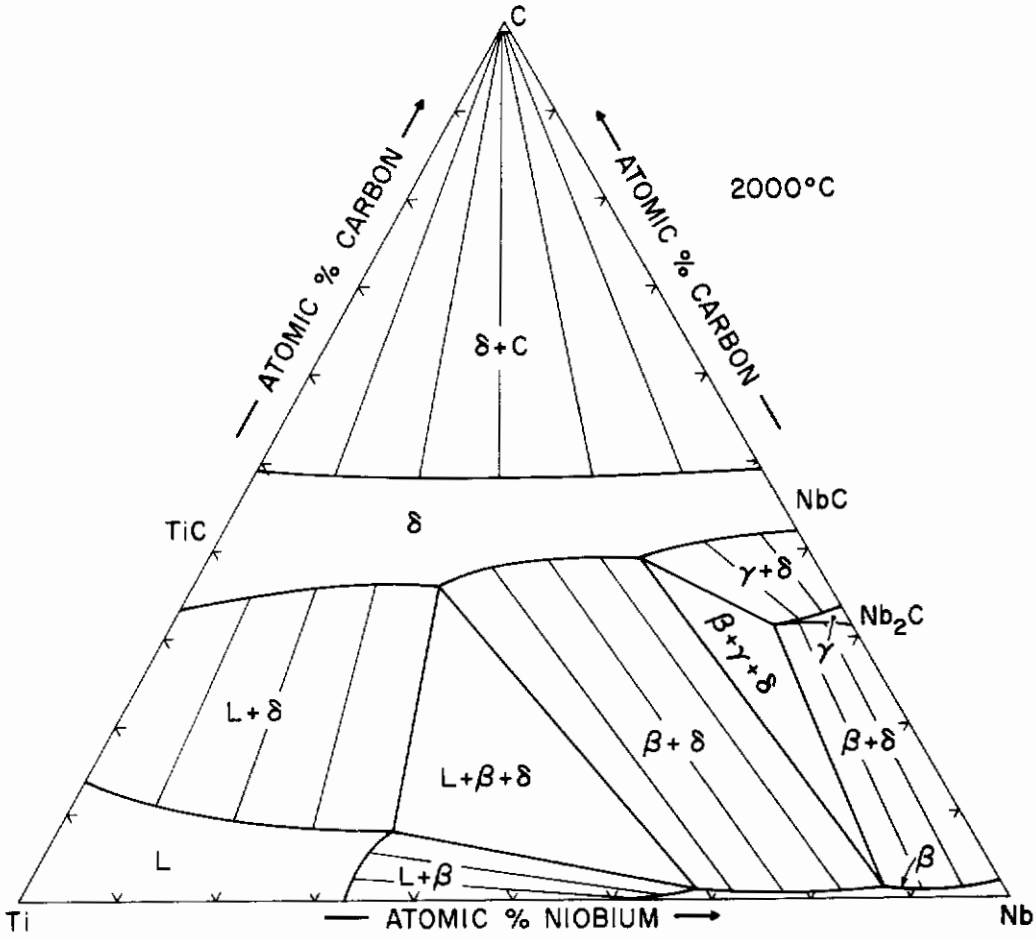

Figure 46. Isothermal Section of the Ti-Nb-C System at 2000°C.

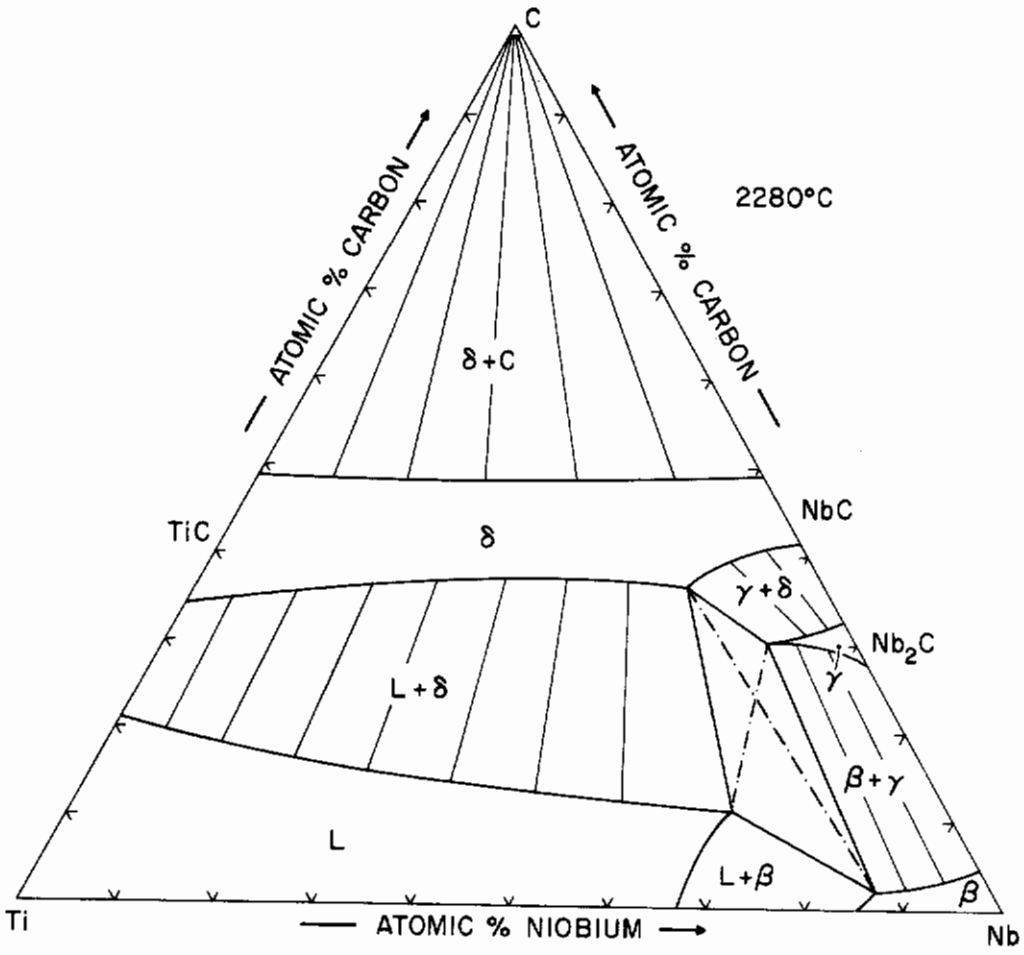

Figure 47. Isothermal Section of the Ti-Nb-C System at 2280°C.

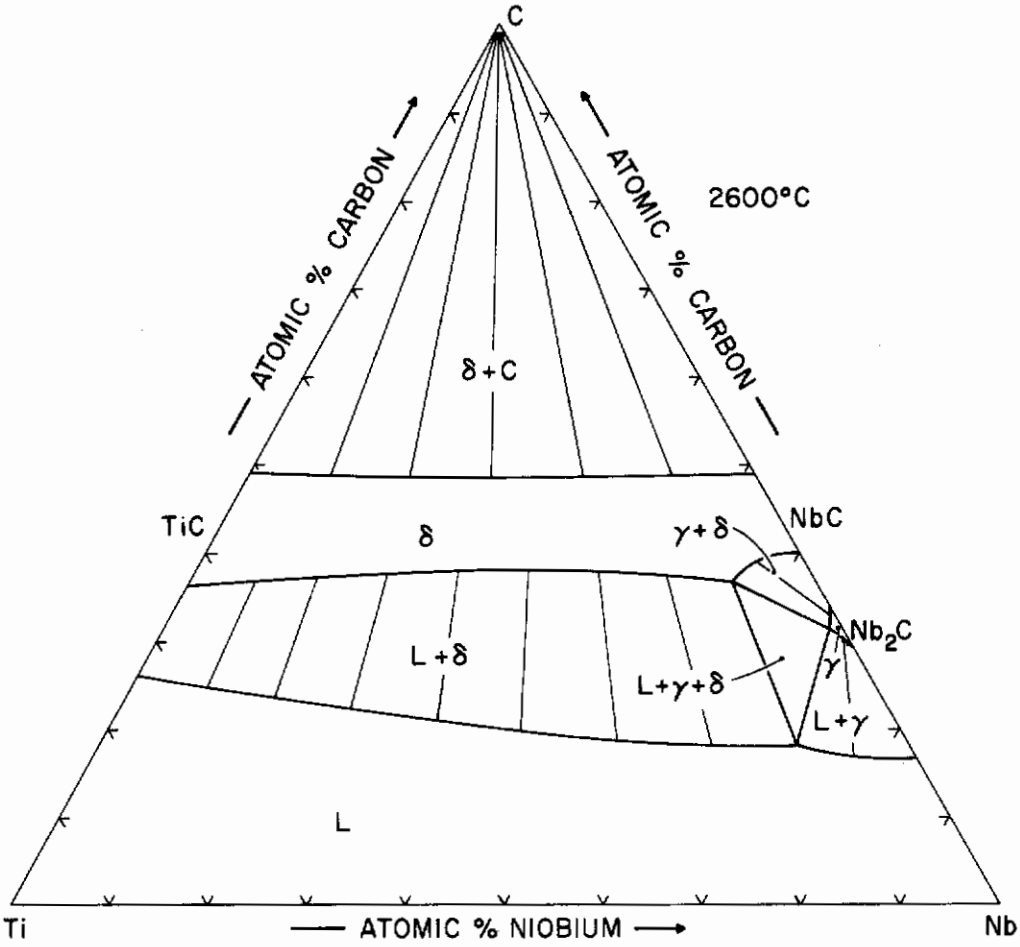

Figure 48. Isothermal Section of the Ti-Nb-C System at 2600° C.

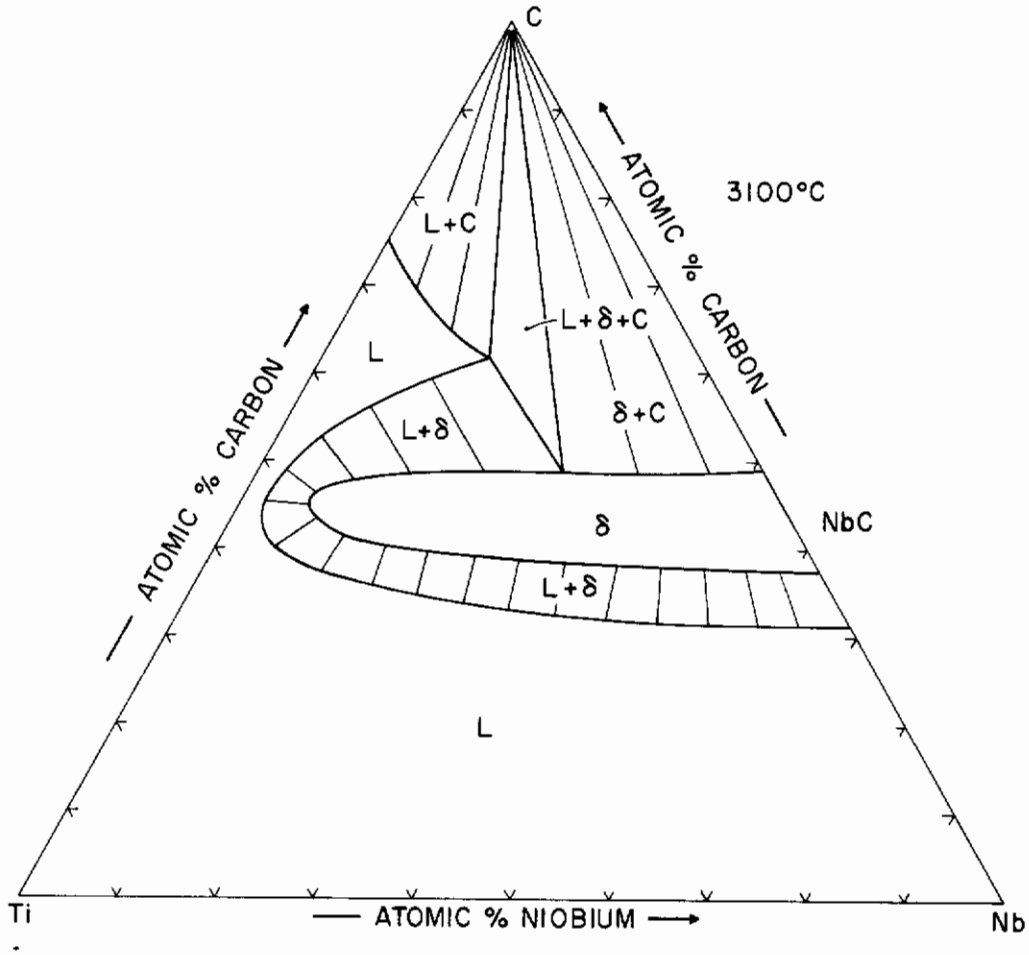

Figure 49. Isothermal Section of the Ti-Nb-C System at 3100° C.

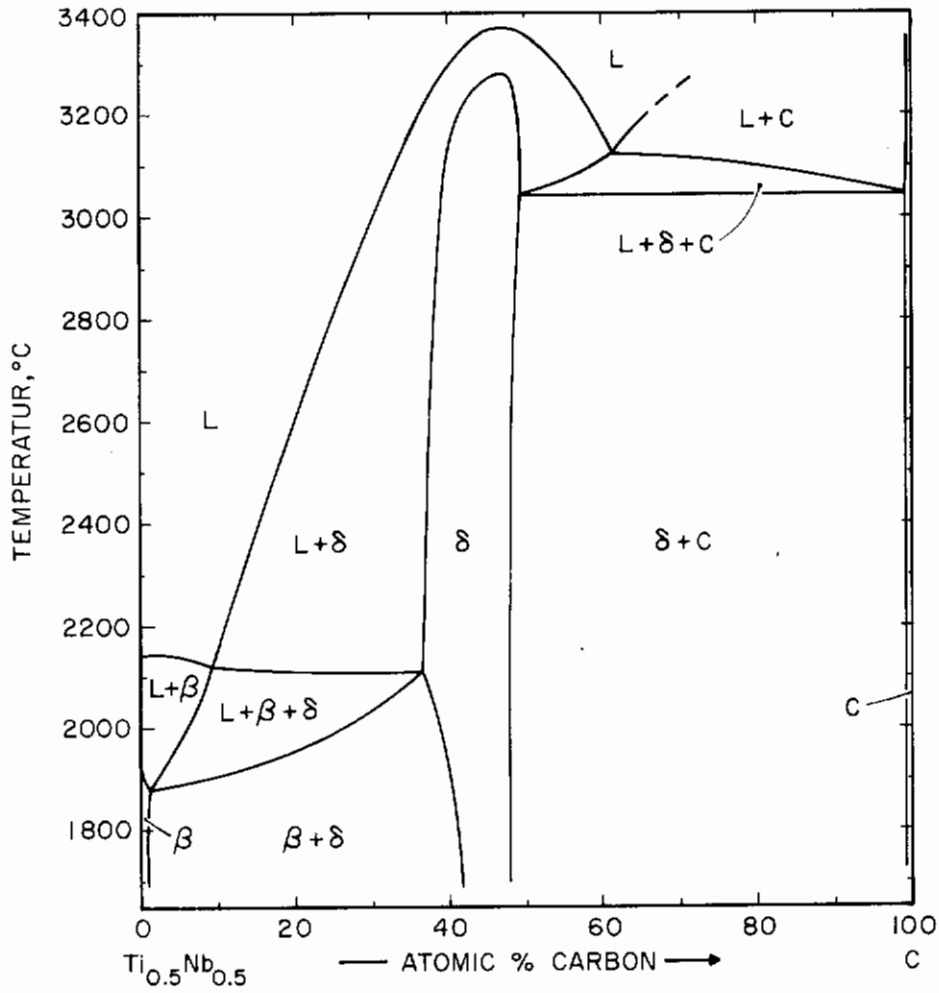

Figure 50. Isopleth $Ti_{0.5}Nb_{0.5}$-C.

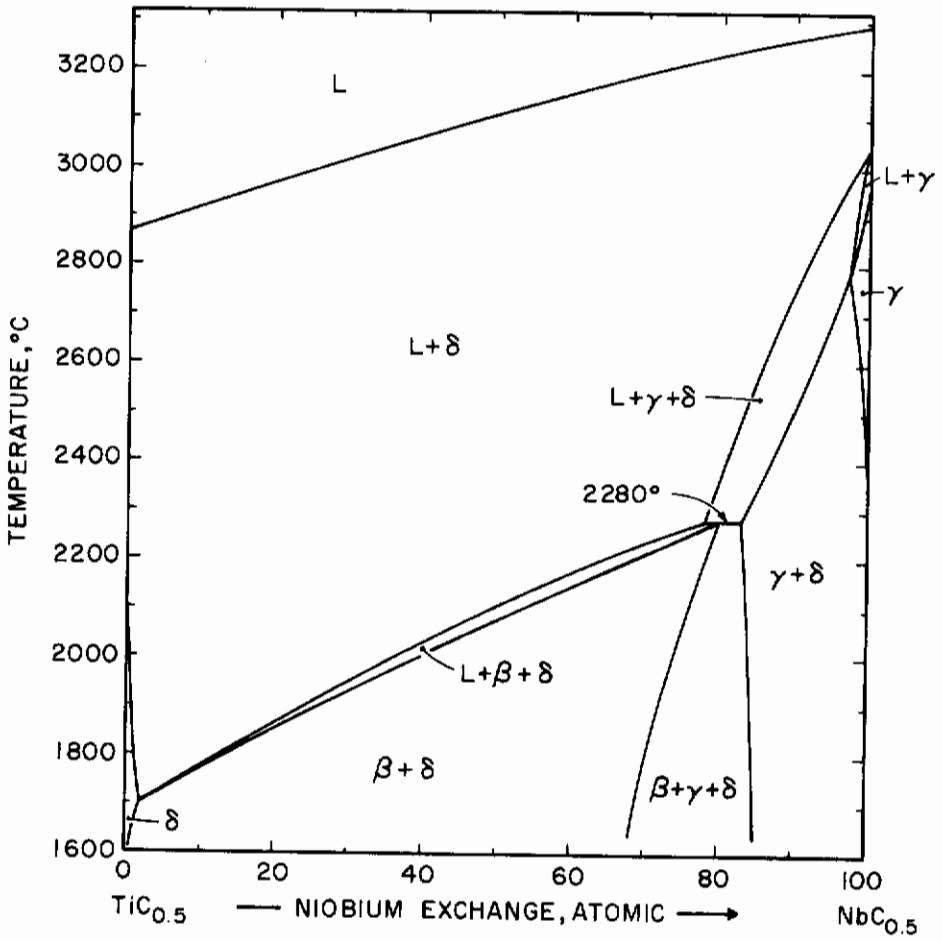

Figure 51. Isopleth $TiC_{0.5}$-$NbC_{0.5}$

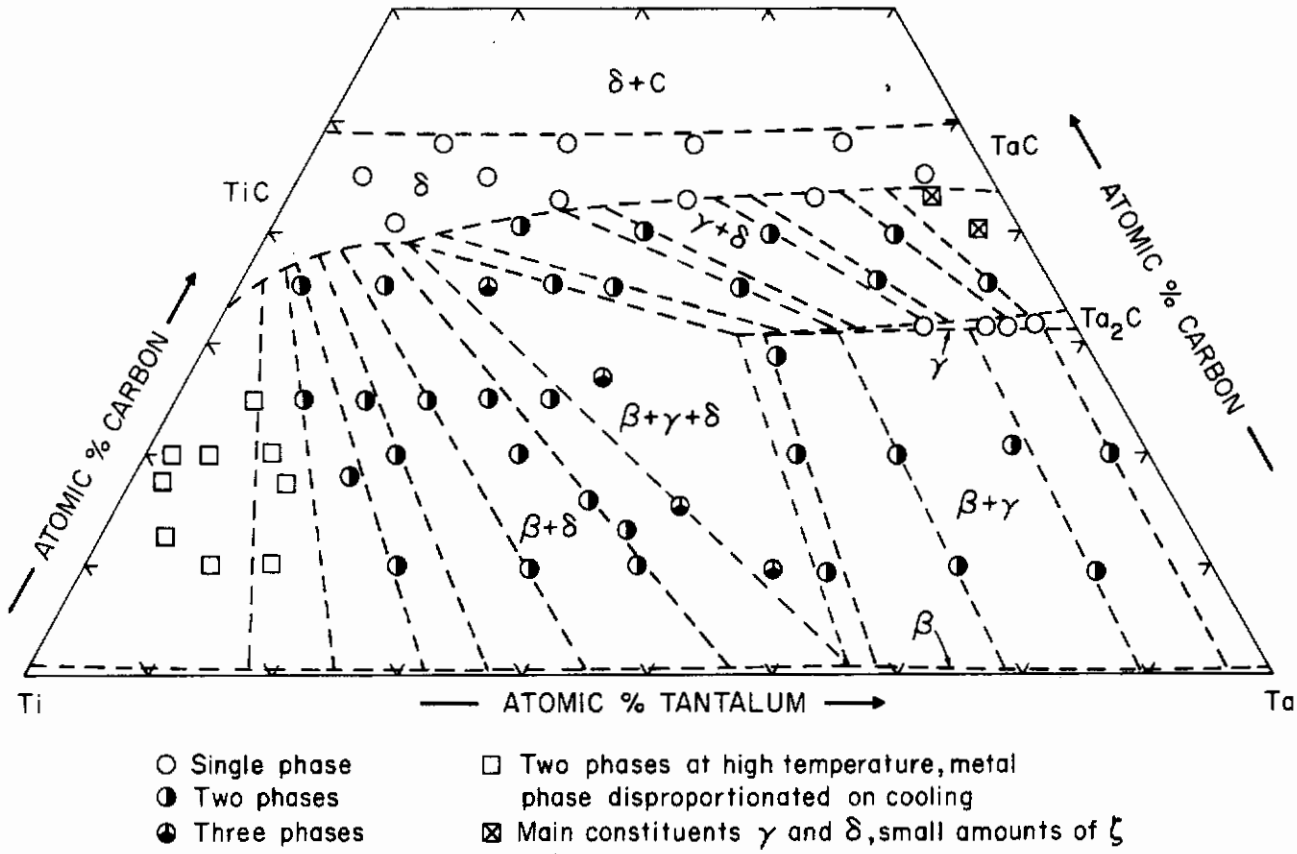

Figure 52. Sample Location and Qualitative (X-ray) Phase Evaluation of the Alloy Series Equilibrated at 1500°C.

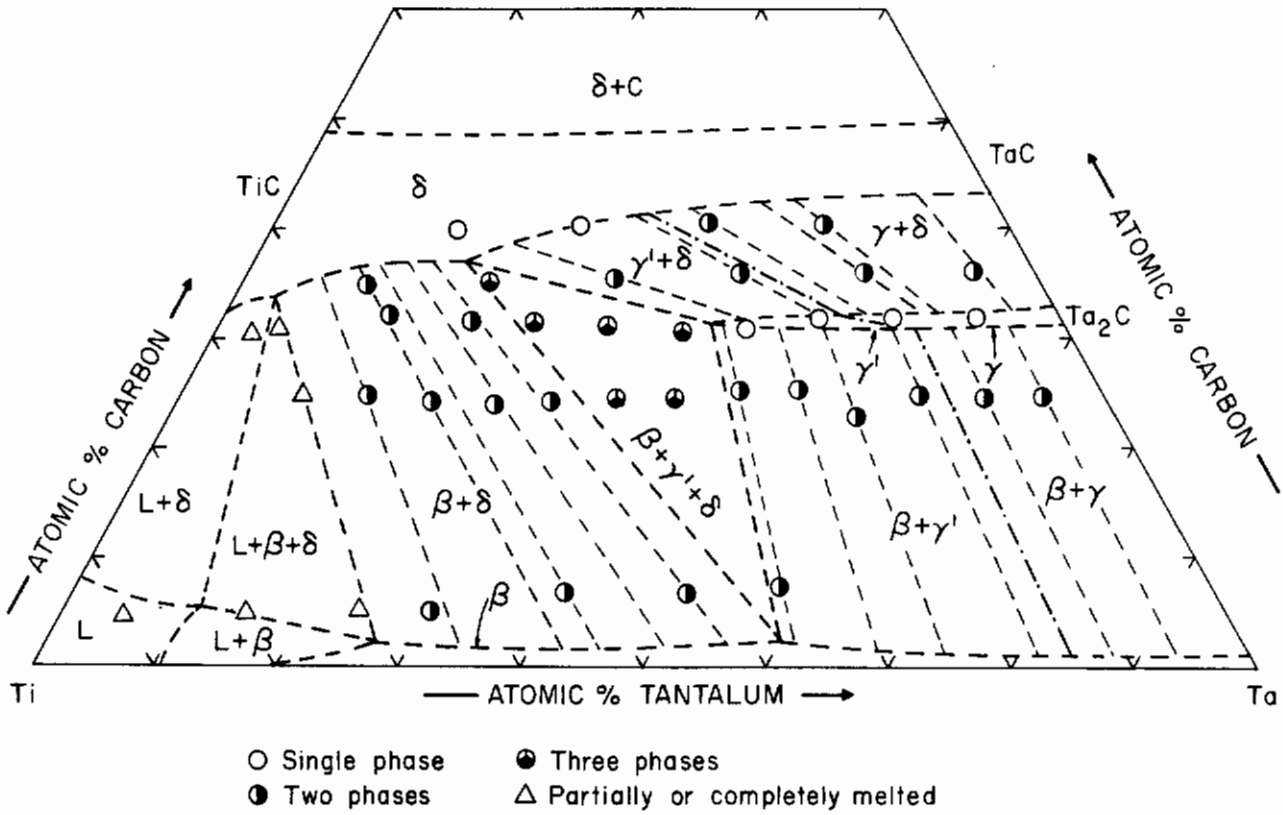

Figure 53. Sample Location and Qualitative Phase Evaluation of the Alloy Series Equilibrated at 1800°C.

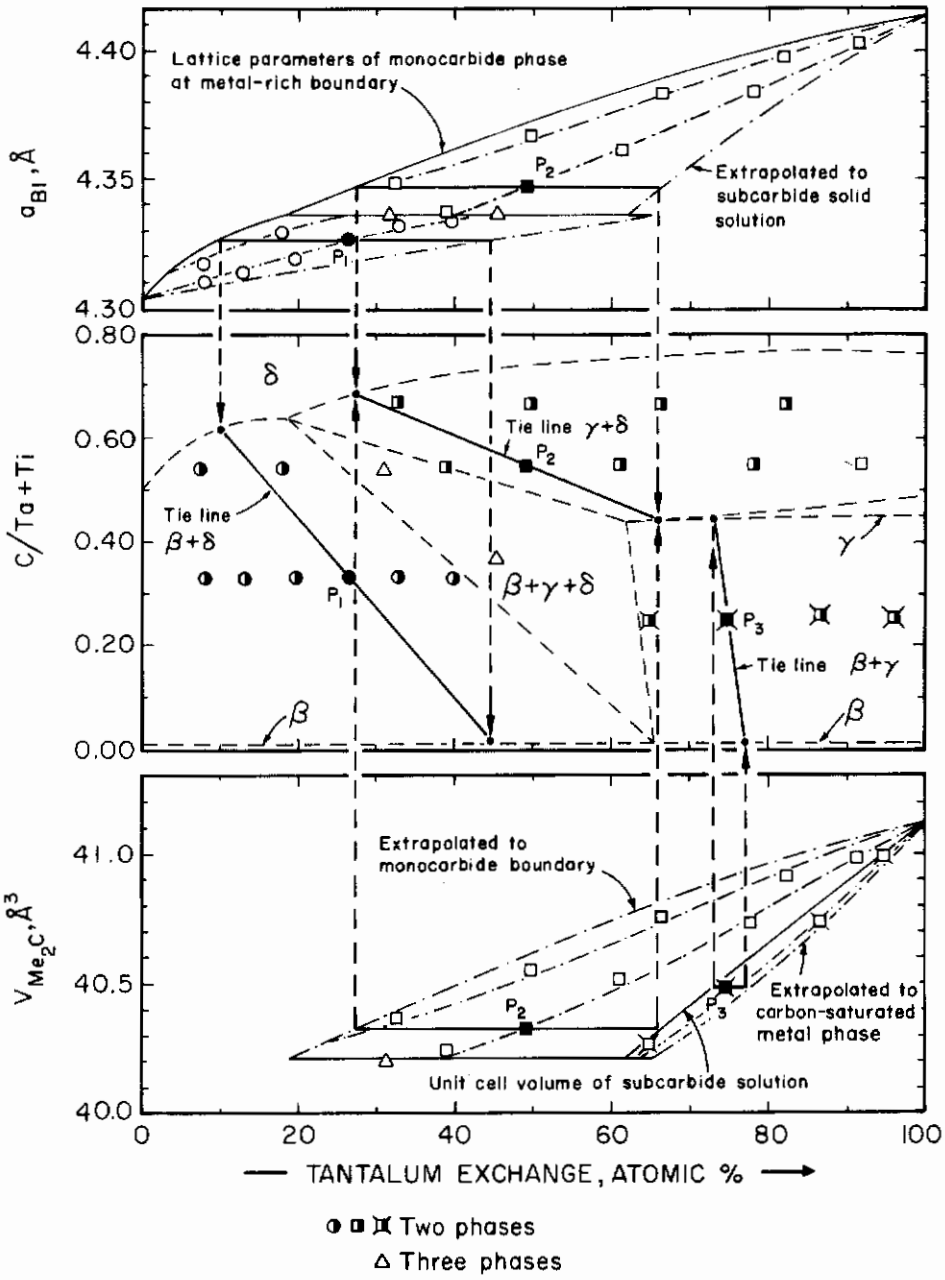

Figure 54. Measured Lattice Parameters for Two- and Three-Phased Ti-Ta-C, Graphical Smoothing of the Tie Lines, and Determination of the Tie Line Distribution in the Two-Phase Fields β + δ, β+ γ, and γ + δ.

(Alloys Equilibrated at 1500° C)

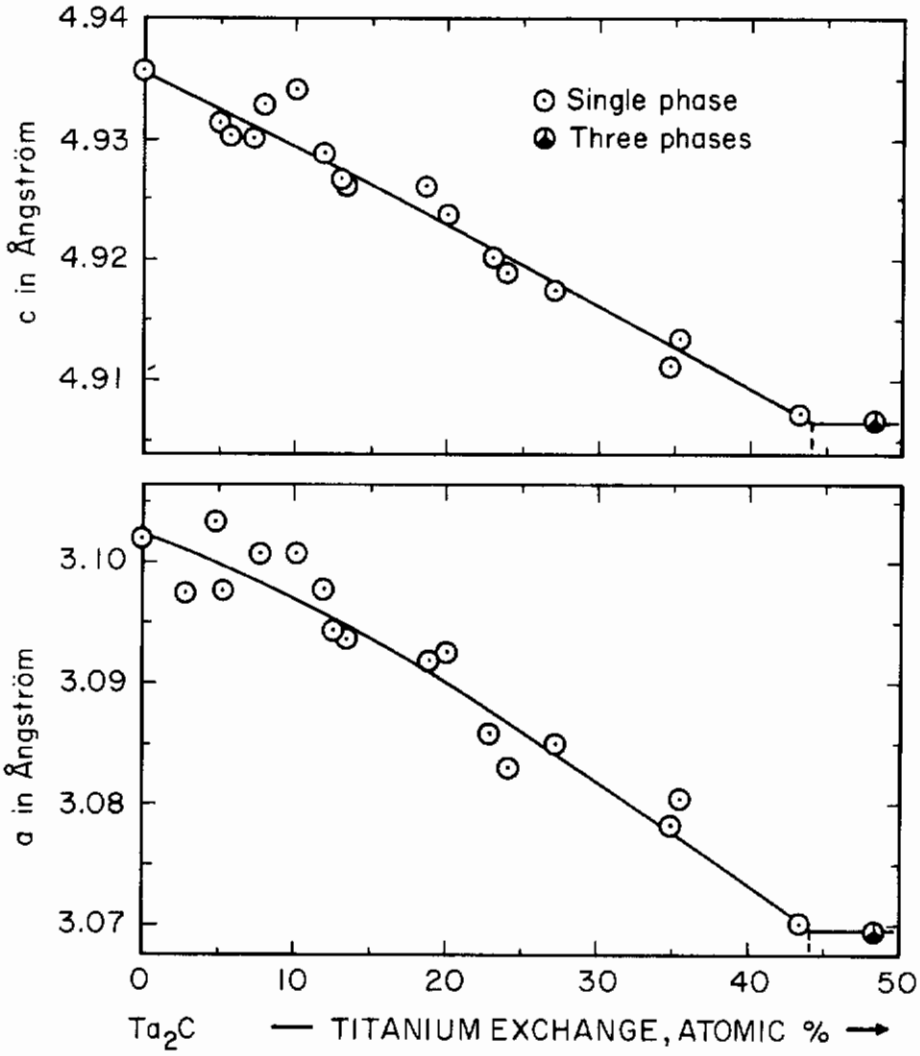

Figure 55. Lattice Parameters of the $(Ti, Ta)_2C$ Solid Solution at 31 to 32 At.% Carbon.

(Alloys Equilibrated at 2000° C)

A very interesting behavior was found in the study of the order-disorder transition of the subcarbide solid solution. Experiments carried out on nearly stoichiometric (32.5 - 33 At.%) alloys revealed a decrease of the transformation temperatures from about 2200° C for the binary phase, to temperatures around 1600° C at the terminal solid solution (Figure 56). Measurements on the substoichiometric carbide yielded a similar variation (Figures 57,58), although the temperature at the equivalent metal exchange are somewhat lower than in the stoichiometric phase. In alloys with excess monocarbide (36 At.% C) a drop from approximately 2020° C at the eutectoid (pseudomonotectoid) isotherm in the binary, to about 1800° C at an apparent titanium exchange of 45 At.% was observed. Correcting the apparent composition with the aid of the tie lines distribution in the two-phase field $Me_2C + MeC_{1-x}$, one finds that at titanium exchanges larger than 11 At.% C the effective transformation temperatures agree closely with those observed in the stoichiometric carbide. No specific discontinuity or break was found at the crossover point of the transformation temperature – concentration curves in the alloy series at 33 and 36 At.% C (Figure 58). Furthermore, the disproportionation of the disordered Me_2C-phase into an ordered substoichiometric alloy and a hyperstoichiometric, disordered phase, which results in a mottled appearance of the sublattice grains, was not observed at titanium exchanges larger than about 10 At.%. From the DTA-data and the results gained by the metallographic studies, the following reaction mechanism concerning the order-disorder transformation of the ternary $(Ti,Ta)_2C$ phase was found to agree best with the experimental observations.

At substoichiometric (<32.5 At.%) compositions the order-disorder transition in the binary Ta_2C phase and in the ternary $(Ti,Ta)_2C$ solid solution proceeds as a homogeneous reaction i.e. no two-phase range is traversed on heating or cooling through the critical temperature range.

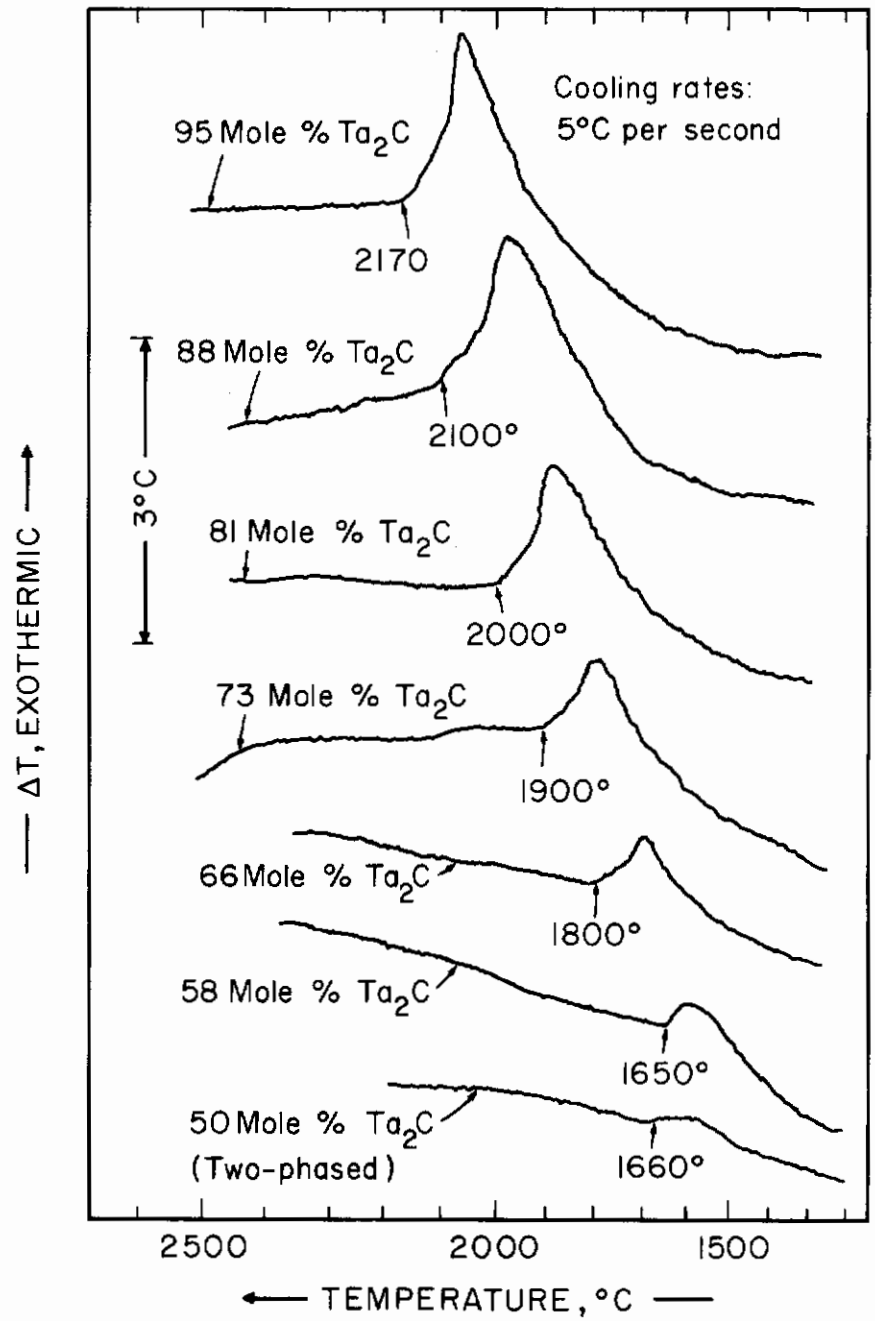

Figure 56. DTA-Thermograms (Cooling), Showing the Order-Disorder Transition in the Primary Ta_2C Phase and in the Ternary $(Ti, Ta)_2C$ Solid Solution. (32.5-33 At.% C).

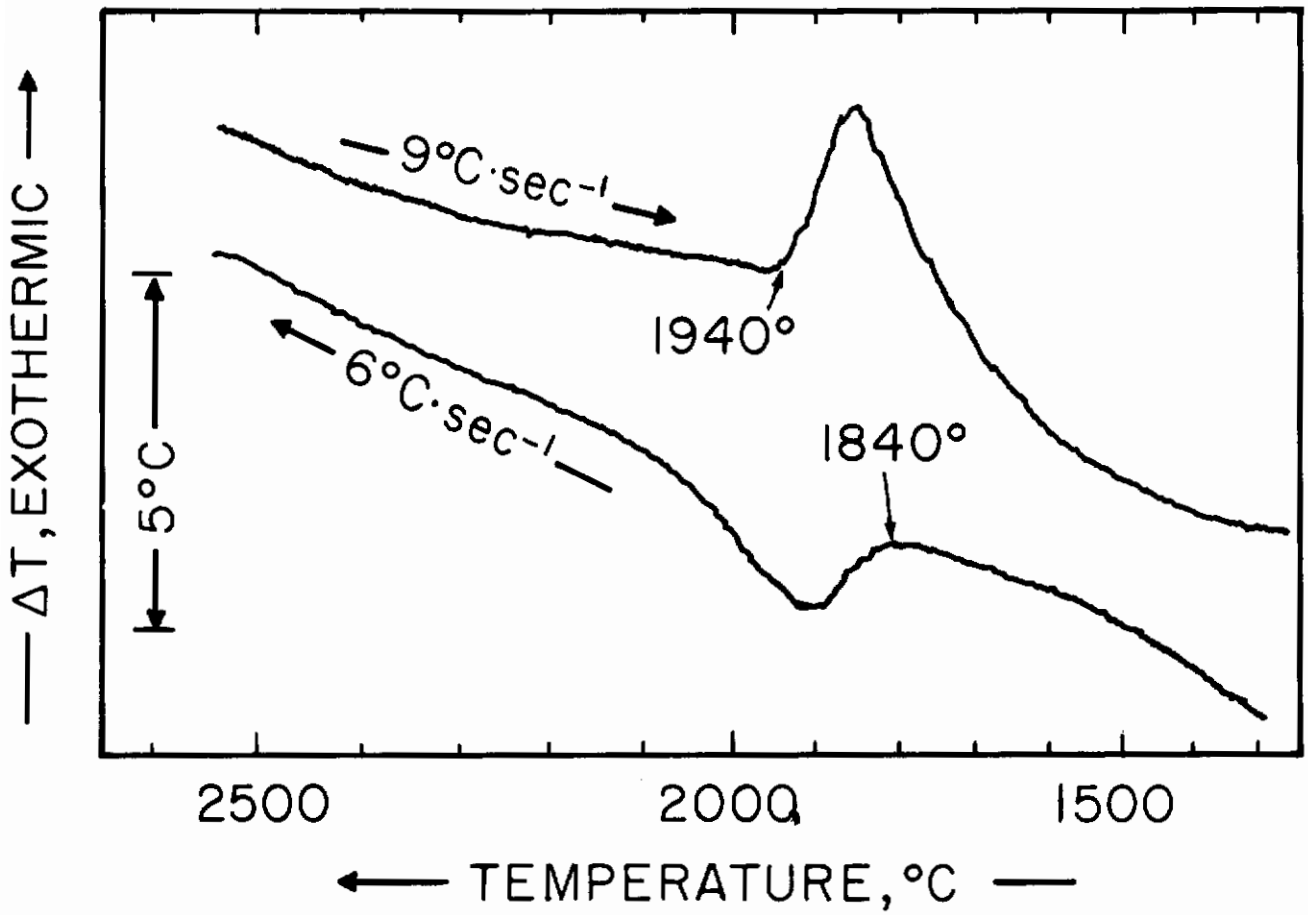

Figure 57. DTA-Thermogram of a Ti-Ta-C (9-63-28 At.%) Alloy, Showing the Order-Disorder Transition in the Substoichiometric $(Ti,Ta)_2C$ Phase.

(Temperatures in Figure refer to Independent Pyrometric Control Measurements).

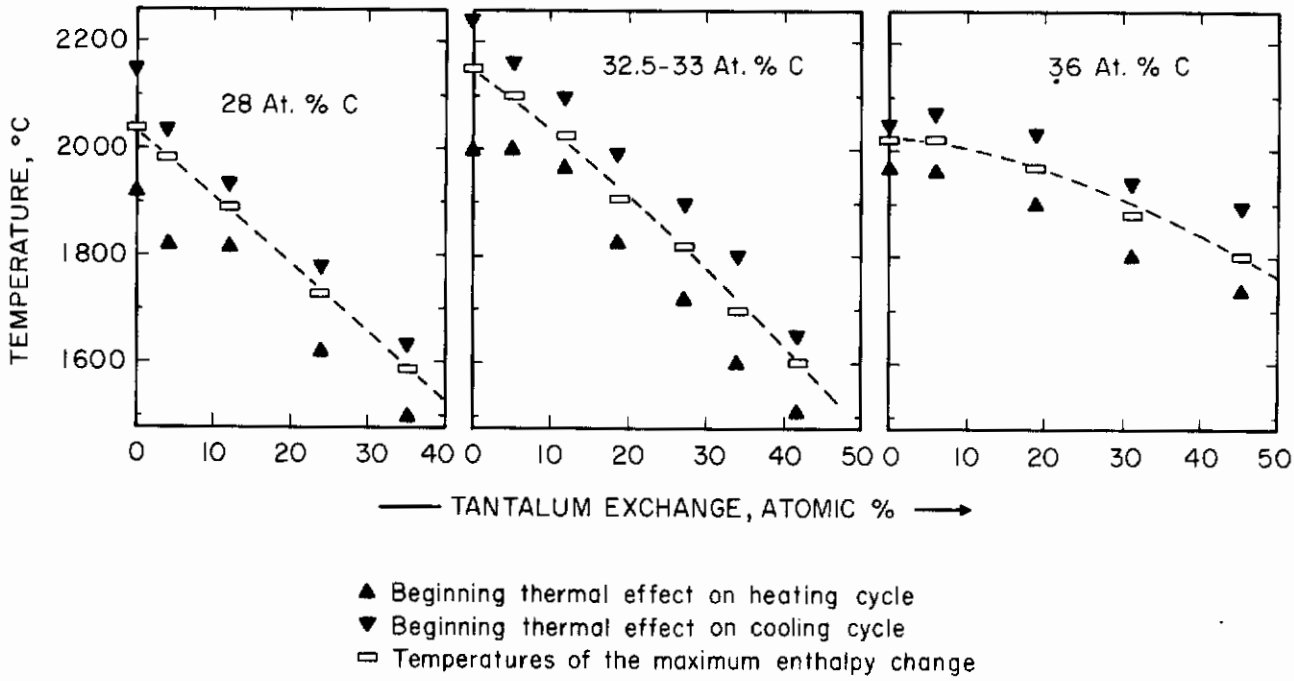

Figure 58. Experimental Order-Disorder Transition Temperatures of the $(Ta, Ti)_2C$-Phase in Samples with Different Carbon Contents.

Substitution of titanium in Ta_2C causes the carbon-rich boundary of the Me_2C-phase to retract to metal-richer compositions, while also lowering the transition temperatures. At an exchange of about 11 At.% Ti, the boundary composition is sufficiently low in carbon so that the heterogeneous ordering reaction ceases to exist[25]. This means, however, that the three-phase equilibrium Me_2C (Ord.) + Me_2C (disord) + MeC_{1-x}, which originates at the eutectoid (pseudomonotectoid) reaction isotherm at 2020° C in the Ta-C binary, vanishes in the ternary. Since no other three-phase equilibria occur in this composition and temperature range, the most likely mechanism leading to a termination of the heterogeneous transition in the ternary is a limiting tie line formed by a degeneration of this single three-phase equilibrium. The temperature sequence of equilibria is shown diagrammatically in Figure 59.

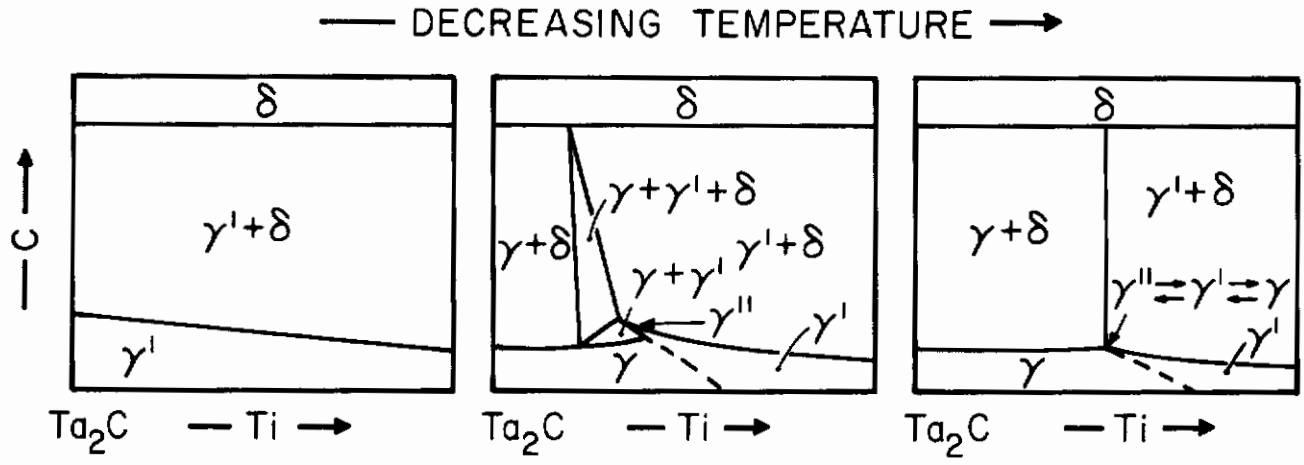

Figure 59. Ti-Ta-C: Diagrammatic Presentation of the Continuation of the Heterogeneous α-β-Ta_2C Phase Transition into the Ternary.

γ' ... Disordered Me_2C-phase

γ ... Ordered Me_2C-phase

δ ... Monocarbide Solid Solution

Measured lattice parameters for carbon-deficient monocarbide alloys, together with derived isoparametric lines, are shown in Figure 60. The parameters obtained for the carbon-saturated solid solution were in good agreement with the numerous measurements reported in the literature (Figure 61).

The melting temperatures of alloys located along the metal-rich eutectic trough vary continuously between the binary, Ti + TiC_{1-x} and Ta + Ta_2C, eutectic temperatures (Figure 62). The boundary lines metal + mono(sub)carbide were derived by microscopic inspection of the as-melted and quenched alloys (Figure 63). A summary of the experimental data obtained

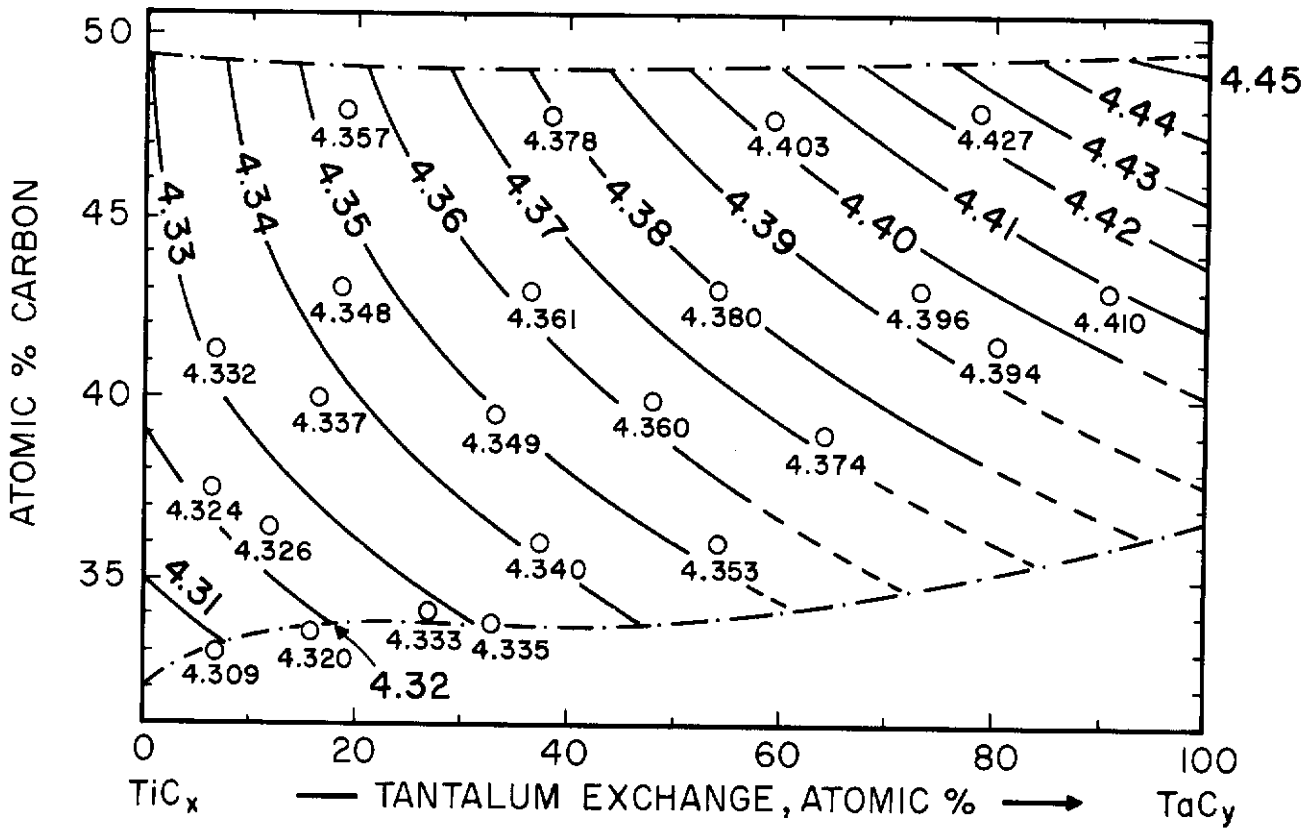

Figure 60. Measured Lattice Parameters and Isoparametric Lines for the (Ti, Ta)C_{1-x} Solid Solution.

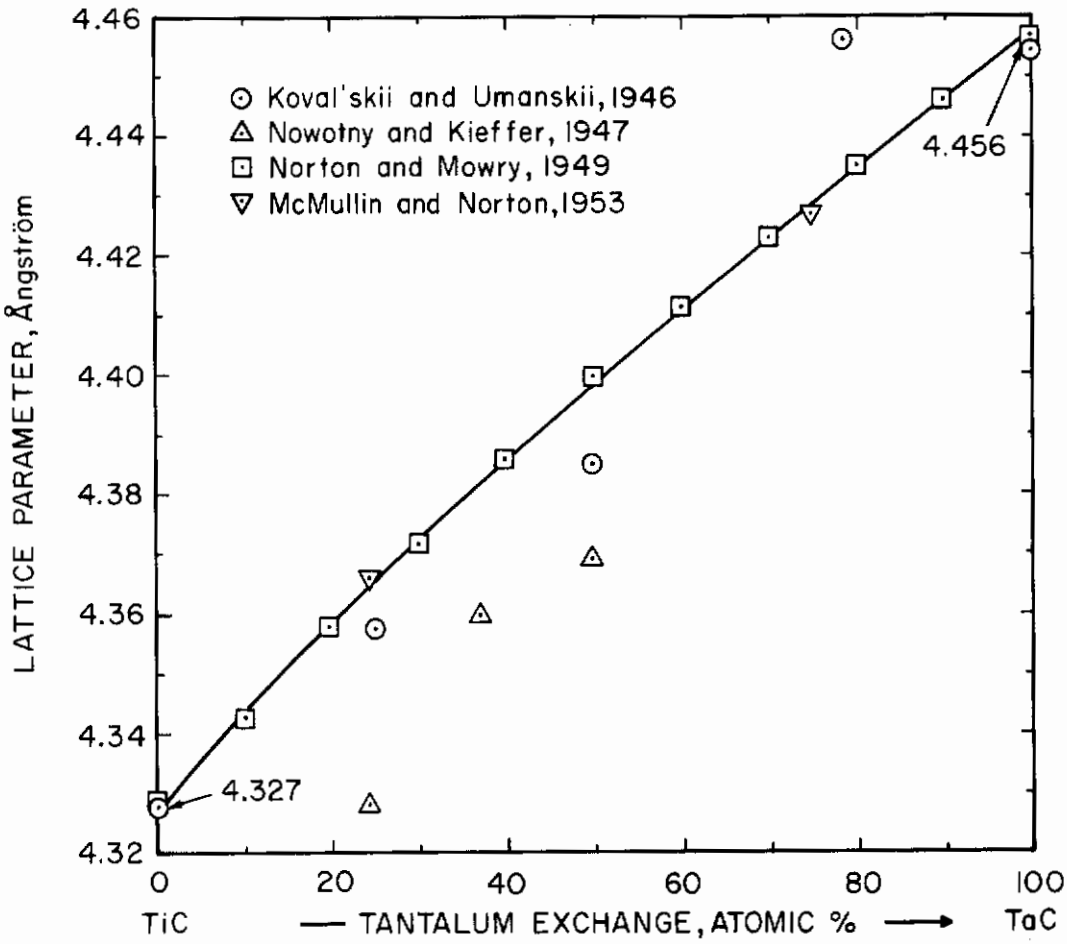

Figure 61. Lattice Parameters of the Cubic Monocarbide Solid Solution.

(Literature Data)[33]

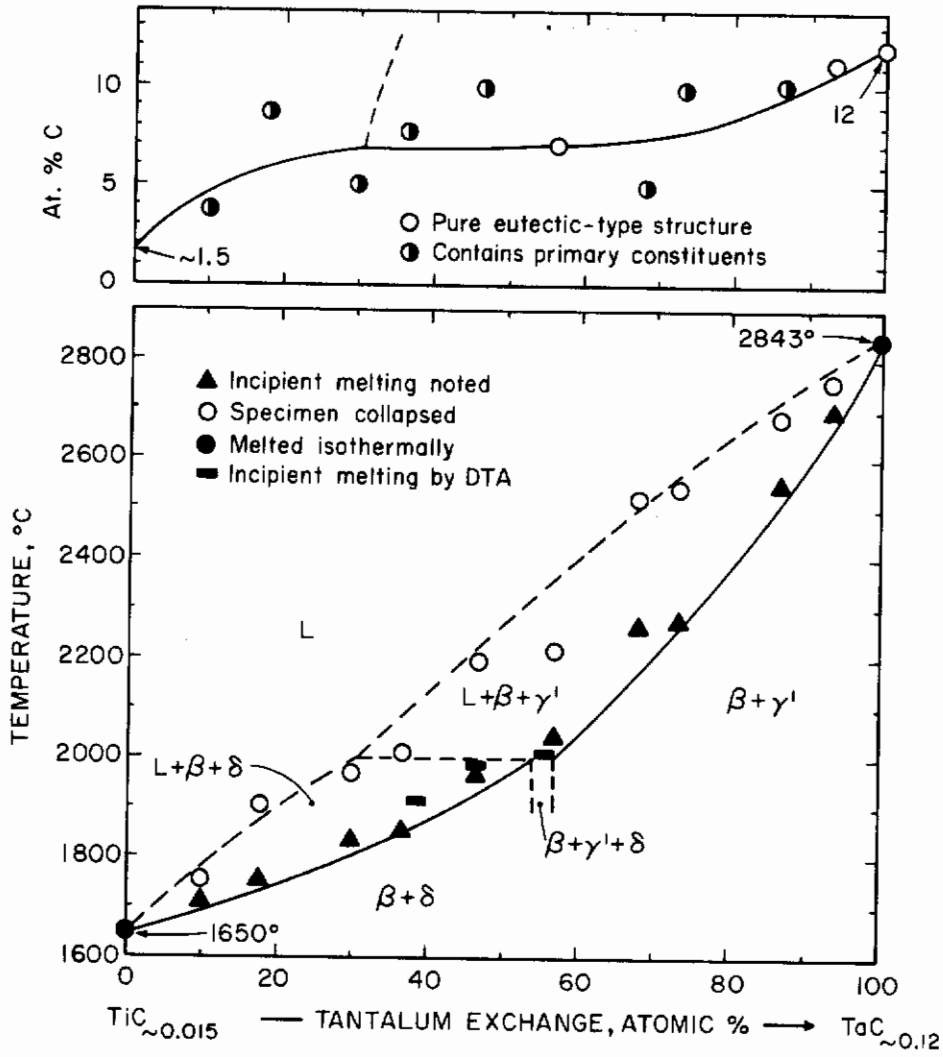

Figure 62. Ti-Ta-C: Melting Temperatures at the Metal-Rich Eutectic Trough and Metallographic Location of the Boundary Line.

Figure 63. Ti-Ta-C (53-40-7 At.%), Quenched from Liquidus Temperatures. X1000

Metal + Monocarbide Eutectic-Like Structure.

at the concentration section $TiC_{1/2}$-$TaC_{1/2}$ is depicted in Figure 64, and the measured solidus envelope for the monocarbide solution in Figure 65. The maximum solidus temperatures of the monocarbide phase, extracted from the data in Figure 65, vary almost linearly between the congruent melting points of the binary phases (Figure 66). The boundary line monocarbide + graphite was determined by a combination of melting point measurements (Figure 67) and metallographic examinations of the melted and rapidly cooled alloys (Figure 68).

The experimental data gathered in the course of the work have been combined to yield the revised phase diagram of the Ti-Ta-C system shown in Figure 4. The phase diagram data are supplemented by a reaction diagram, depicting the flow of isothermal binary and ternary reactions, Figure 5, a projection of the liquidus surface, Figure 6, and isothermal and concentration sections of the phase diagram, shown in Figures 69 through 78.

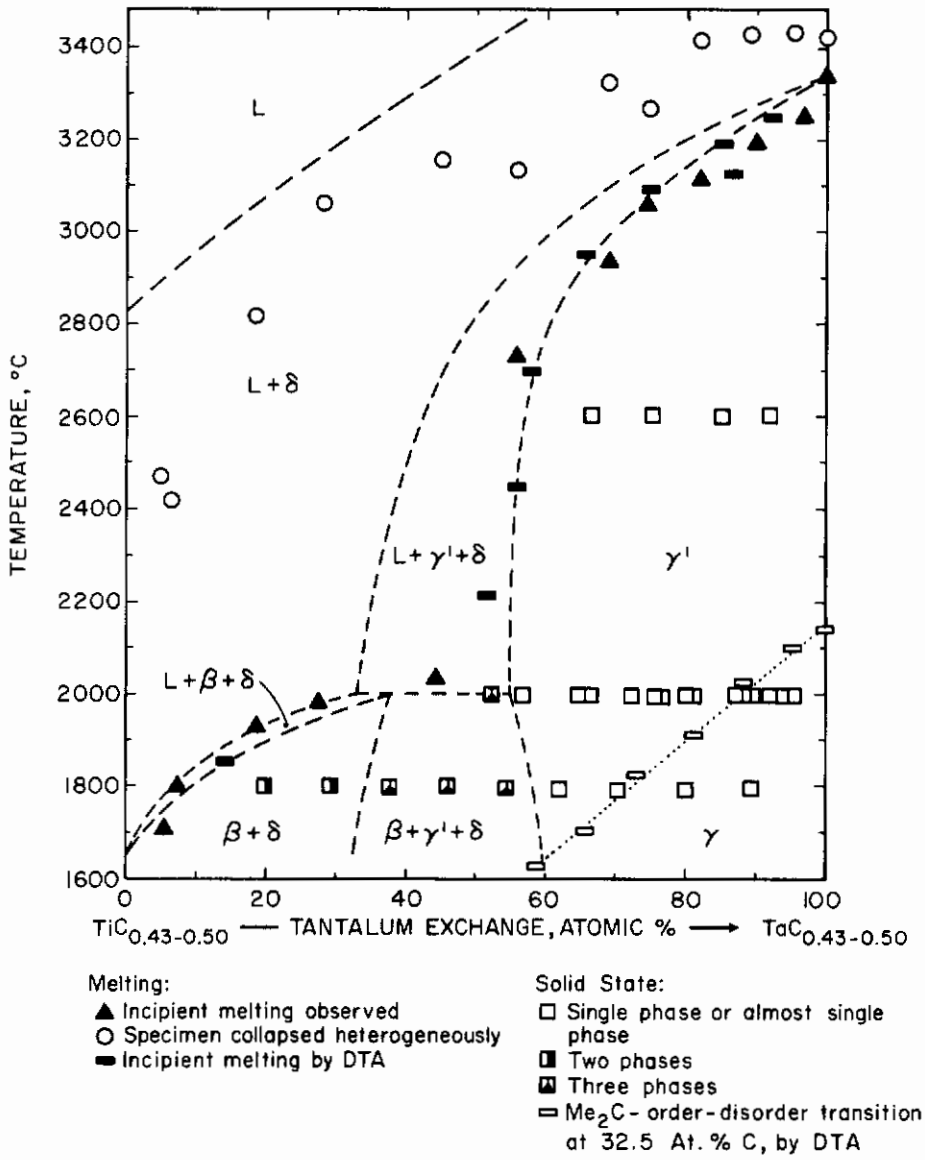

Figure 64. Melting Temperatures, Solid State Transitions, and Qualitative Phase Evaluation of Ti-Ta-C Alloys Containing Between 30 and 33 At.% Carbon.

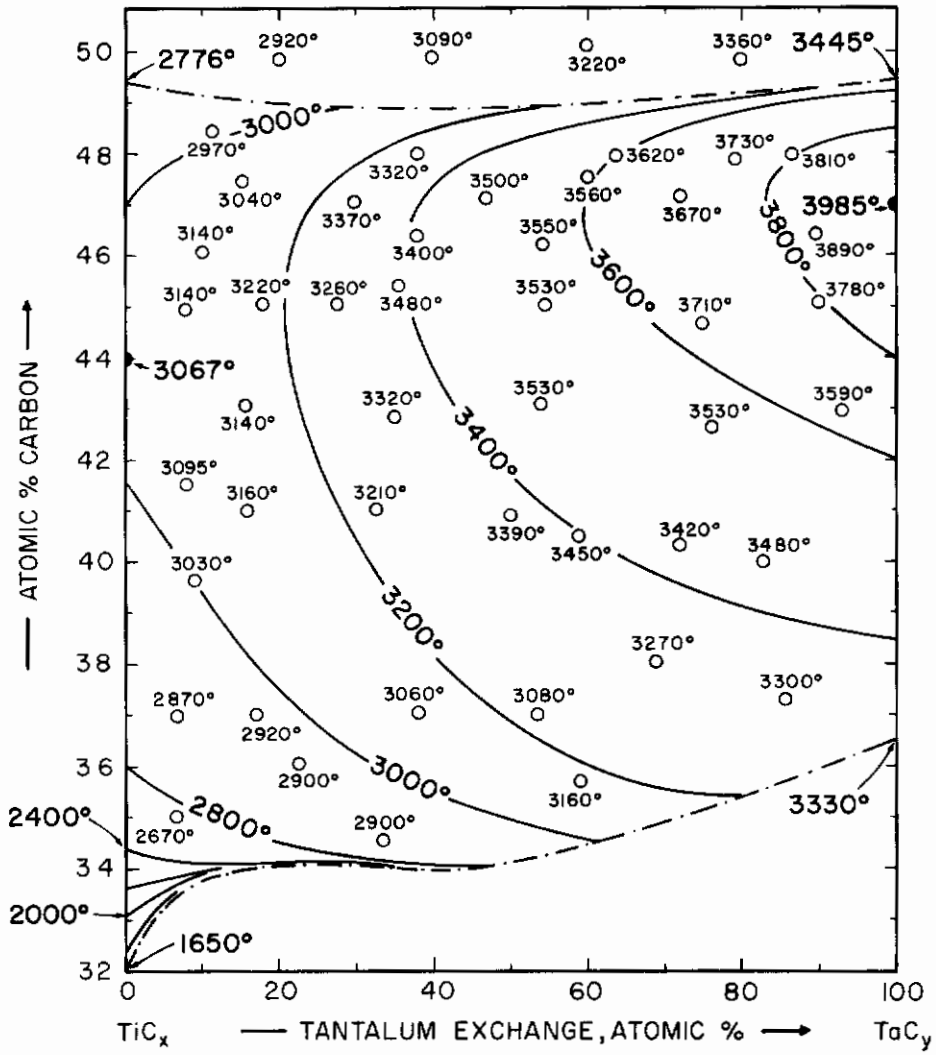

Figure 65. Experimental Solidus Surface and Derived Solidus Isotherms for the Monocarbide Solid Solution in the Ti-Ta-C System.

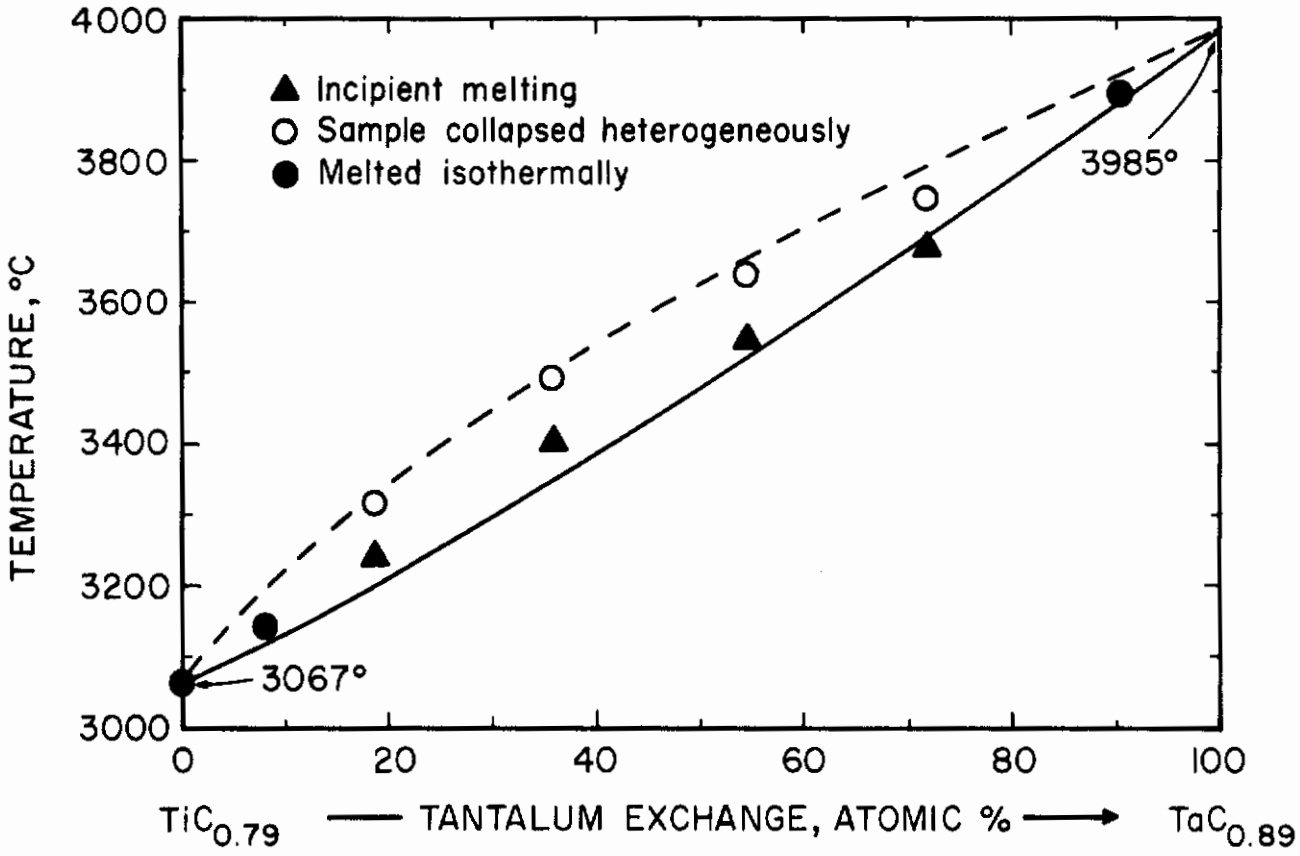

Figure 66. Maximum Solidus Temperatures of the $(Ti, Ta)C_{1-x}$ Solid Solution.

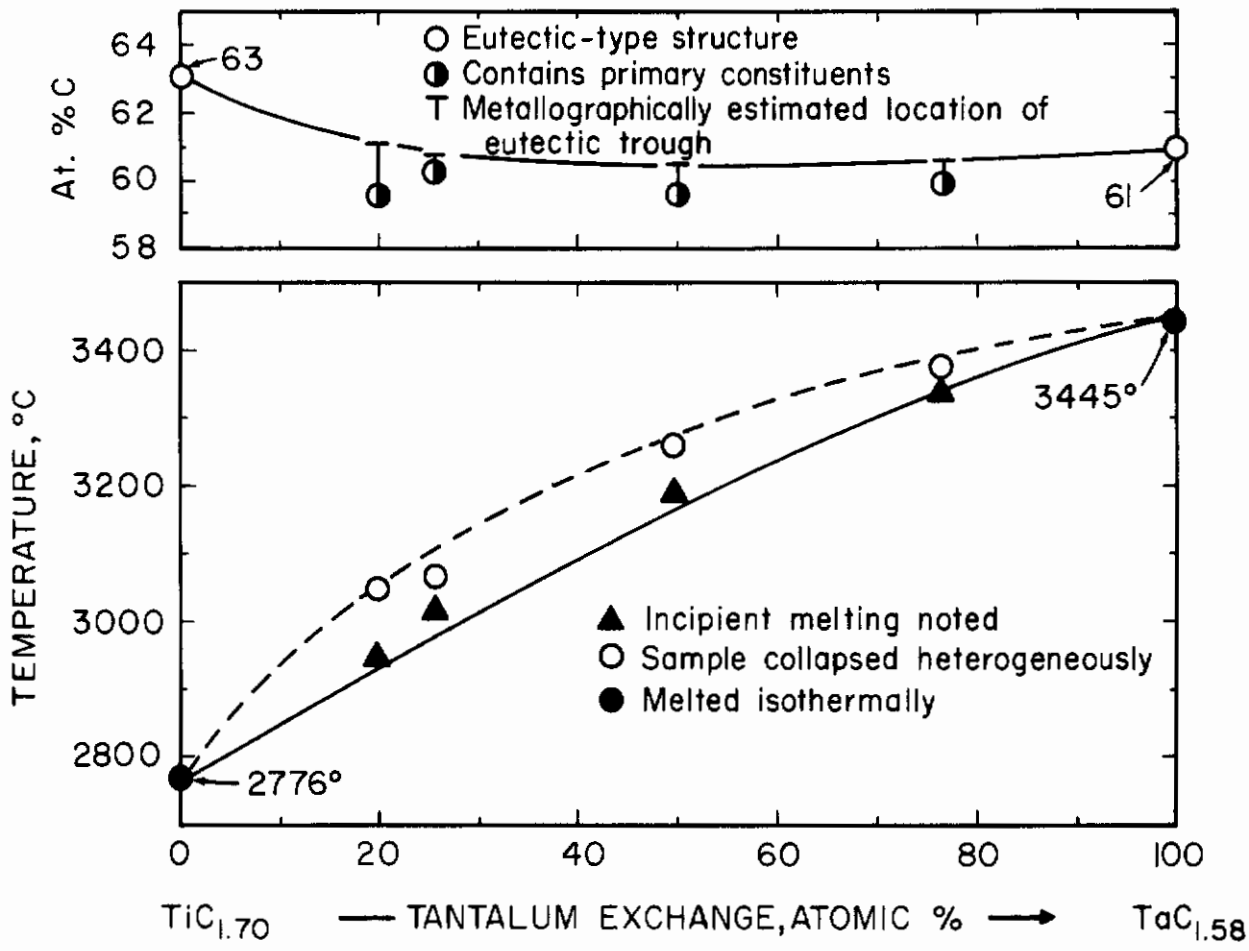

Figure 67. Melting Temperatures of Two-Phased, Monocarbide + Graphite Ti-Ta-C Alloys and Metallographic Location of Eutectic Trough.

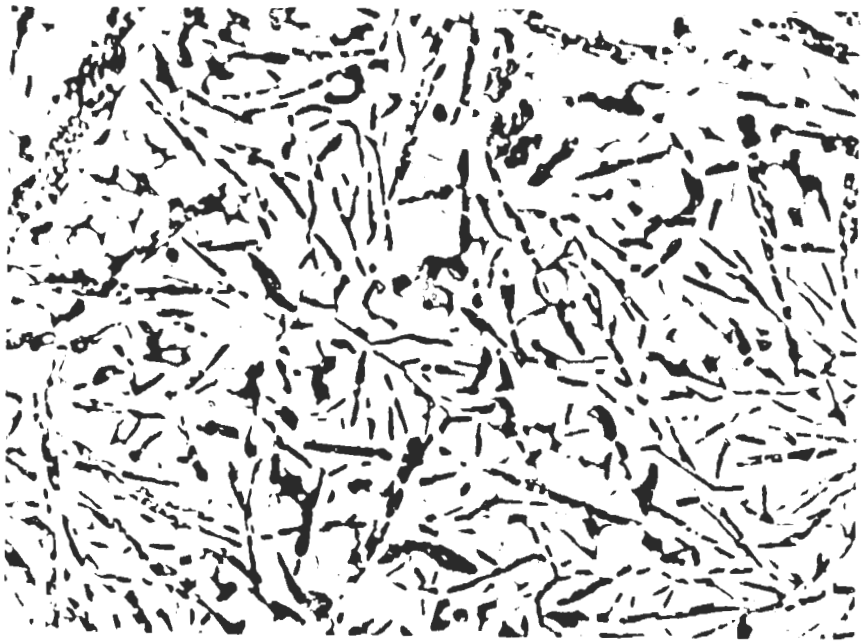

Figure 68. Ti-Ta-C (20-20-60 At.%), Quenched from Liquidus Temperatures. X100

Bivariant Monocarbide + Graphite Eutectic Structure.

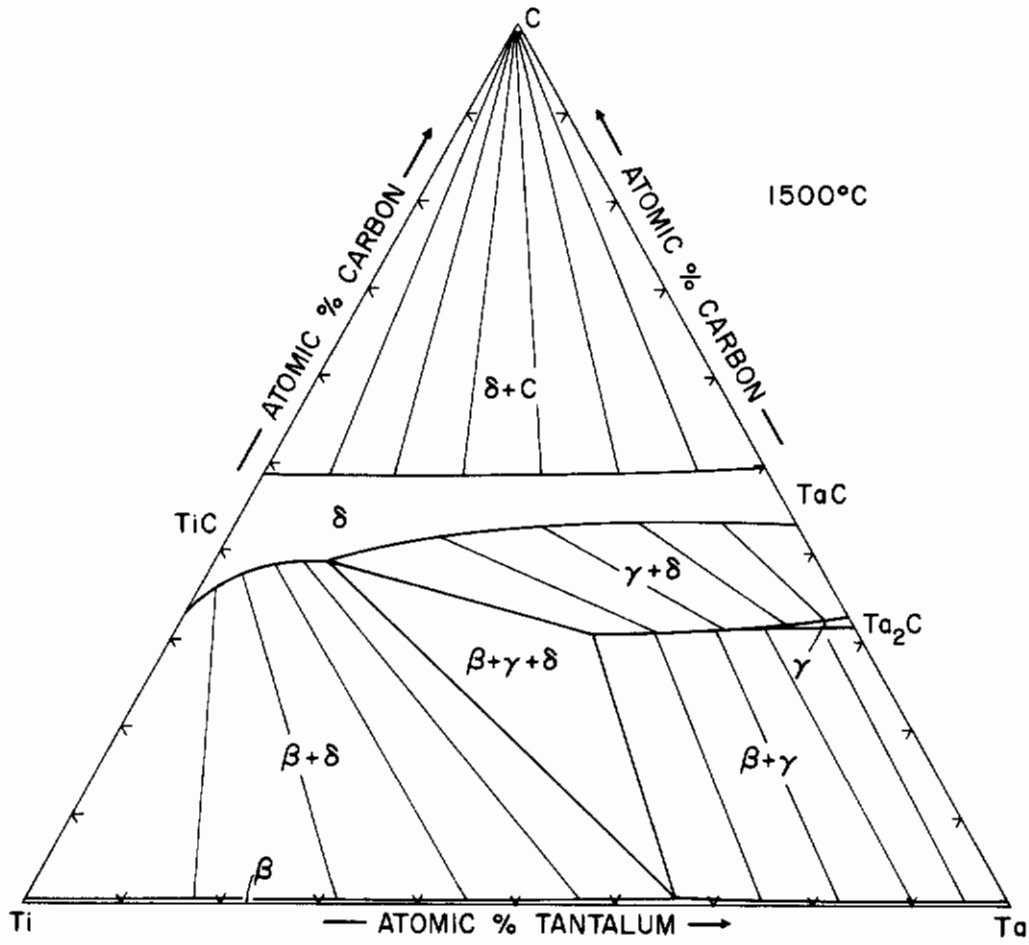

Figure 69. Isothermal Section of the Ti-Ta-C System at 1500° C.

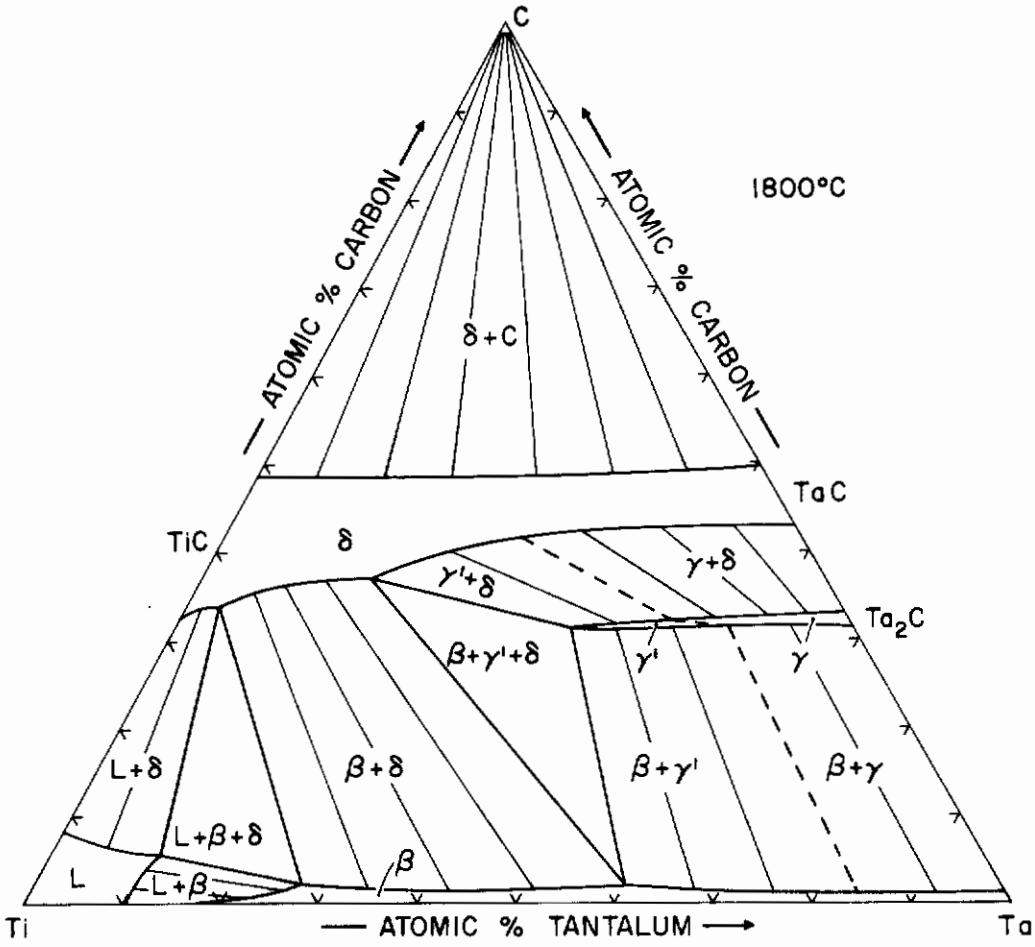

Figure 70. Isothermal Section of the Ti-Ta-C System at 1800° C.

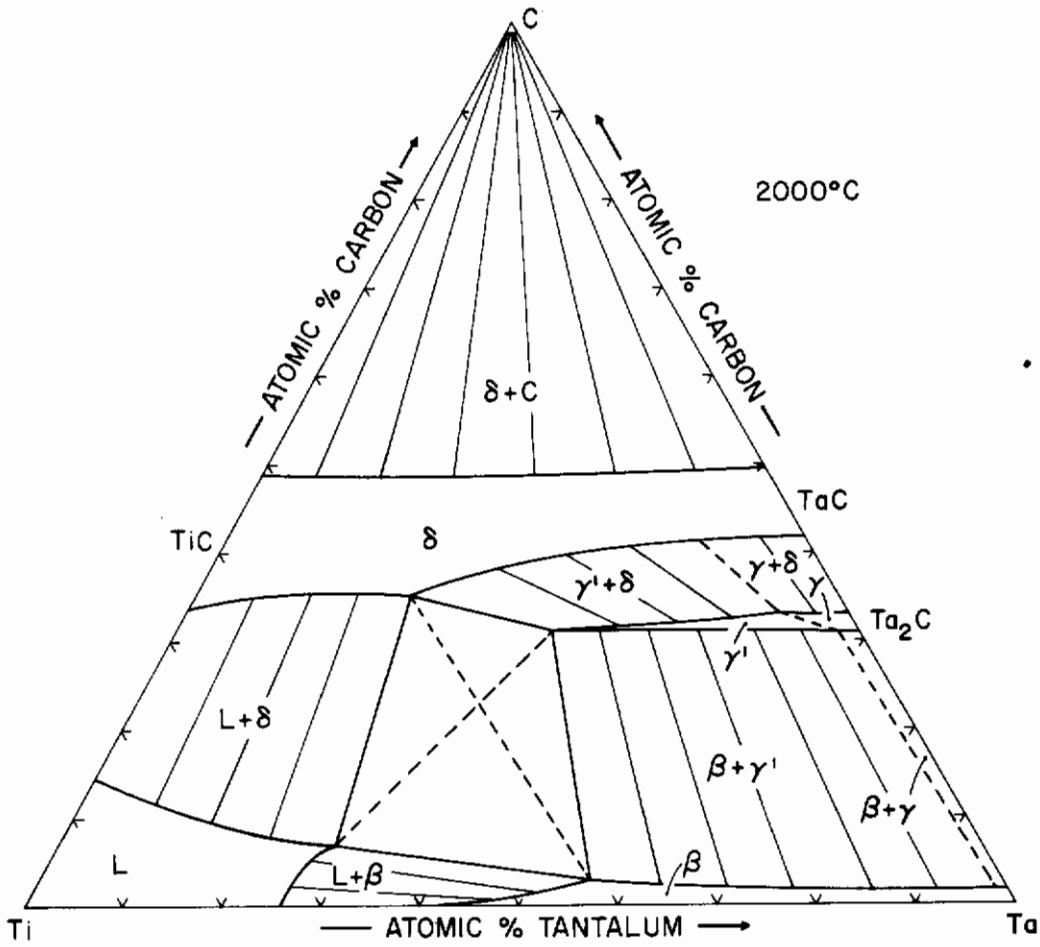

Figure 71. Isothermal Section of the Ti-Ta-C System at 2000° C.

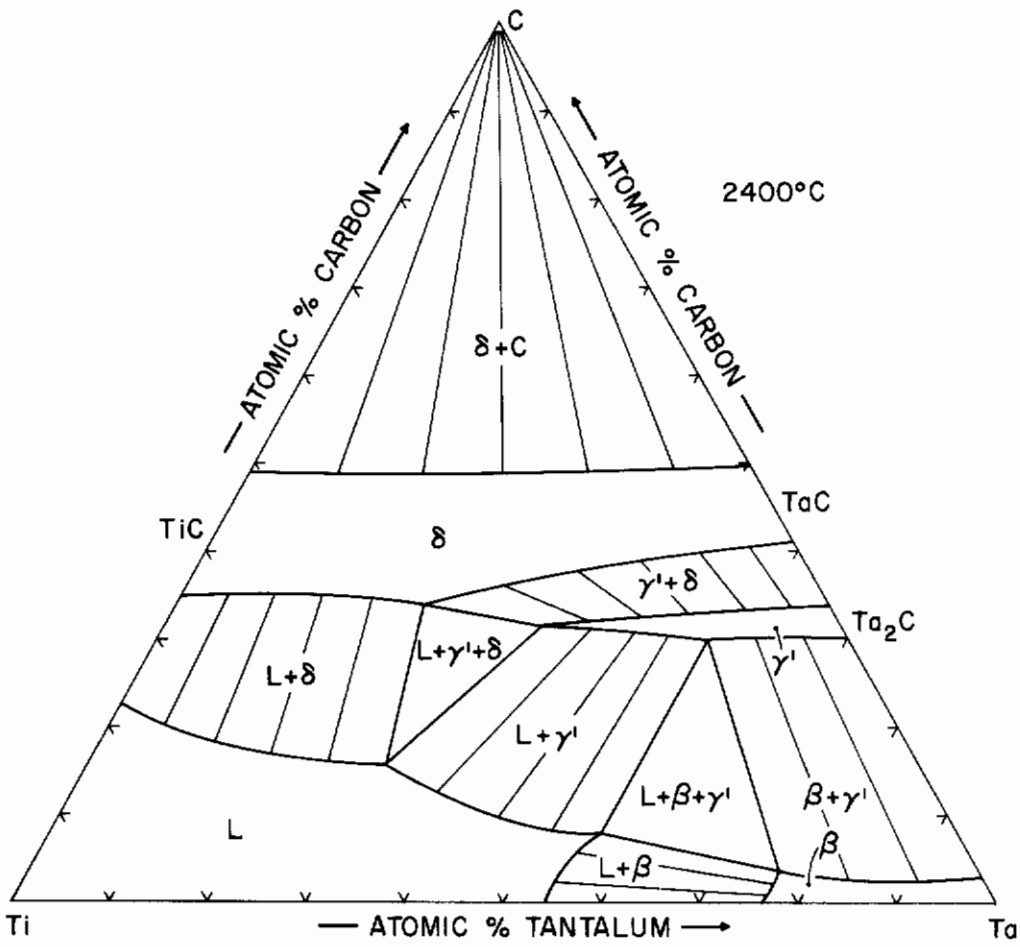

Figure 72. Isothermal Section of the Ti-Ta-C System at 2400° C.

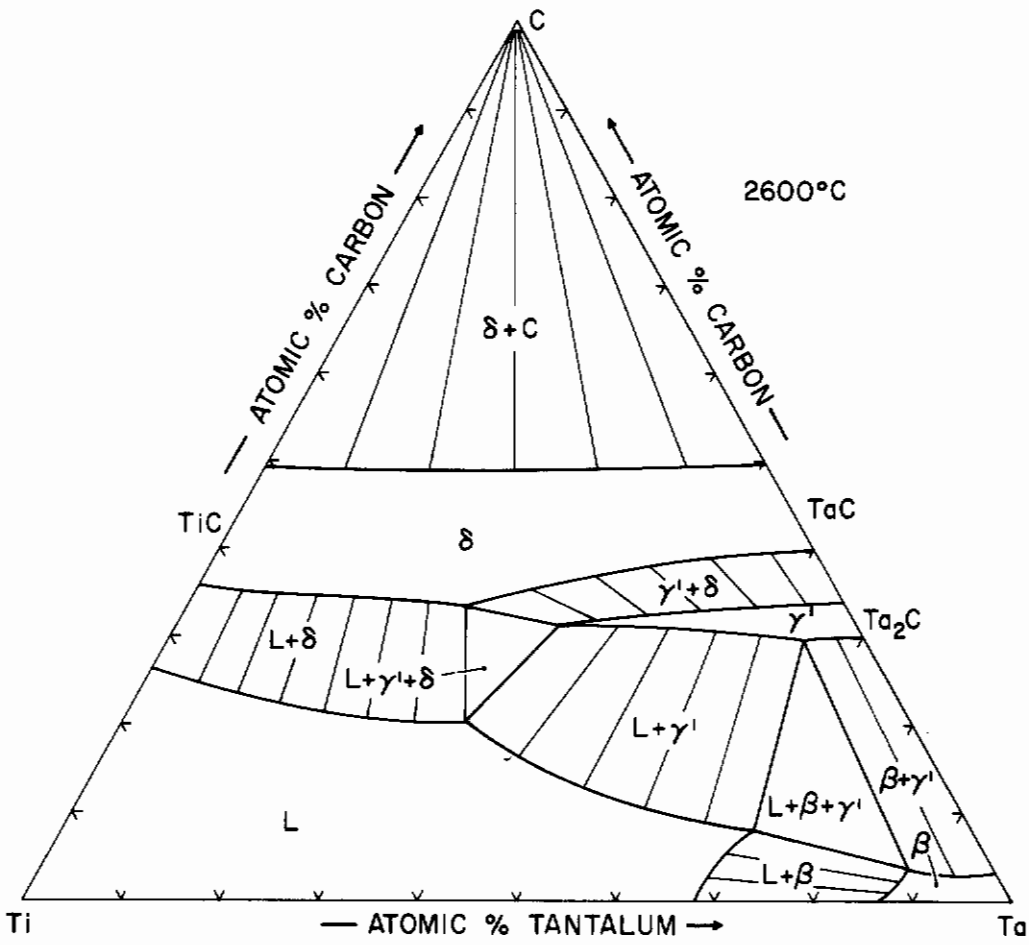

Figure 73. Isothermal Section of the Ti-Ta-C System at 2600° C.

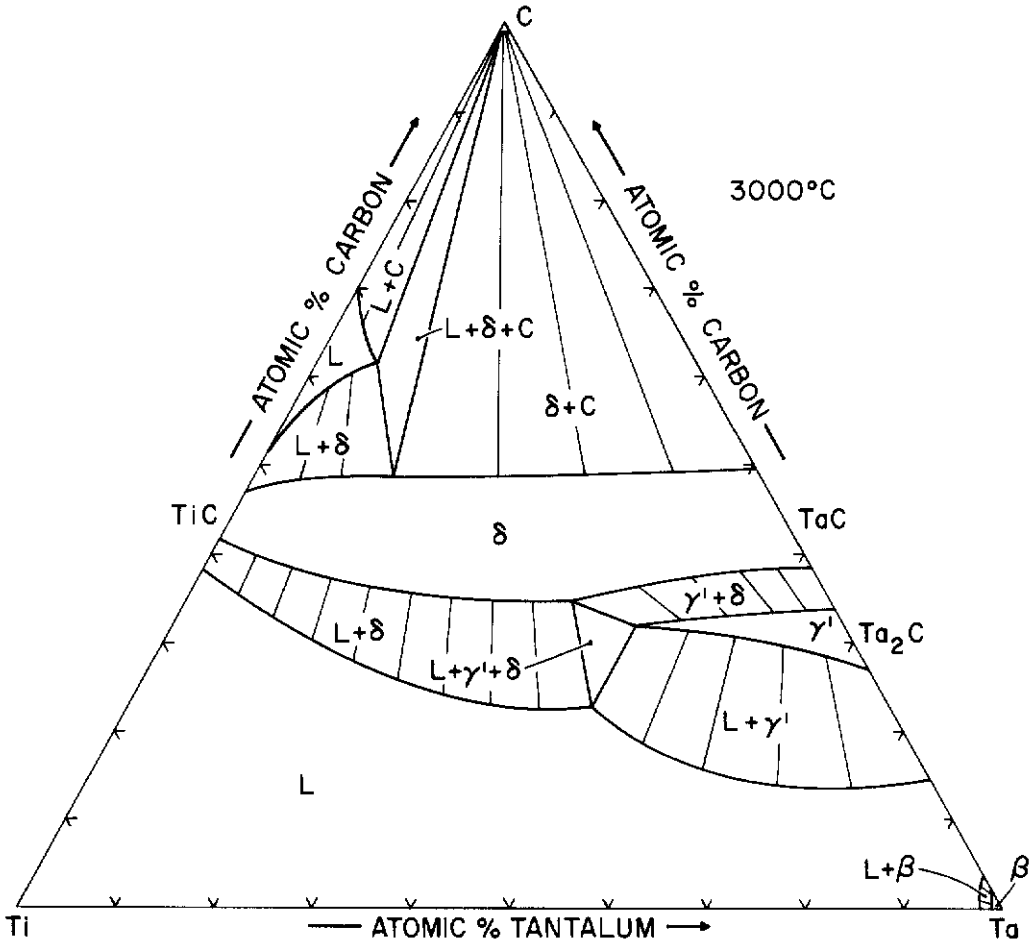

Figure 74. Isothermal Section of the Ti-Ta-C System at 3000° C.

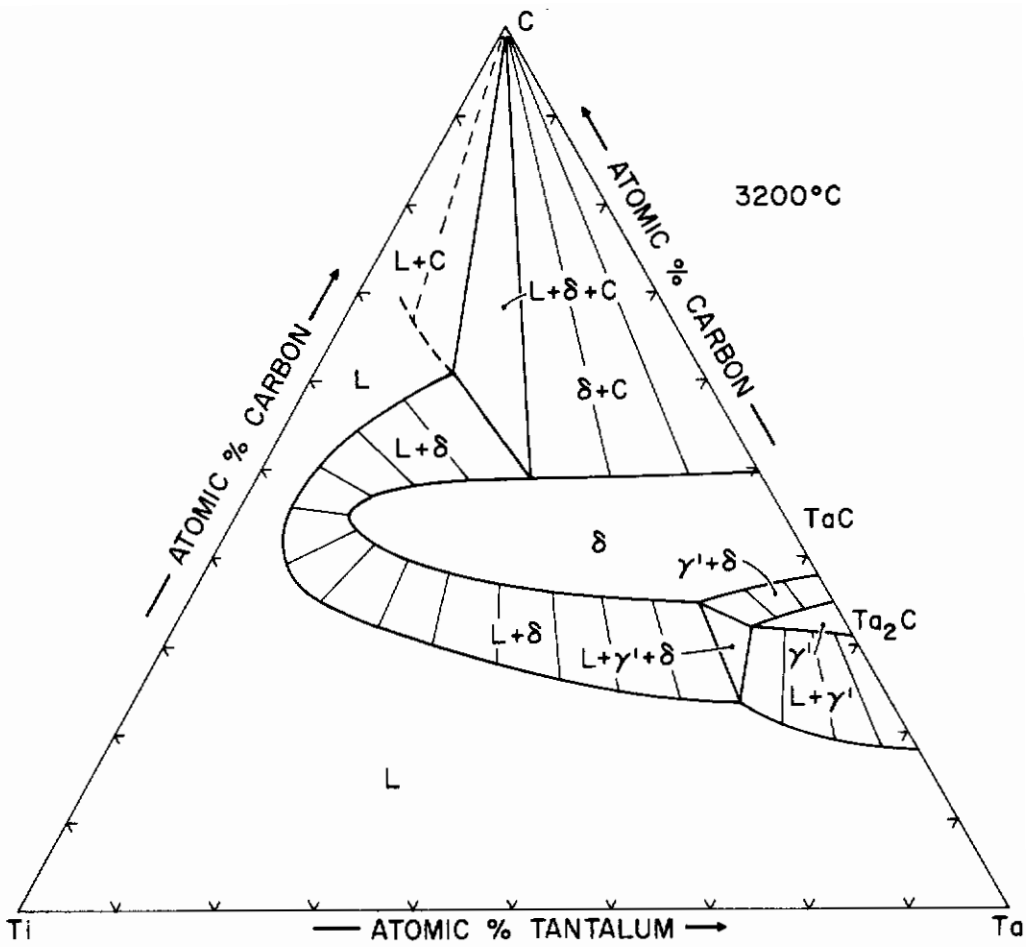

Figure 75. Isothermal Section of the Ti-Ta-C System at 3200°C.

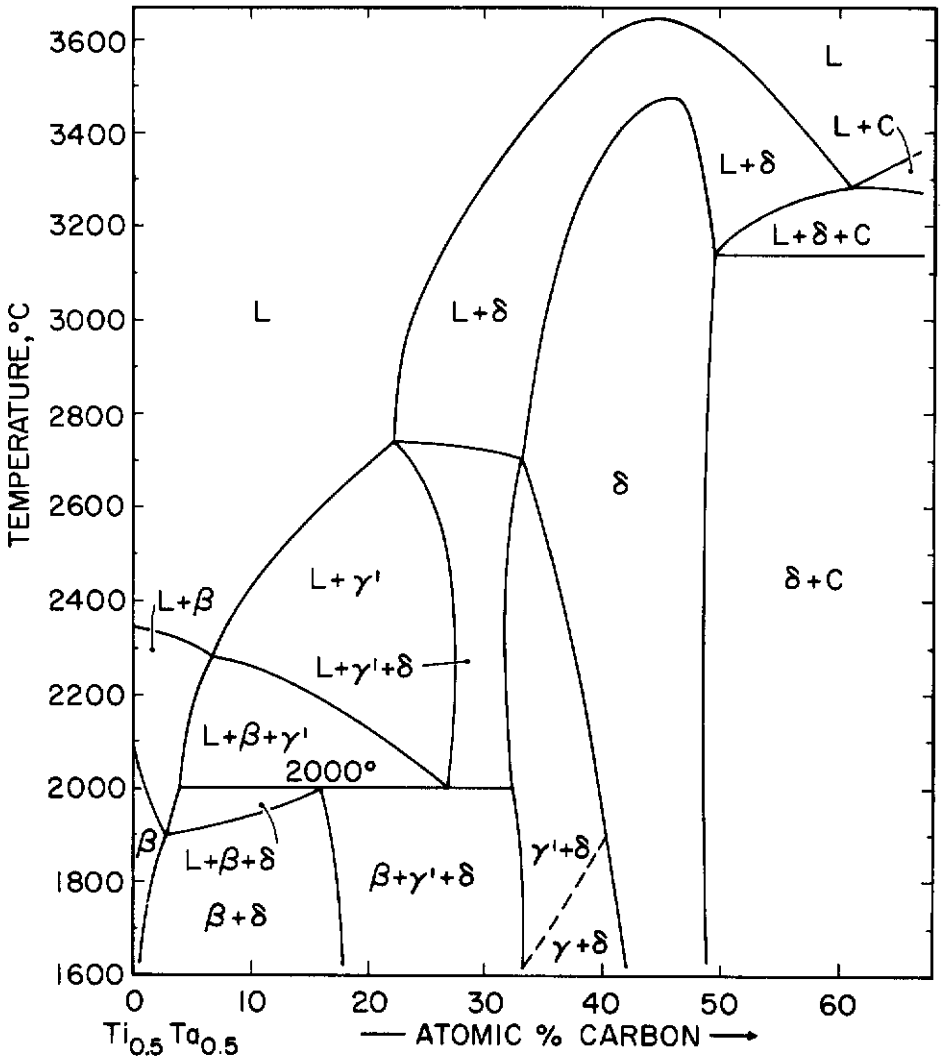

Figure 76. Isopleth $Ti_{0.5}Ta_{0.5}$-C.

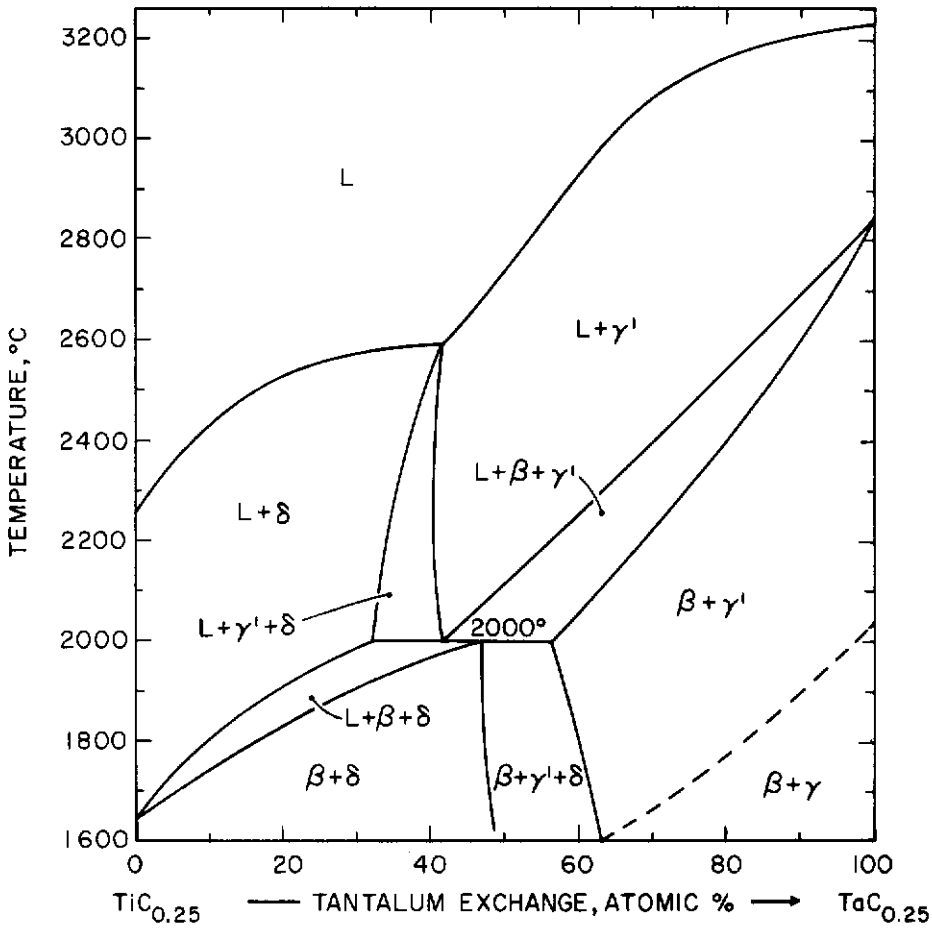

Figure 77. Isopleth $TiC_{0.25}$-$TaC_{0.25}$

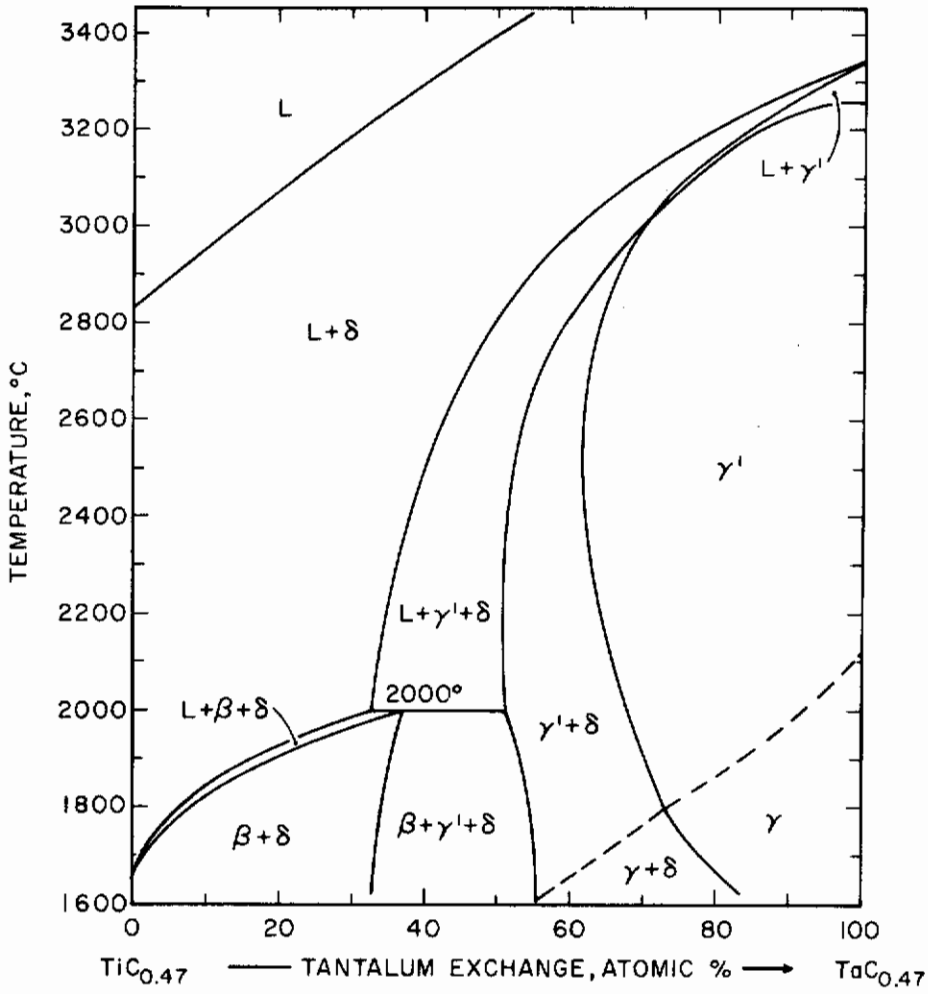

Figure 78. **Isopleth $TiC_{0.47}$-$TaC_{0.47}$.**

D. Ti-Mo-C SYSTEM

Qualitative and quantitative X-ray and metallographic analysis of the alloy series equilibrated at 1500° C and 2100° C established the phase relationships outlined in Figures 79 and 80. As can be seen from a comparison of the two isothermal sections, the principal phase relationships do not vary appreciably within this comparatively wide temperature range. Within the solid state region, titanium-rich (> 50 At.%) monocarbide solid solution alloys are in equilibrium with the metal phase ranging from titanium to about 98 At.% molybdenum.

The homogeneity range of the cubic monocarbide phase extends to a molybdenum exchange of approximately 91 At.% at 1500° C (a= 4.327Å for TiC, a= 4.273Å at the homogeneity limit), while the η-phase seems to be stabilized in the ternary. Lattice parameters varying between a=3.010 to 3.014Å, and c= 14.64 to 14.67Å, for the η-phase in ternary alloys are only insignificantly different from unit cell dimensions of a= 3.010Å and c= 14.64Å measured for the pure, binary carbide.

The Mo_2C-phase, which substitutes less than 5 At.% titanium at 1500° C, is constrained by a three-phase equilibrium (Ti,Mo) + Mo_2C-ss + $(Ti,Mo)C_{1-x}$ in the ternary. Lattice parameters of a= 3.004 to 3.012Å and c= 4.742 to 4.746 Å, for Mo_2C in three phased, Me + Me_2C + MeC_{1-x}, alloys fall into the range of parameters for the binary carbide. In view of the low solid solubility of titanium in molybdenum, the sublattice order-disorder transition temperatures for the ternary subcarbide phase are practically the same as in the binary alloy (Figure 81).

The swing of the tie-lines in the two-phase field metal + monocarbide, determined by lattice parameter measurements on two-three-phased alloys (Figures 82 and 83) are indicative of the large stability difference between TiC and the cubic molybdenum carbide.

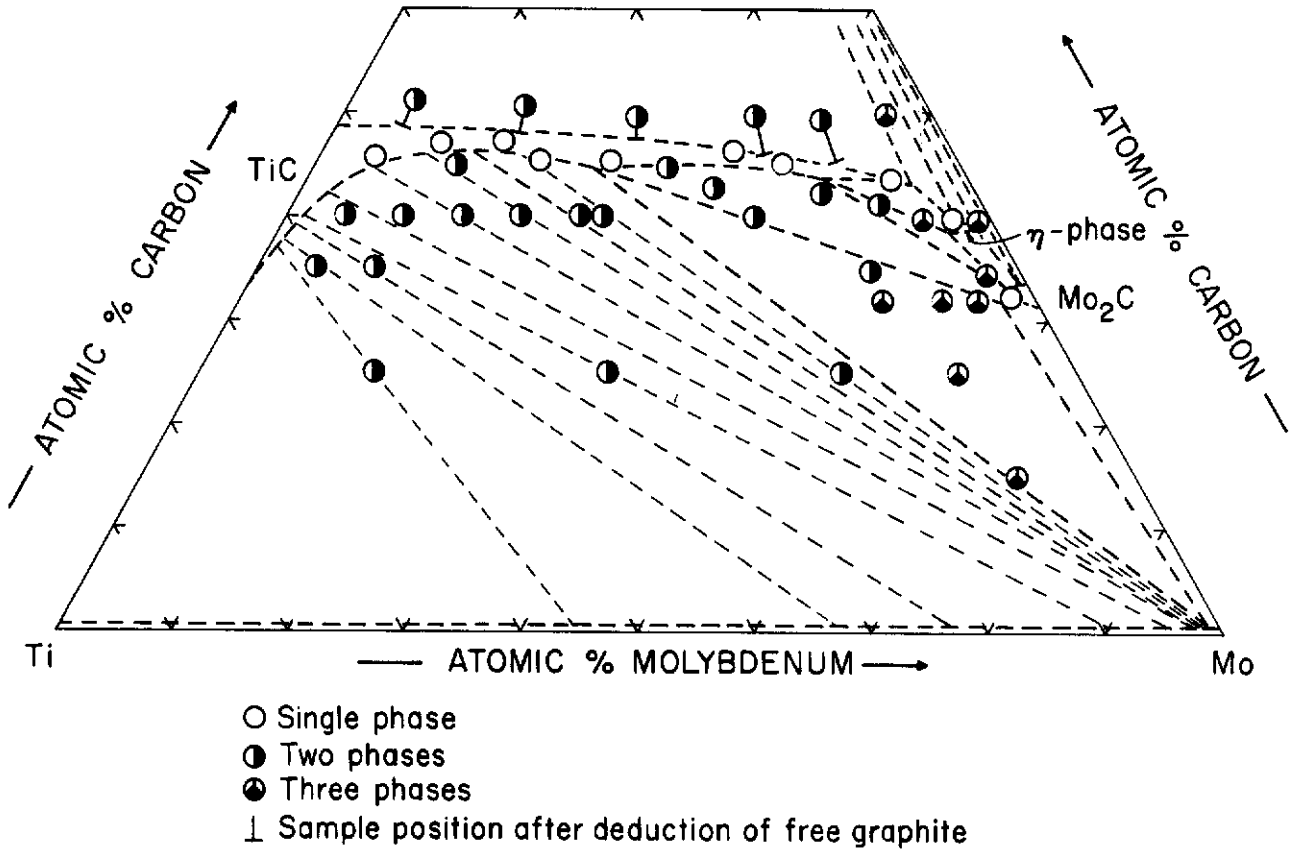

Figure 79. Sample Location and Qualitative Phase Evaluation of the Alloy Series Equilibrated at 1500° C.

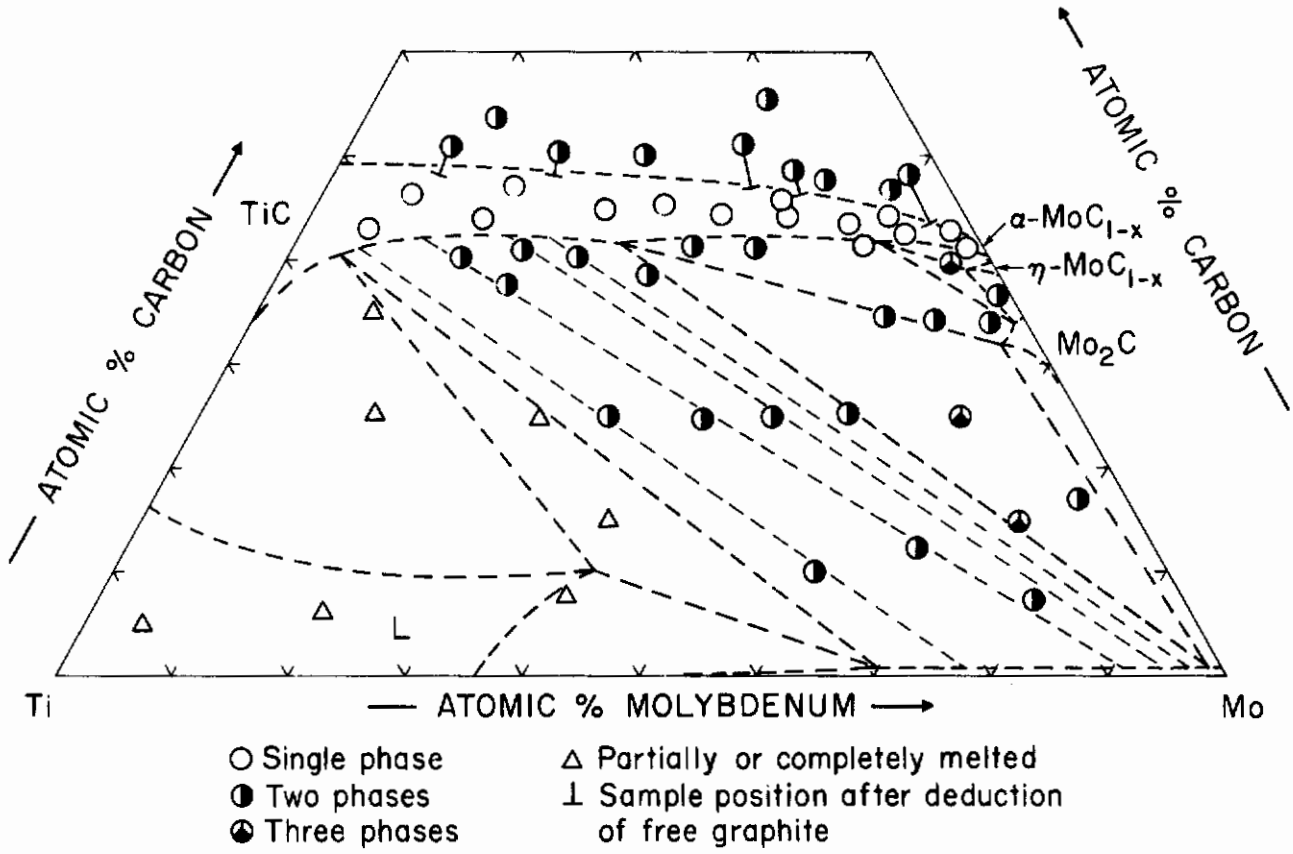

Figure 80. Sample Location and Qualitative Phase Evaluation of the Alloy Series Equilibrated at 2100° C.

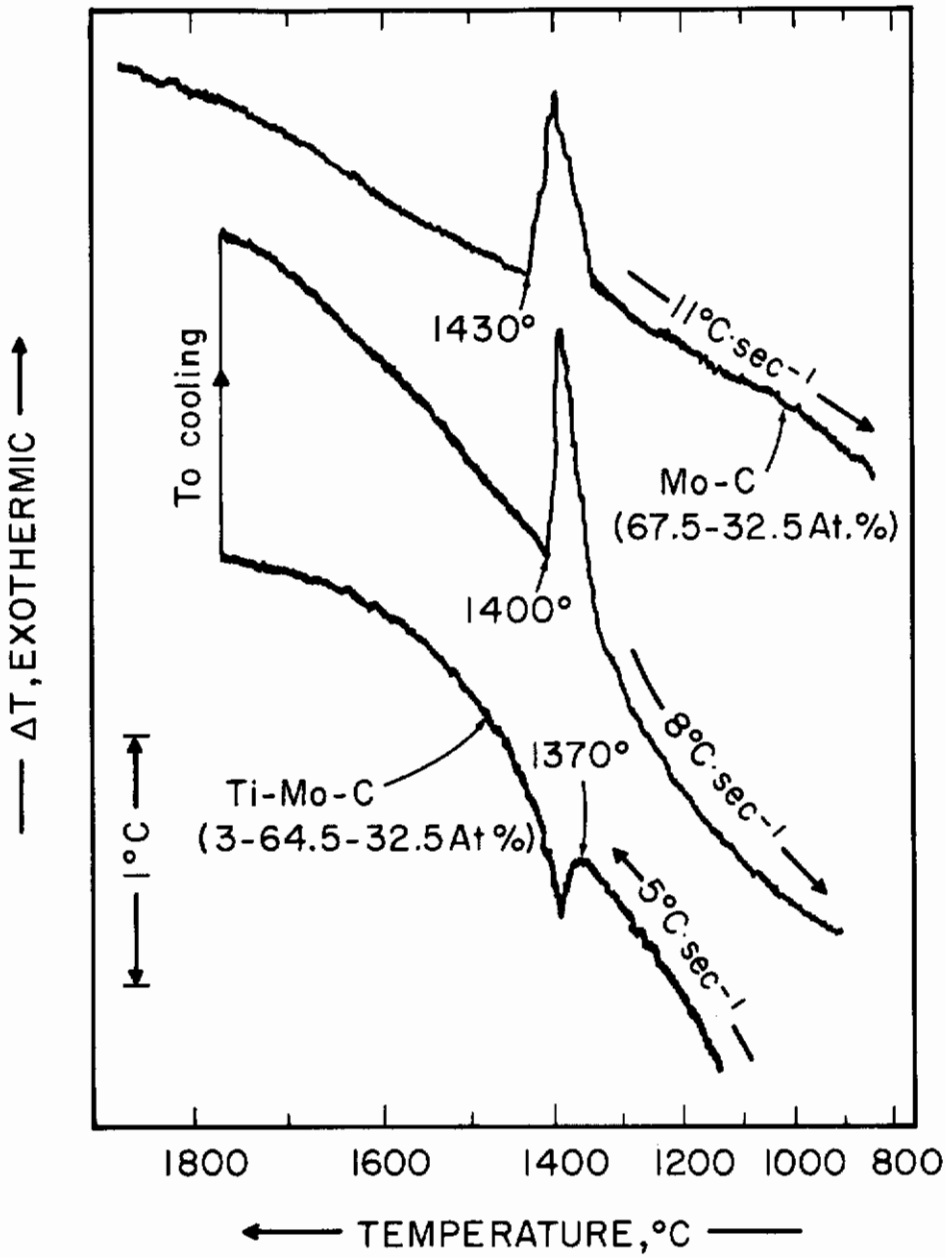

Figure 81. DTA-Thermograms Showing the Order-Disorder Transition in Binary Mo_2C and a Ternary Subcarbide Alloy Containing 3 At.% Titanium.

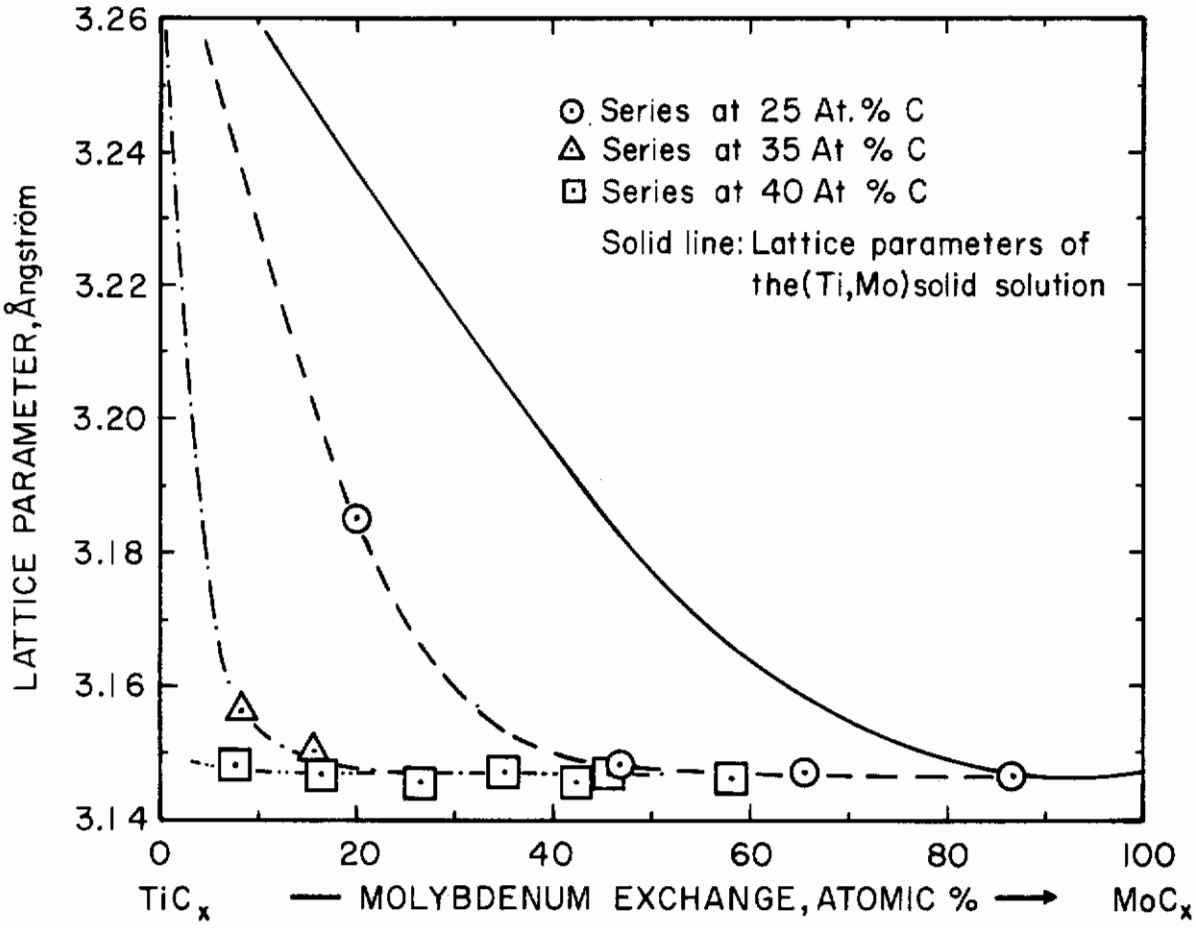

Figure 82. Lattice Parameters of the Cubic (A2) Metal Phase in Two-Phased, β+ δ, Alloys.

(Alloys Homogenized at 1500° C)

Solid Line = Parameters of the β-(Ti,Mo) Solid Solution).

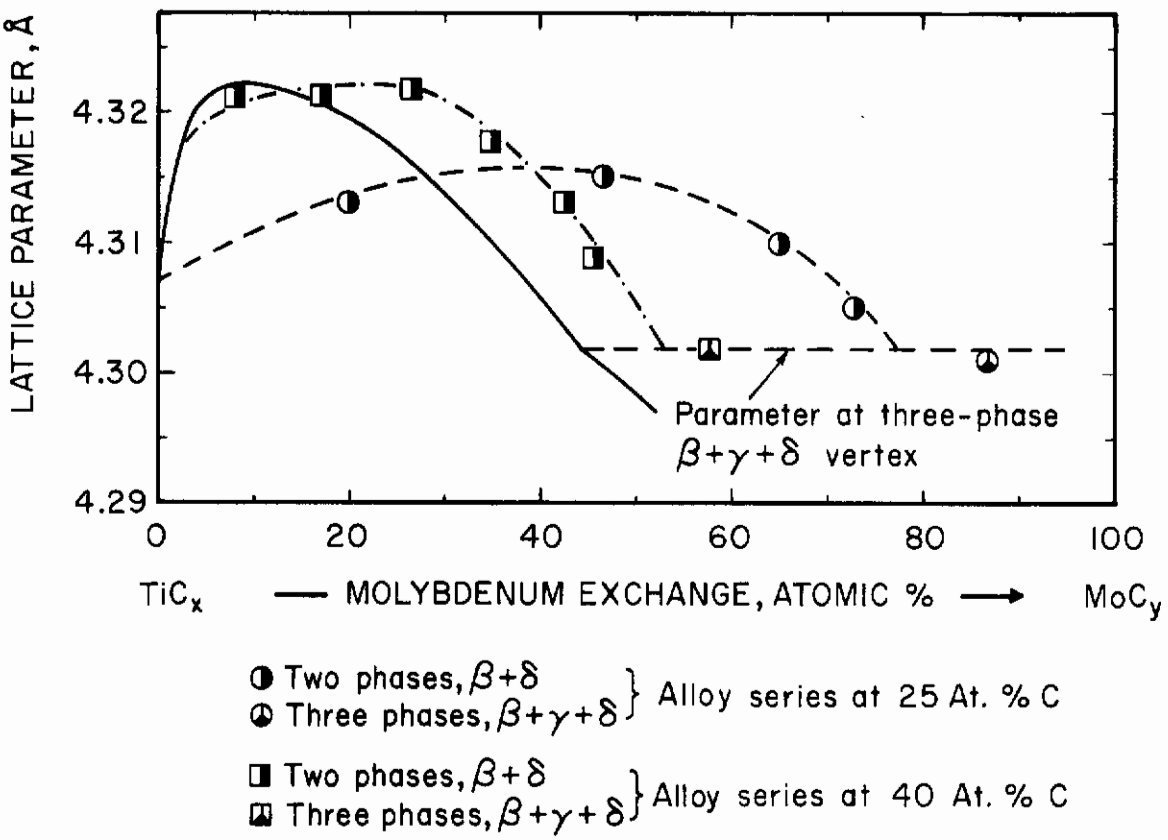

Figure 83. Parameters of the Monocarbide at the Metal-Rich Phase Boundary and in Two-Phased, $\beta + \delta$, and Three-Phased, $\beta + \gamma + \delta$, Alloys. (Alloys Homogenized at 1500° C).

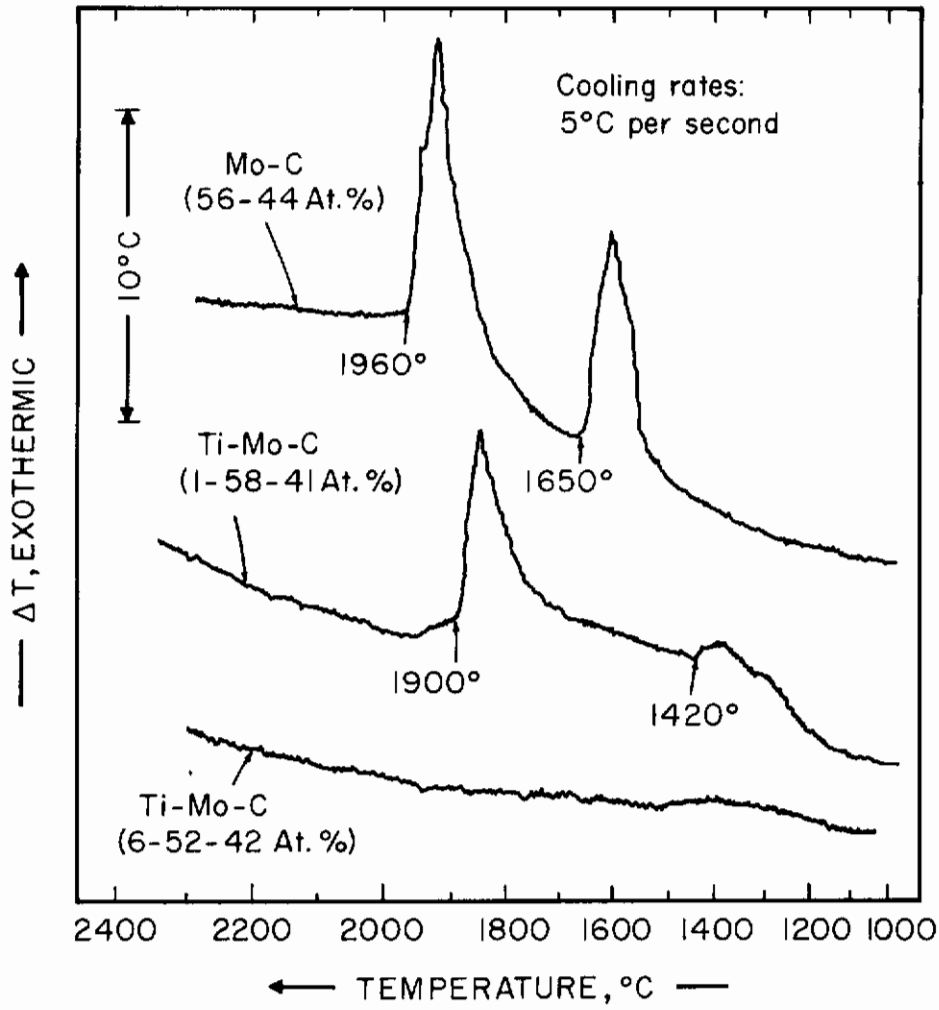

Figure 84. Decomposition of the β-MoC_{1-x} and η-MoC_{1-x} Phases Upon Cooling in Binary Mo-C and Ternary Ti-Mo-C Alloys.

Above 1960° C, the eutectoid decomposition temperature for the binary molybdenum carbide, the cubic carbides in the boundary systems Ti-C and Mo-C form a complete series of solid solutions. Below this temperature, the ternary homogeneity range of the cubic monocarbide phase becomes temperature-dependent. The decomposition rates in solid solutions with more than about 10 At. % molybdenum exchange are so slow that it proved difficult to attain equilibrium at temperatures below 1500° C. This behavior is also borne out by the results of the differential-thermoanalytical studies: Thus, while the decomposition rates of the pure binary phases are high and the phases can be retained to room temperature only by severe quenching, decomposition of the cubic carbide in an alloy Ti-Mo-C (1-58-41 At.%) occurs at a lower temperature and also much more sluggishly (Figure 84). The decomposition of the cubic carbide in an alloy Ti-Mo-C (6-52-42 At.%) could not be observed within the range of cooling rates (0.5° to 20° C per second) of the DTA-apparatus.

The lattice parameter-concentration relationships for the carbon-saturated monocarbide solid solution appears to show an abnormally large positive deviation from Vegards law (Figure 85). A similar variation has also been observed in the Ti-W-C system[30] and was attributed to changes in the band structure[39]. A closer examination, however, reveals that Vegard's relationship is quite well obeyed if the changing carbon content of the carbon-rich boundary is taken into account. Extrapolation of the lattice parameters of the cubic molybdenum carbide[25] to 50 At.% yields a_{MoC} = 4.325Å, which nearly coincides with the unit cell edge length of a= 4.327Å for TiC. As can be seen from the top section in Figure 85, the carbon content of the boundary decreases only slightly at molybdenum exchanges up to 40 At.% and, as a result, the parameters are nearly independent of the metal exchange. Towards higher molybdenum contents, however, the boundary

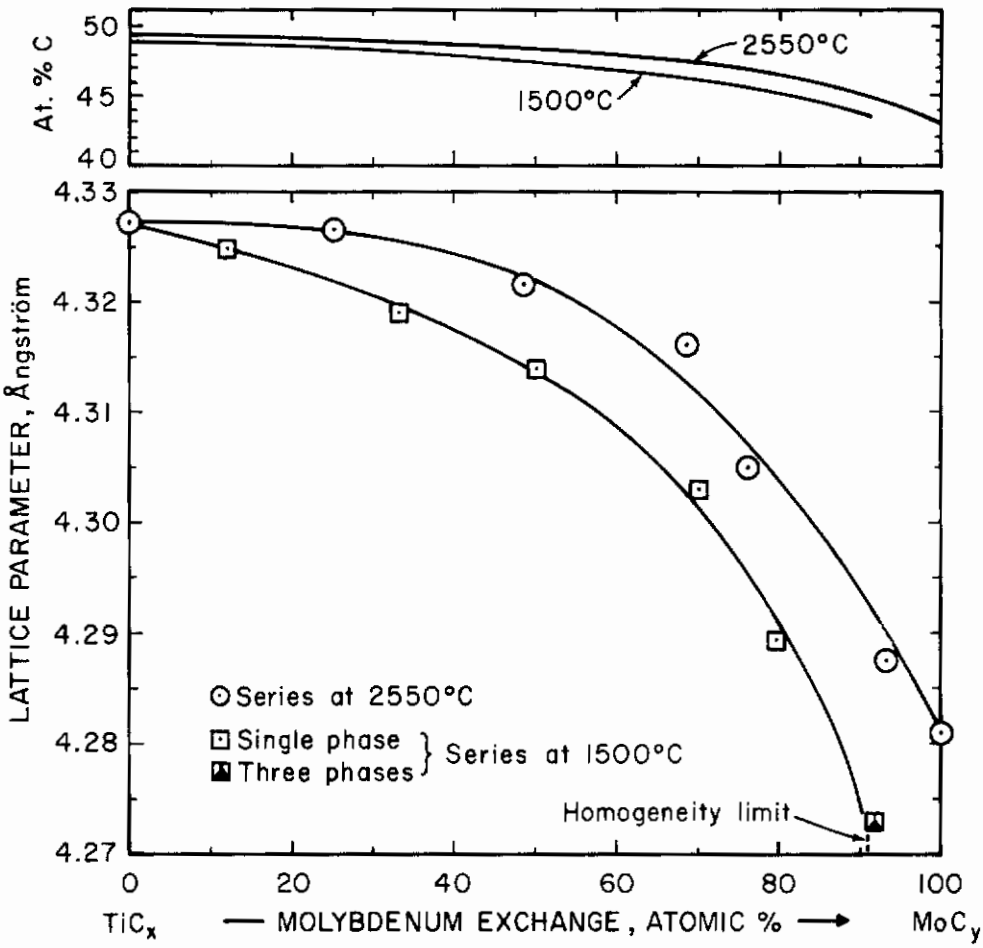

Figure 85. Lattice Parameters of the Carbon-Saturated Monocarbide Phase at 1500° C and 2550° C.

retracts more rapidly to lower carbon contents, and the steeper parameter-concentrations gradient of the molybdenum carbide also becomes more important. As a consequence, the unit cell dimensions show a pronounced dip about 50 At.% Mo. The lattice parameters shown for the alloy series heat treated at 2550° C (Figure 85) can be reproduced within the error limits of the experimental curve by assuming a variation of the parameter according to a linear relationship, i.e.

$$A_{ss} = x_{Mo} \cdot a_{MoC_{1-x}} + x_{Ti} \cdot a_{TiC_{1-x}}$$

whereas a_{ss} is the parameter of the ternary solid solution, x_{Mo} and x_{Ti} the metal exchanges in the monocarbide, and $a_{MoC_{1-x}}$ and $a_{TiC_{1-x}}$ the lattice parameters of the binary carbides referred to the same carbon content as the ternary carbide.

A microscopic study of the monocarbide decomposition reaction indicated that in low carbon carbon alloys the decomposition reaction invariably nucleated at the grain boundaries, from which it then spread to the interior of the grains (Figure 86). In monocarbide alloys located at, or close to, the carbon-rich boundary and which were equilibrated at high temperatures, nucleation occurred at inter- and intragranular graphite precipitates which had formed during cooling; the gross decomposition rates in such alloys were therefore considerably higher than in the homogeneous alloys and higher cooling speeds were necessary to retain the alloys single-phased to room temperature (Figure 88).

Melting point measurements on alloys located along the metal-rich eutectic trough revealed the existence of a melting point maximum at a molybdenum exchange of about 70 At.% (17 At.% C), and a melting point minimum at about 85 At.% Mo (Figure 89). The melting point maximum at at 2240° C was shown from X-ray and metallographic studies to be due to the formation of a pseudobinary eutectic equilibrium between a molybdenum-rich metal, and a titanium-rich monocarbide, solid solution. The melting point minimum at 2200° C was identified to be a ternary eutectic between metal, sub-carbide, and monocarbide. Typical microstructures of melted alloys from the metal-rich (< 35 At.% C) region of the system are shown in Figures 90 through 97.

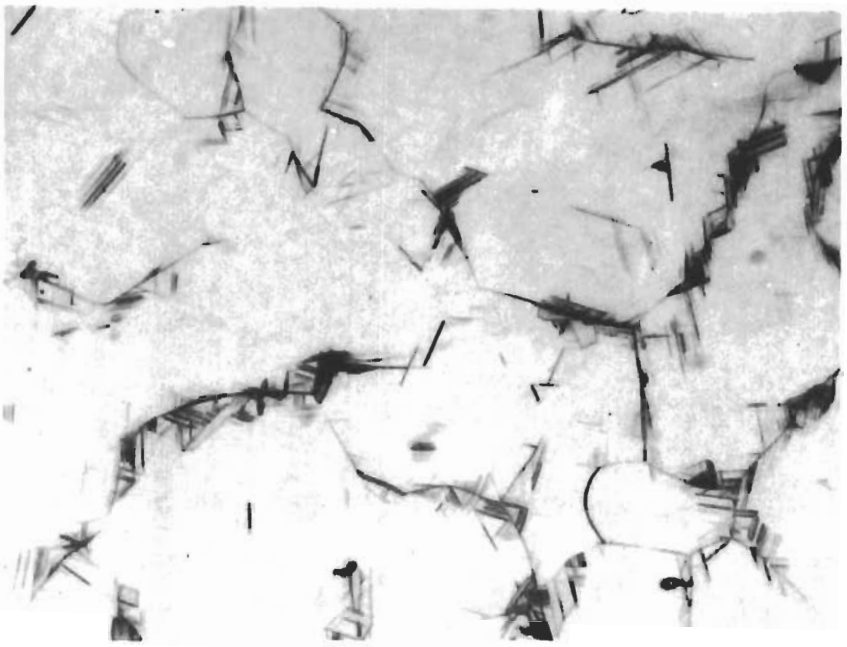

Figure 86. Ti-Mo-C (2-58-40 At.%), Equilibrated at 2500° C and Cooled at ~30° C per Second. X375

$(Ti,Mo)C_{1-x}$ Solid Solution. Note Nucleation of Decomposition Reaction at Grain Boundaries.

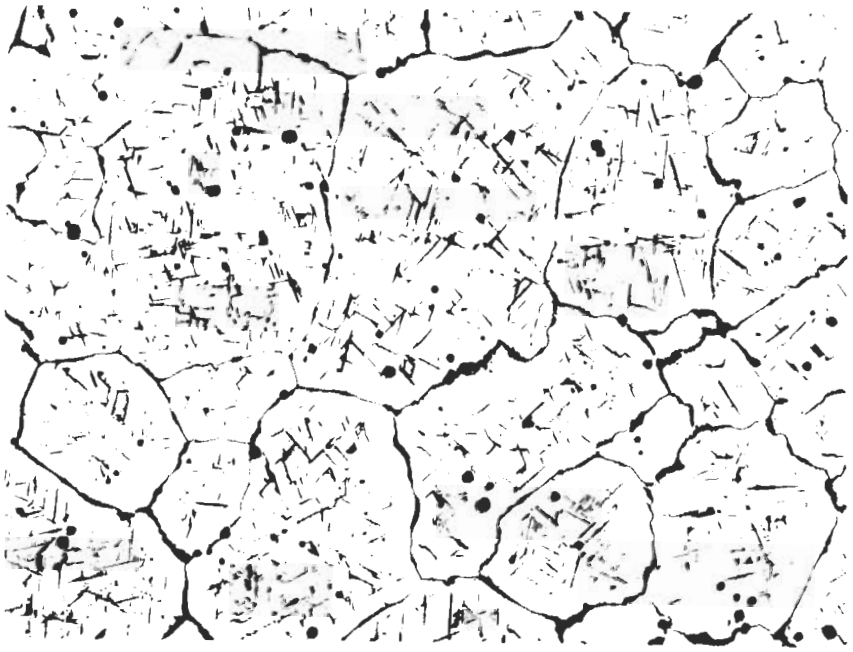

Figure 87. Ti-Mo-C (1-57-42 At.%), Equilibrated at 2350° C and Cooled at 12° C per Second. X80

Monocarbide, Disproportionated into Graphite and η-MoC_{1-x} During Cooling. Note Segregation of Graphite to Grain Boundaries.

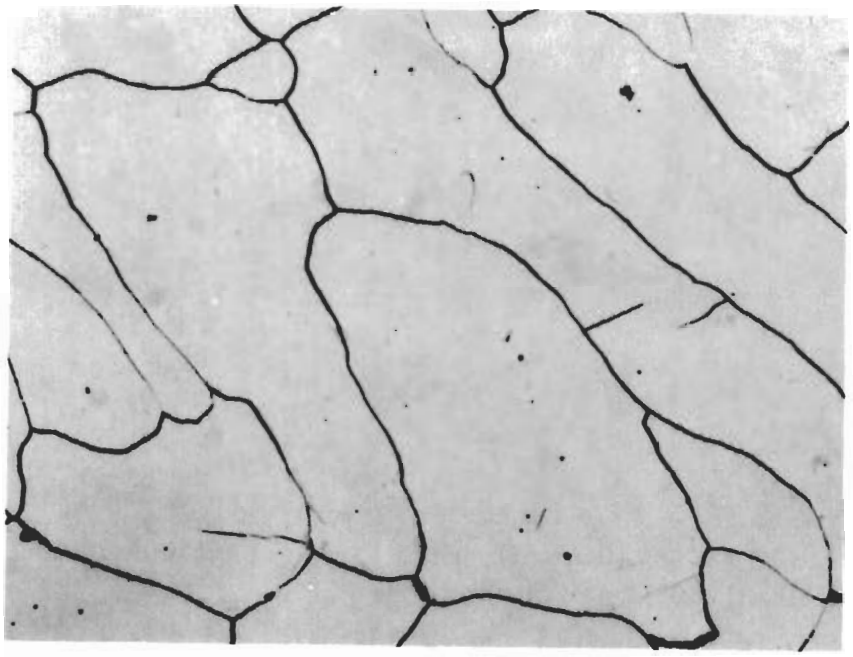

Figure 88. Ti-Mo-C (7-50-43 At.%), Melted, Equilibrated for 1 Minute at 2600° C, and Cooled at ~30° C per Second. X325

Single-Phased Monocarbide Solid Solution.

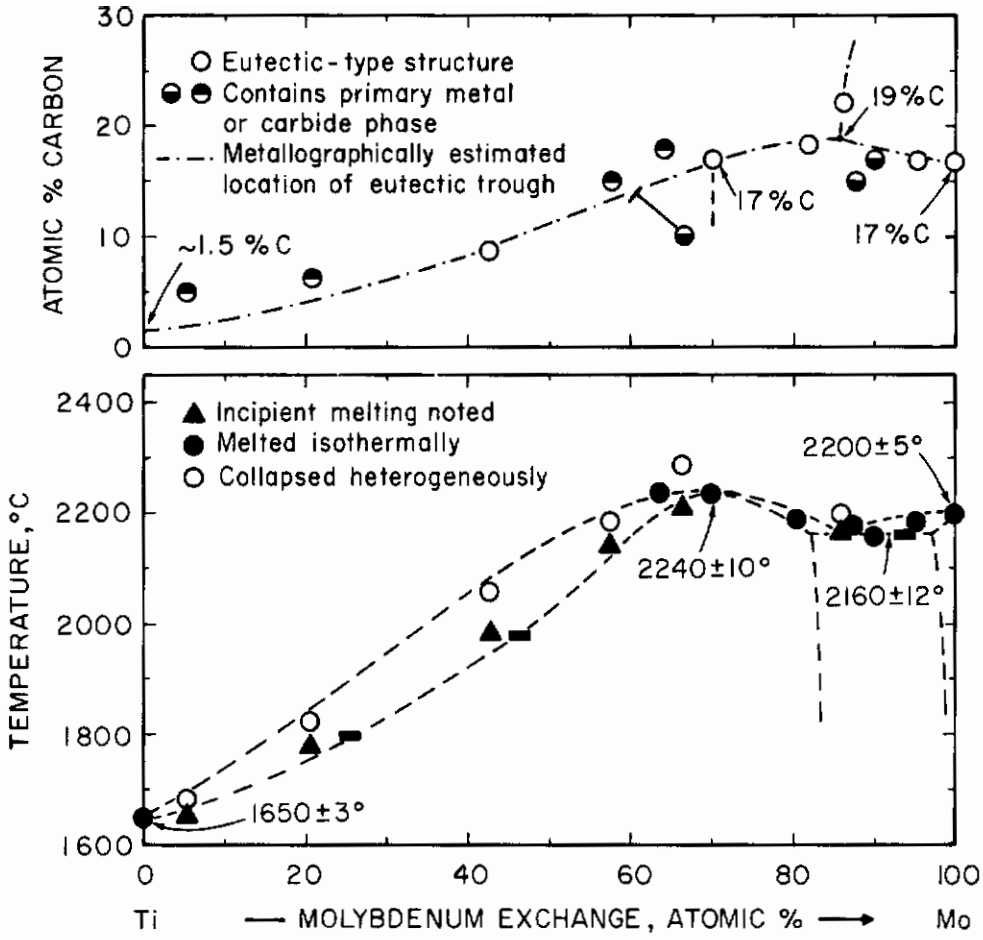

Figure 89. Ti-Mo-C: Melting Temperatures of Alloys Located Along the Metal-Rich Eutectic Trough and Metallographically Estimated Boundary Line.

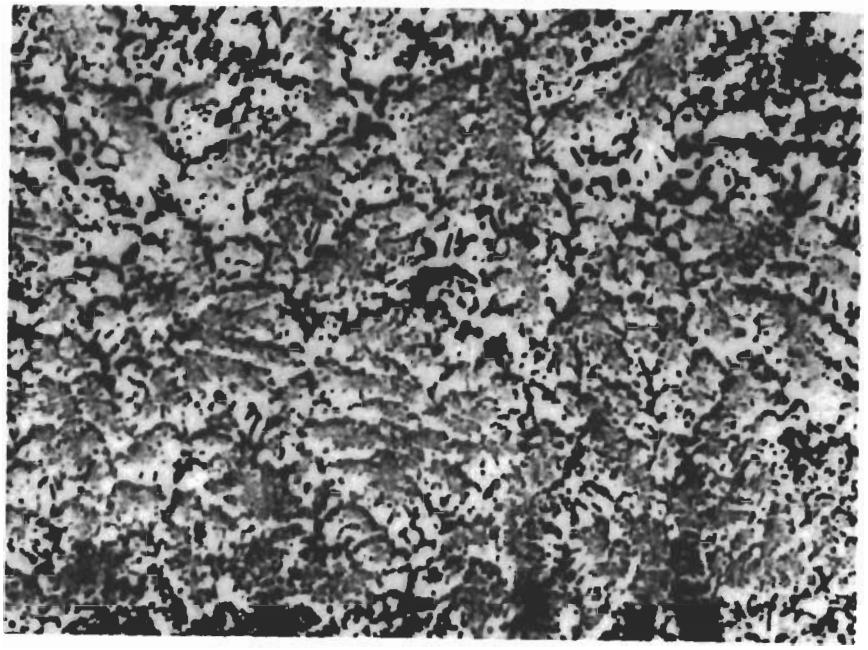

Figure 90. Ti-Mo-C (52-40-8 At.%), Quenched from Liquidus Temperatures. X625

Primary Metal in a Matrix of Bivariant Metal + Monocarbide Eutectic.

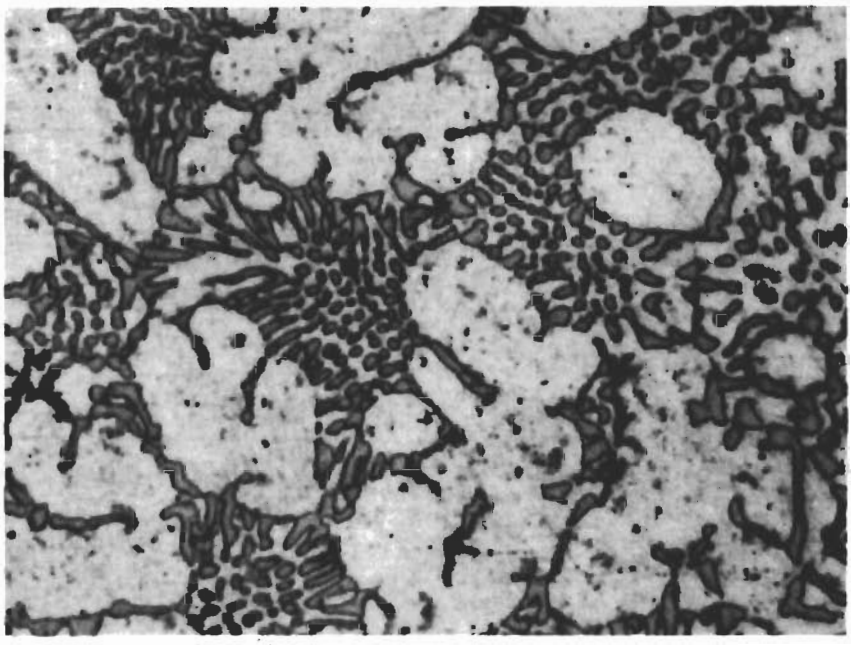

Figure 91. Ti-Mo-C (30-60-10 At.%), Melted and Rapidly Cooled. X1000

Primary Metal Grains in a Eutectic-Like Metal + Monocarbide Matrix.

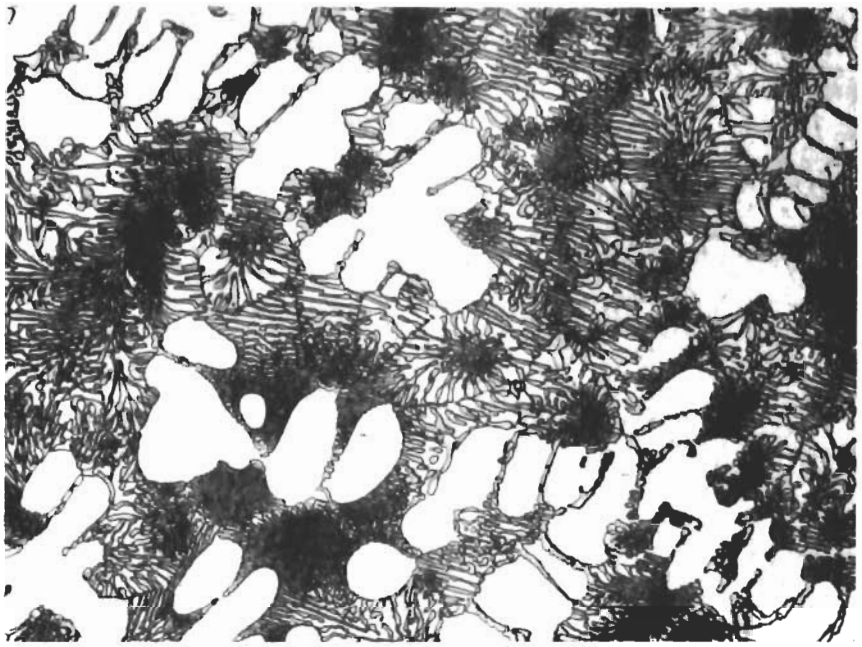

Figure 92. Ti-Mo-C (20-68-12 At.%), Melted and Rapidly Cooled. X600

Primary Mo-Rich Metal Alloy and Pseudobinary Me + MeC_{1-x} Eutectic.

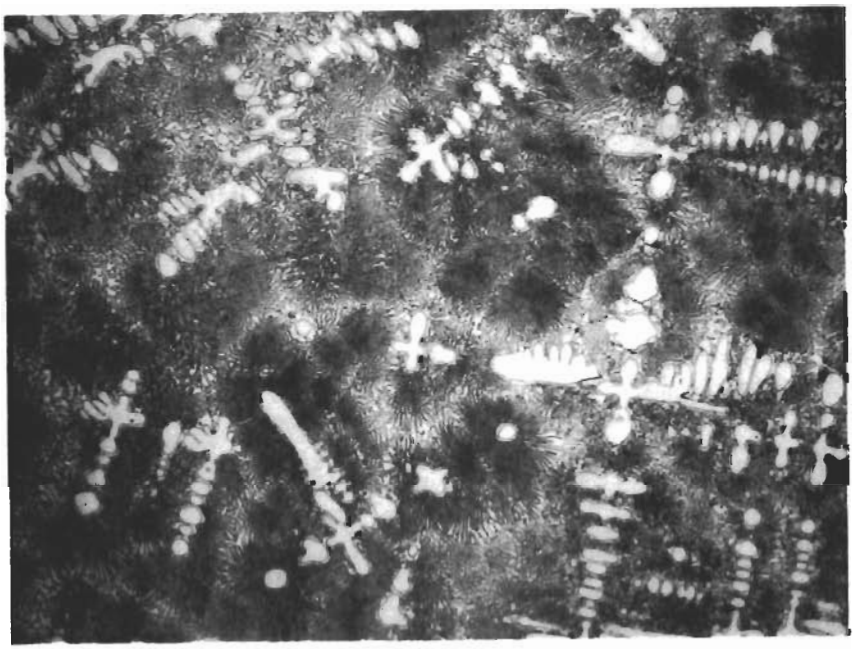

Figure 93. Ti-Mo-C (28-54-18 At.%) Small Amounts of Binary Monocarbide in a Pseudobinary Me + MeC_{1-x} Eutectic Matrix. X400

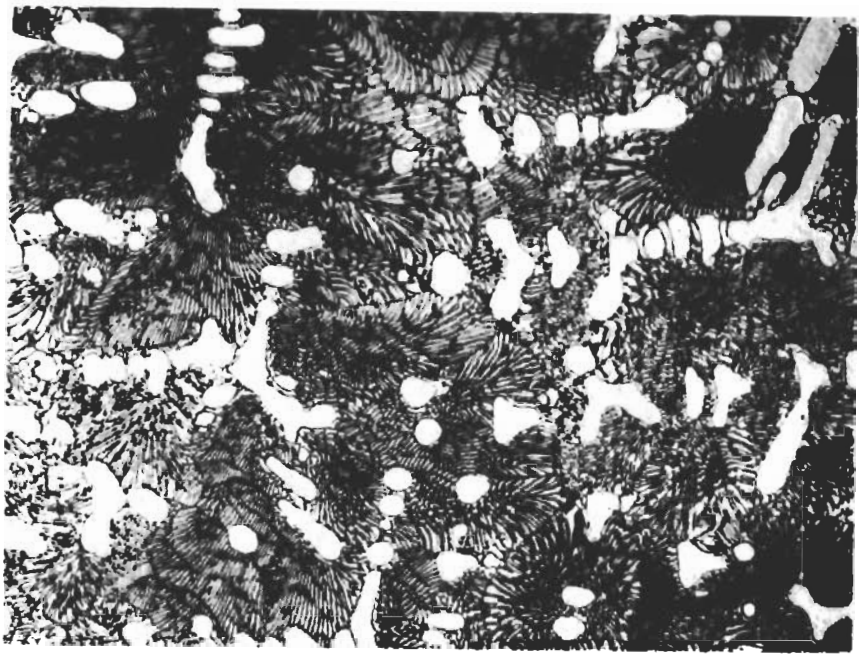

Figure 94. Ti-Mo-C (10-75-15 At.%), Melted and Rapidly Cooled. X400

Primary Metal (Light Grains) in a Matrix of Ternary Eutectic Me + Me_2C + MeC_{1-x}.

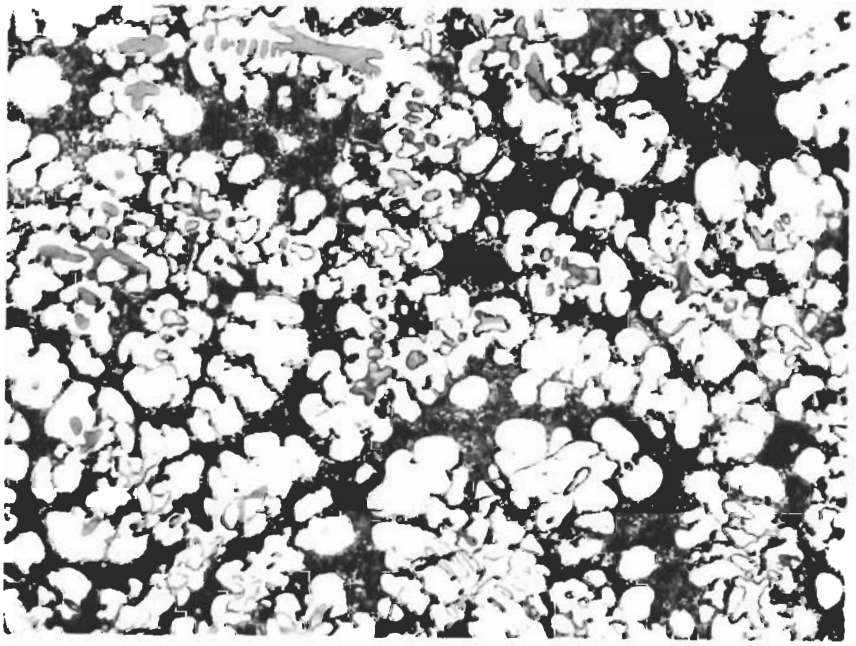

Figure 95. Ti-Mo-C (10-65-25 At.%), Melted and Quenched X350

Cocrystallized (Primary) Subcarbide and Monocarbide Alloy and Ternary Eutectic, Me + Me_2C + MeC_{1-x}.

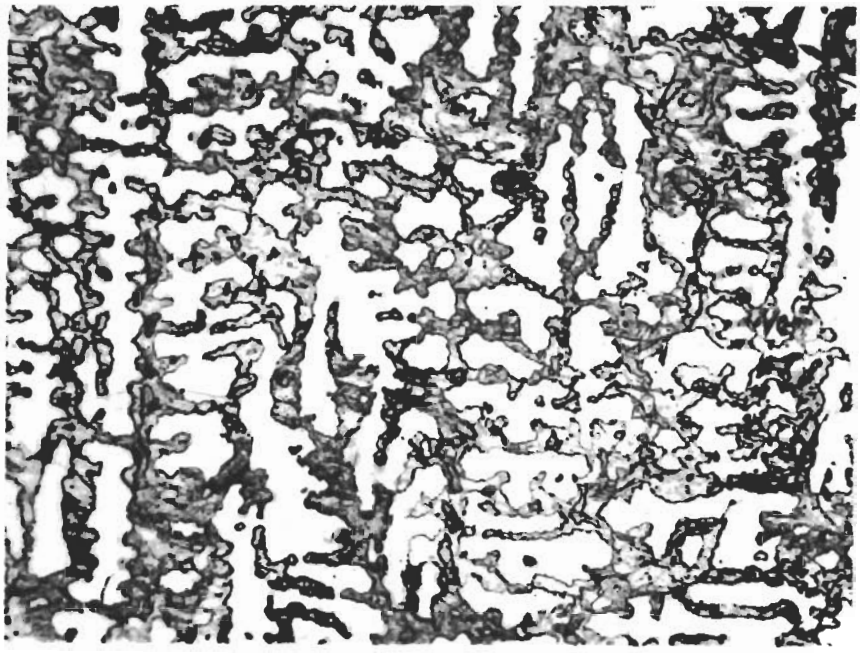

Figure 96. Ti-Mo-C (13-53-34 At.%), Melted and Rapidly Cooled. X350

Primary Monocarbide in a Bivariantly Solidified Matrix of Mo_2C and Small Amounts of Monocarbide.

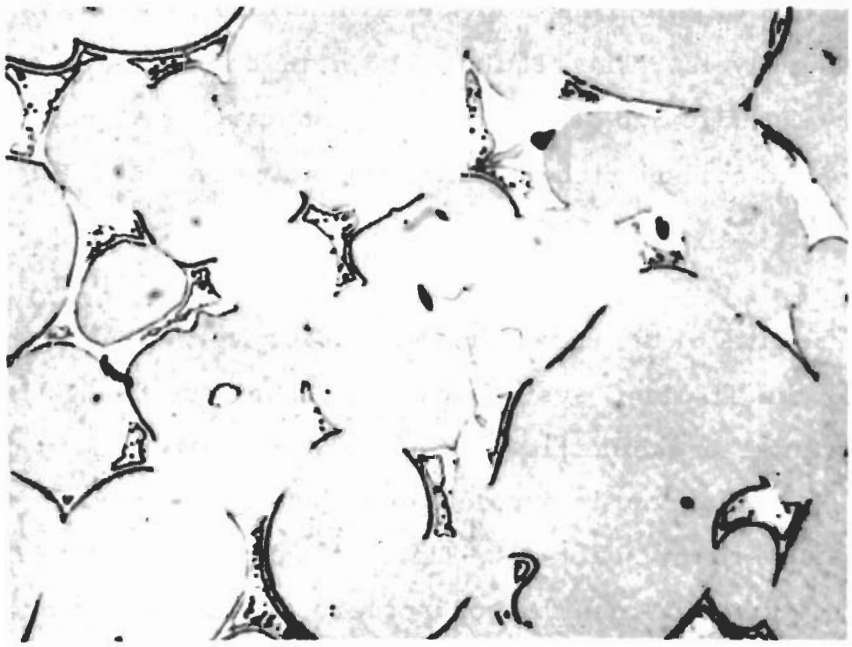

Figure 97. Ti-Mo-C (53-13-34 At.%), Equilibrated at 2200° C and Quenched. X840

Monocarbide with Eutectic(Divorced) of Grain Boundaries.

The temperature variation of the metal-rich boundary of the monocarbide solid solution at solidus temperatures was determined metallographically by the disappearance of grain boundary metal (Figure 97) and also by differential-thermal analysis by detecting the entropy change during melting of excess metal (Figure 98).

The monocarbide solid solution shows a regular melting behavior (Figure 99). The relatively wide separation of the solidus and liquidus surfaces in the middle concentration ranges resulted in heavily cored samples when quenched from the melt (Figure 100) and the X-ray diffraction patterns of such alloys were correspondingly diffuse; a one- to three-minute heat treatment of the melted alloys at slightly subsolidus temperatures usually proved sufficient to reestablish homogeneity.

Melting along the carbon-rich eutectic trough was studied independently by pyrometric melting point determinations as well as by differential thermal analysis. The results of both methods were in good agreement (Figure 101). Eutectic-type structures of monocarbide + graphite alloys located at, or near, the carbon-rich eutectic trough are shown in Figures 102, 103, and 104.

The results of the experimental studies were used to develop a phase diagram for the Ti-Mo-C system for the temperature range from 1500°C through melting; an isometric view of the proposed diagram is shown in Figure 7. The phase diagram is supplemented by a flow diagram for the isothermal binary and ternary reactions, Figure 8, and a projection of the liquidus, shown in Figure 9. A number of isothermal and concentration (T-X) sections, Figures 105 through 114, were prepared from the available data, and show more clearly and in greater detail the phase distributions in the systems and the thermal reaction behavior of phases along given composition lines.

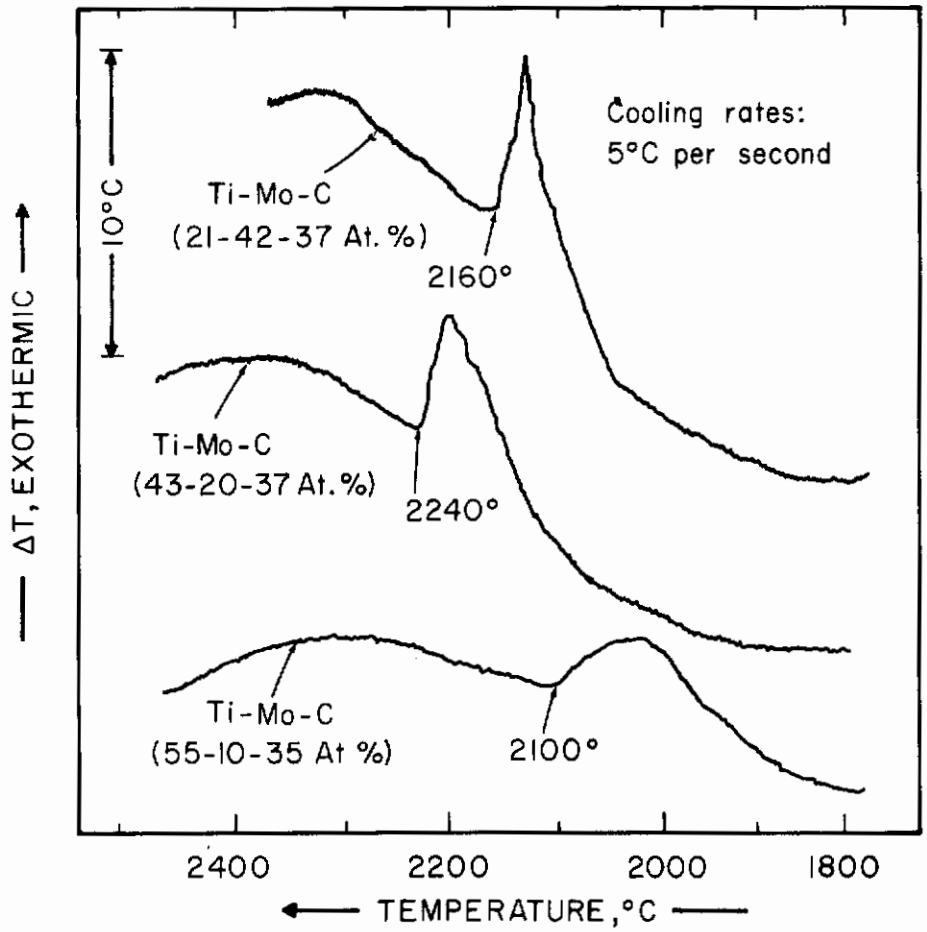

Figure 98. Ti-Mo-C Alloys Showing Solidification of Rest-Eutectic in Alloys Located Near the Monocarbide Phase Boundary.

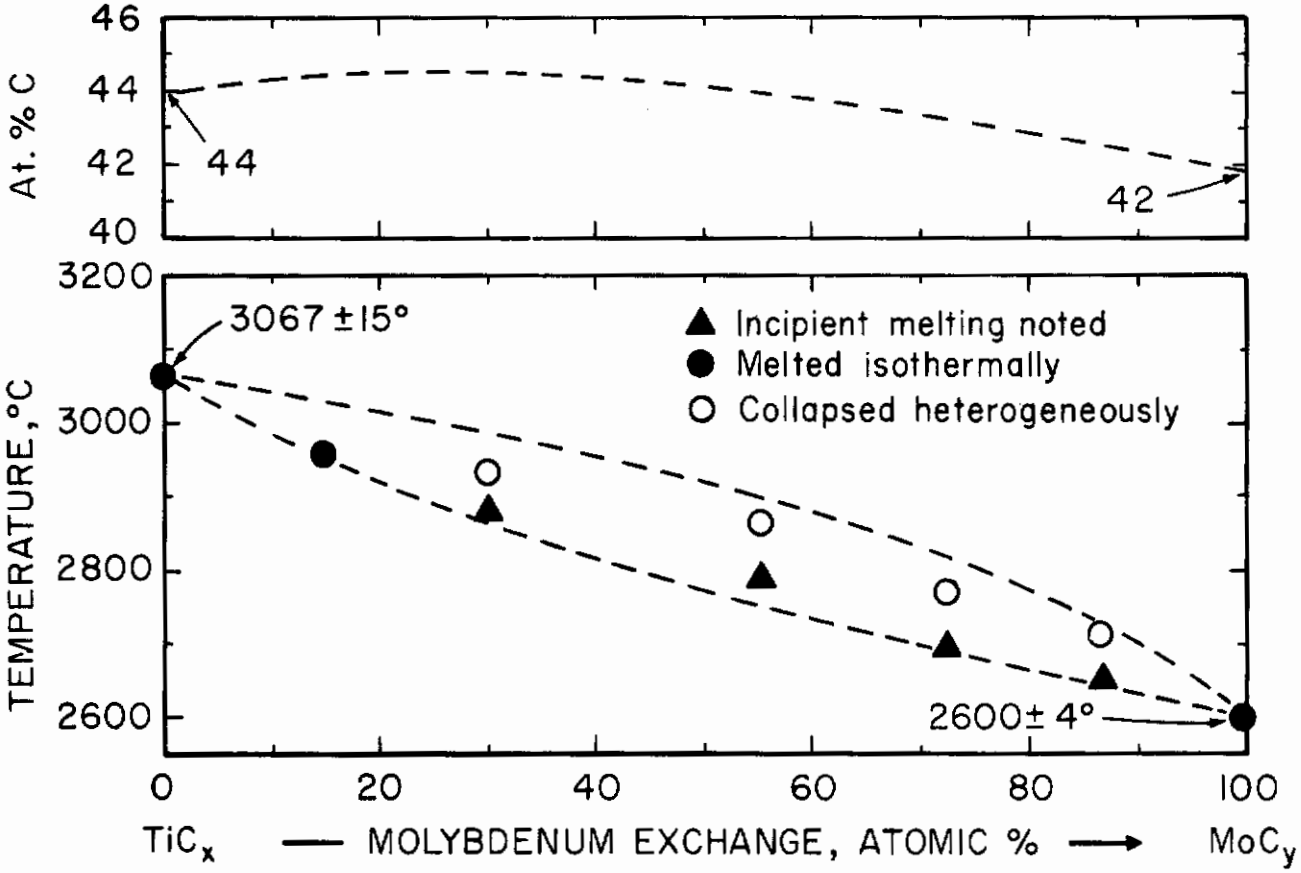

Figure 99. Maximum Solidus Temperatures of the $(Ti,Mo)C_{1-x}$ Solid Solution.

Top: Locus of Concentration Points Corresponding to the Highest Melting Alloys.

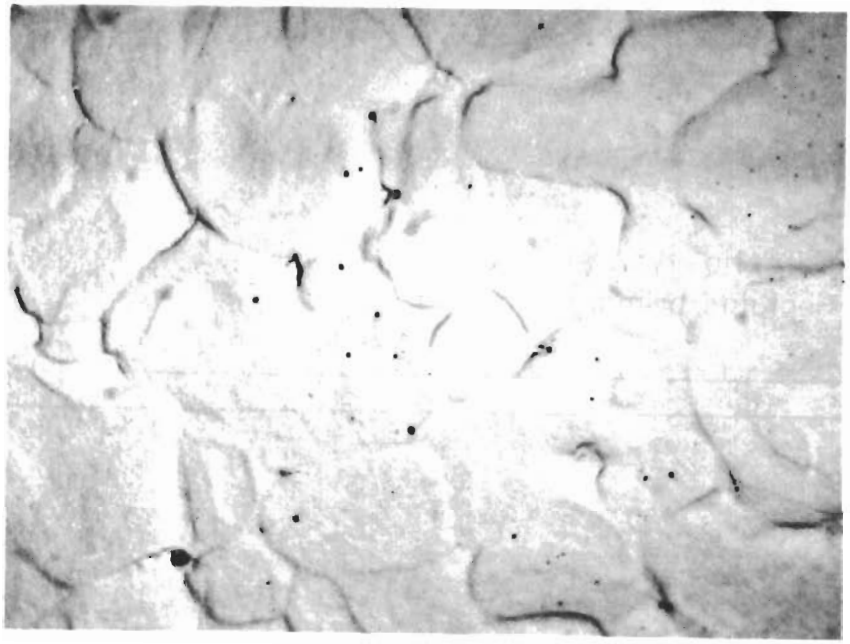

Figure 100. Ti-Mo-C (34-24-42 At.%), Partially Melted at 2600°C and Rapidly Cooled. X600

Cored Monocarbide Solution.

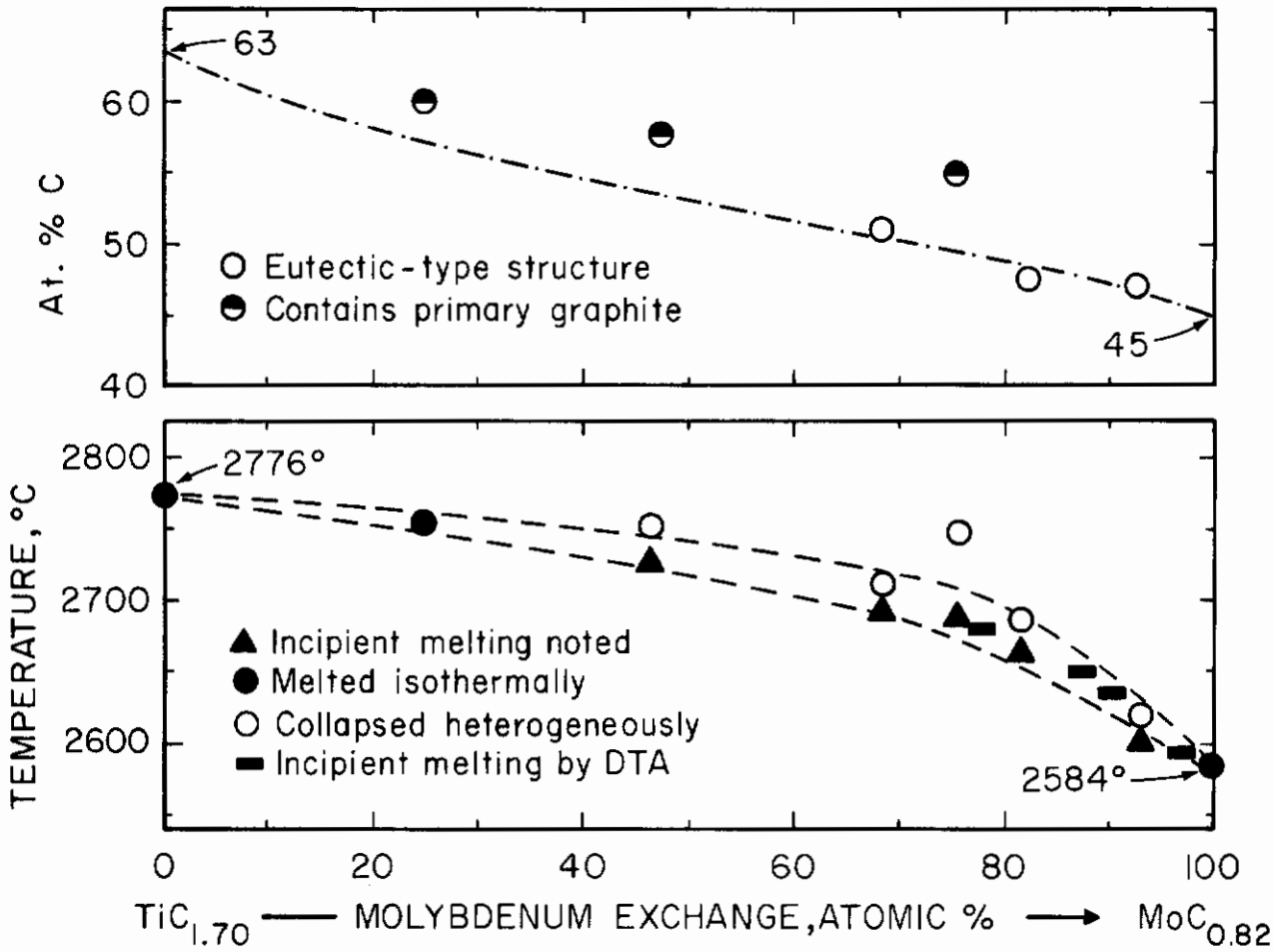

Figure 101. Melting Temperatures of Ti-Mo-C Alloys Located at, or Near, the Monocarbide + + Graphite Eutectic Trough.

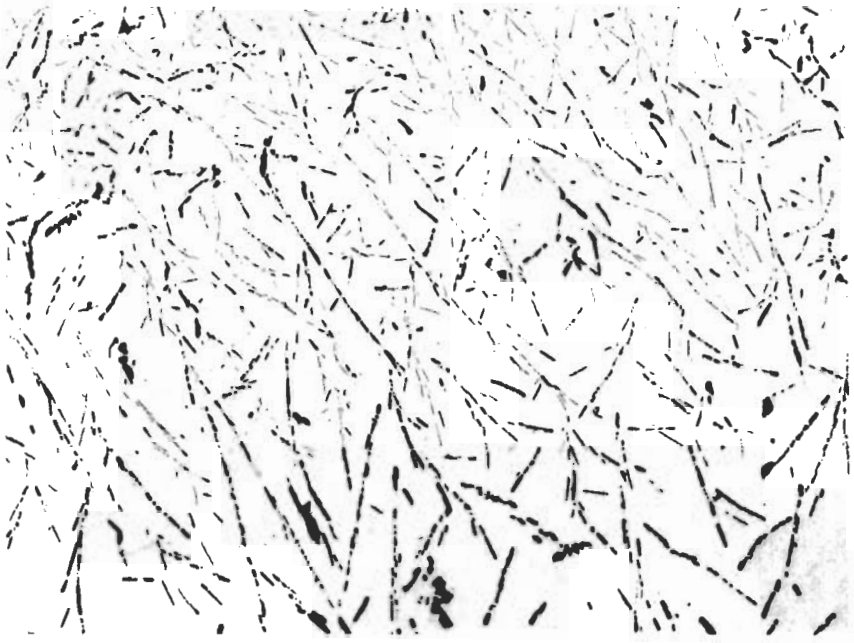

Figure 102. Ti-Mo-C (10-43-47 At.%), Rapidly Cooled from Liquidus Temperatures. X175

Small Amounts of Primary Monocarbide in a Matrix of Bivariantly Solidified Monocarbide + Graphite Eutectic.

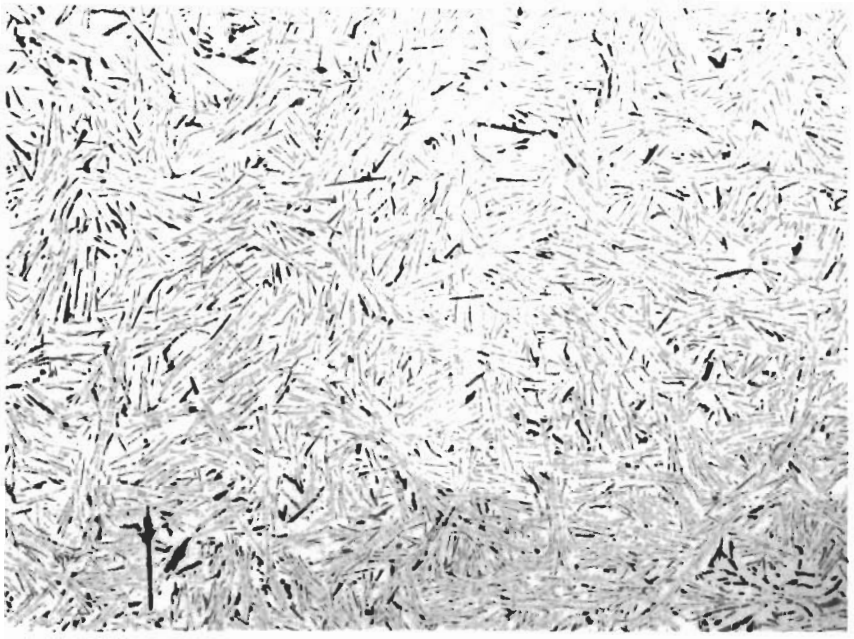

Figure 103. Ti-Mo-C (16-34-50 At.%), Quenched from Liquidus Temperatures. X175

Eutectic-Like Structure at the Monocarbide + Graphite Boundary Line.

Figure 104. Ti-Mo-C (22-20-58 At.%), Melted and Rapidly Cooled. X140

Plate-Shaped Primary Graphite in a Monocarbide + Graphite Eutectic-Like Matrix.

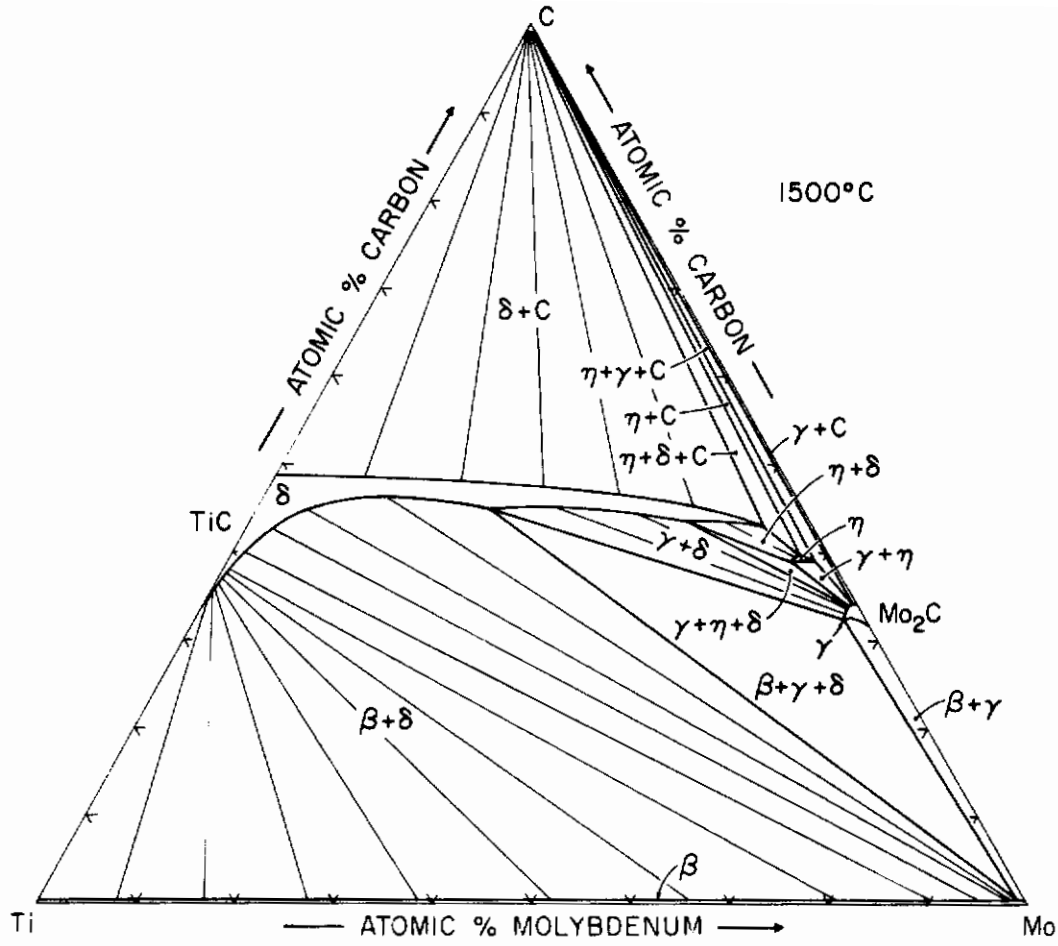

Figure 105. Isothermal Section of the Ti-Mo-C System at 1500° C.

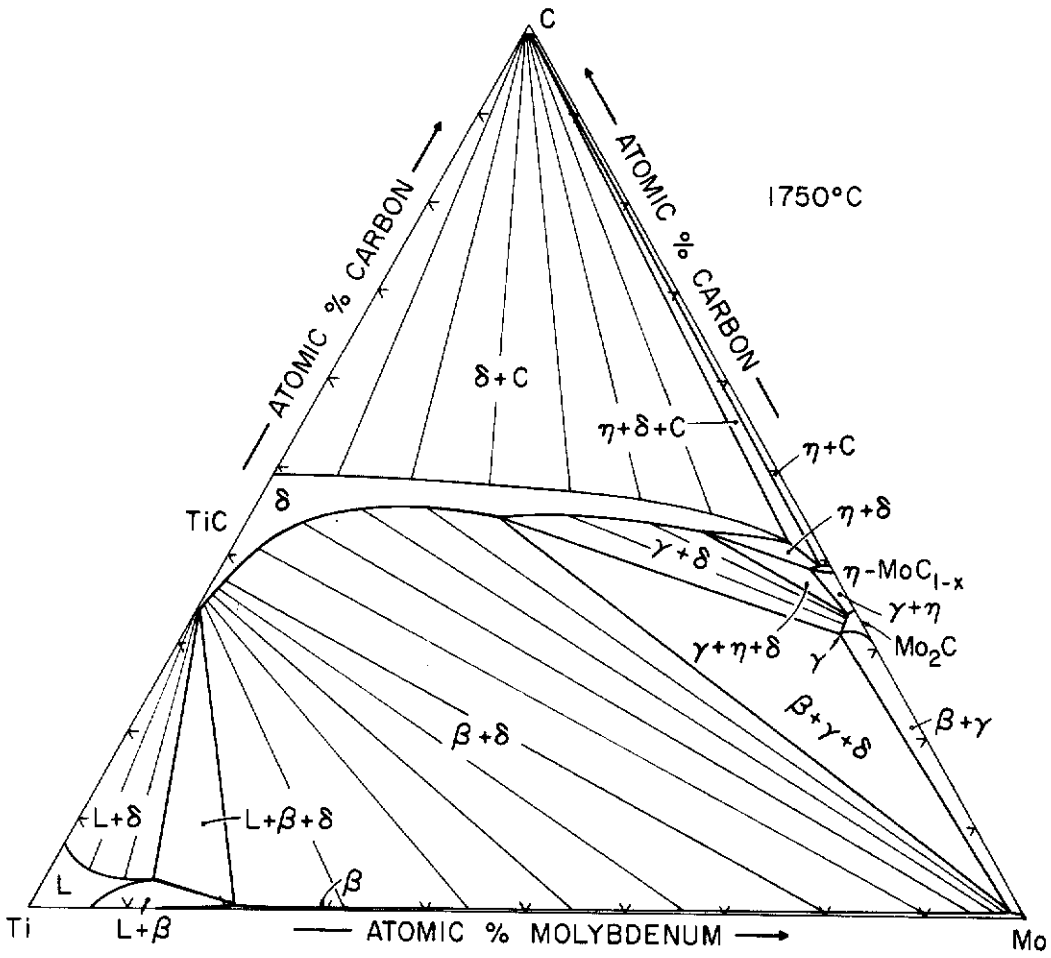

Figure 106. Isothermal Section of the Ti-Mo-C System at 1750° C.

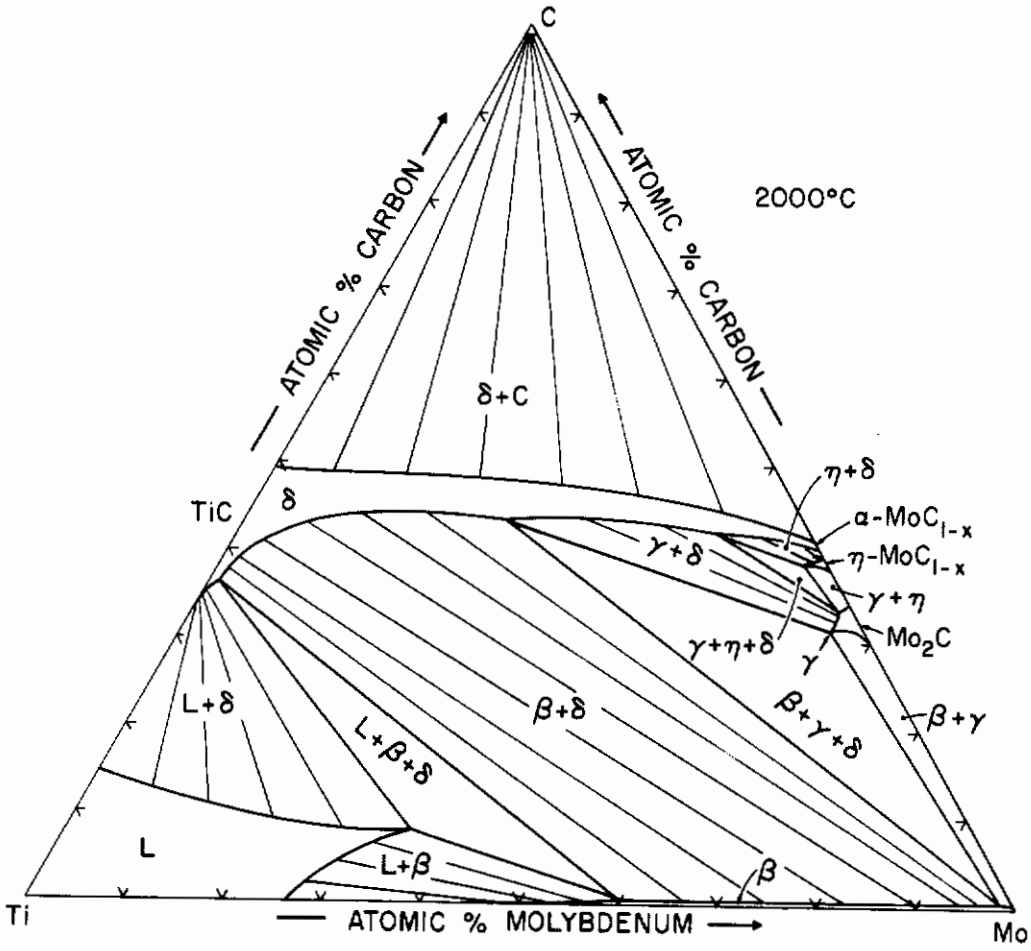

Figure 107. Isothermal Section of the Ti-Mo-C System at 2000° C.

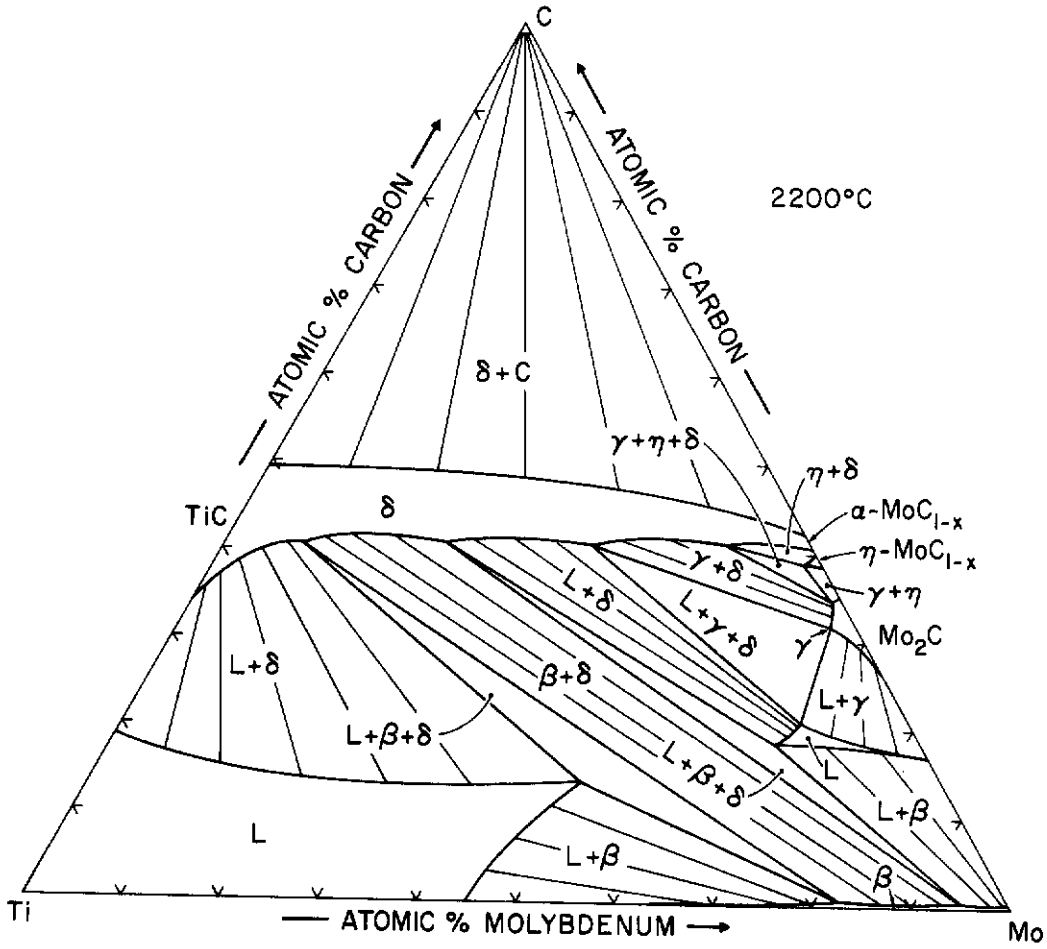

Figure 108. Isothermal Section of the Ti-Mo-C System at 2200°C.

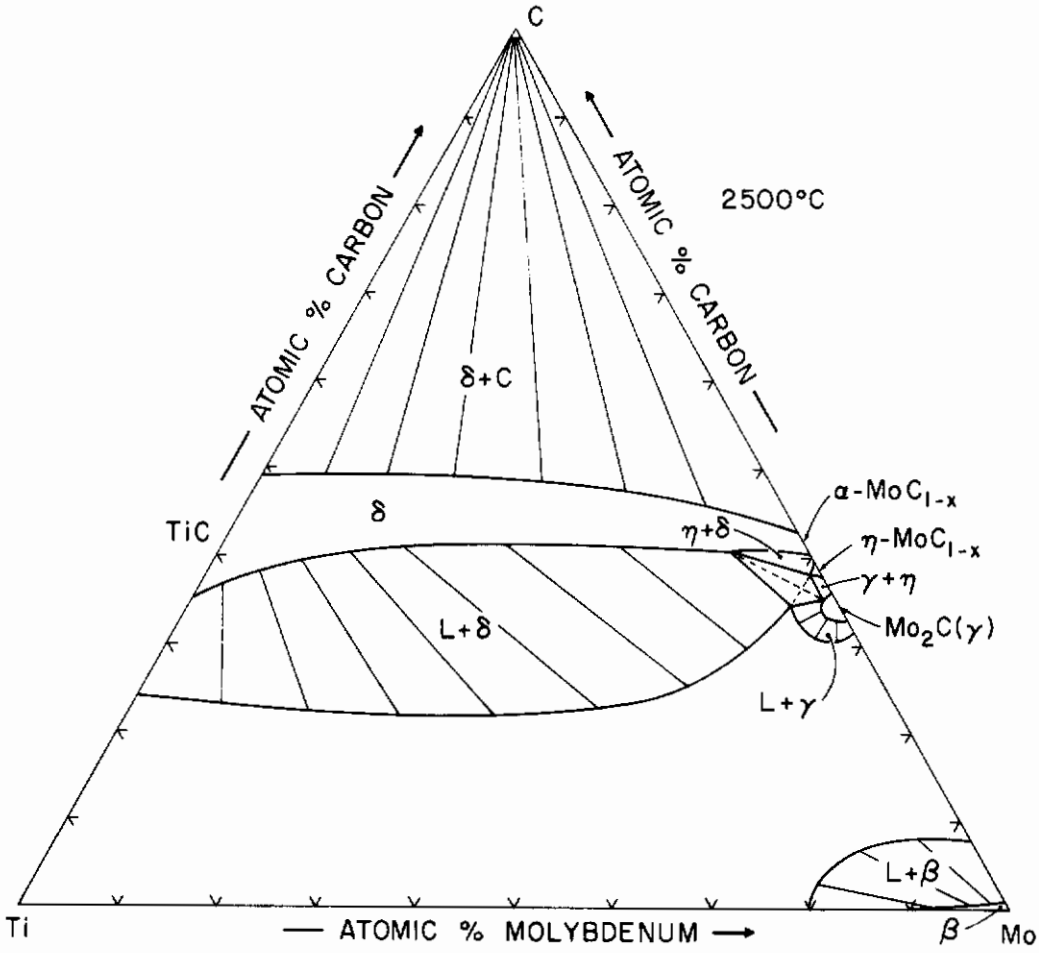

Figure 109. Isothermal Section of the Ti-Mo-C System at 2500°C.

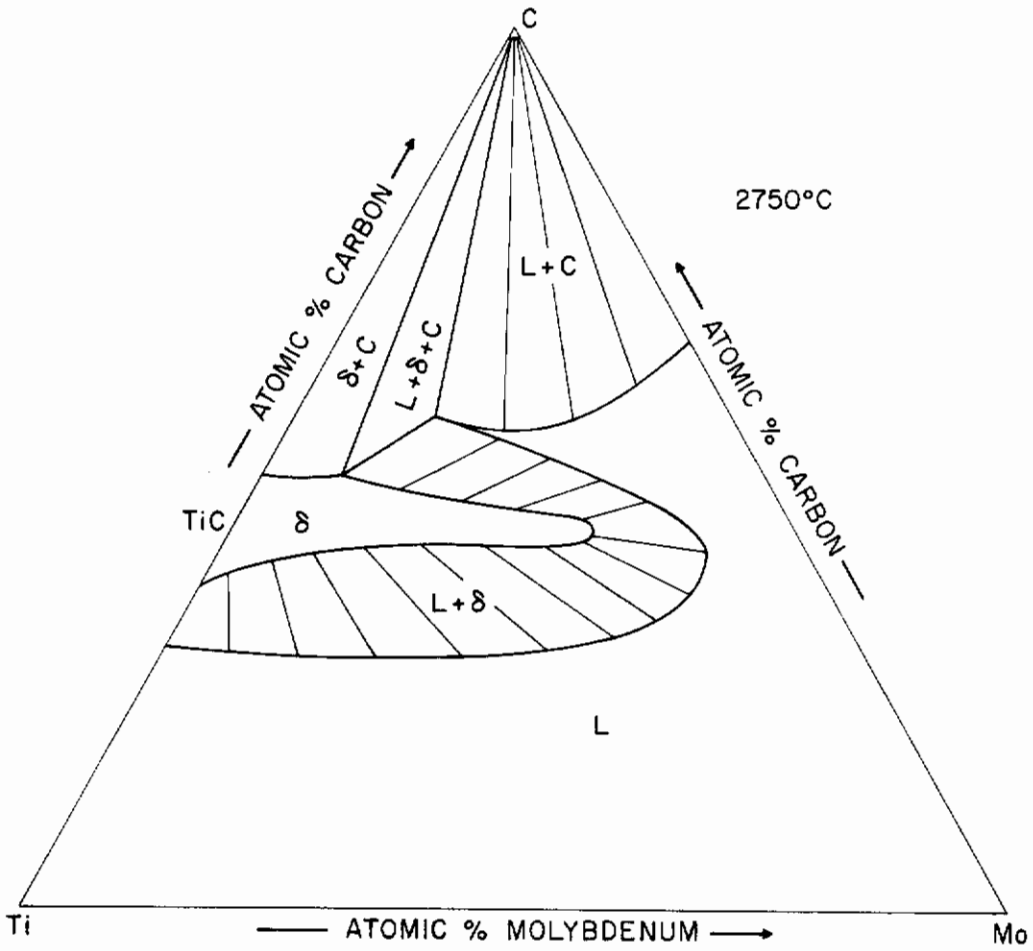

Figure 110. Isothermal Section of the Ti-Mo-C System at 2750°C.

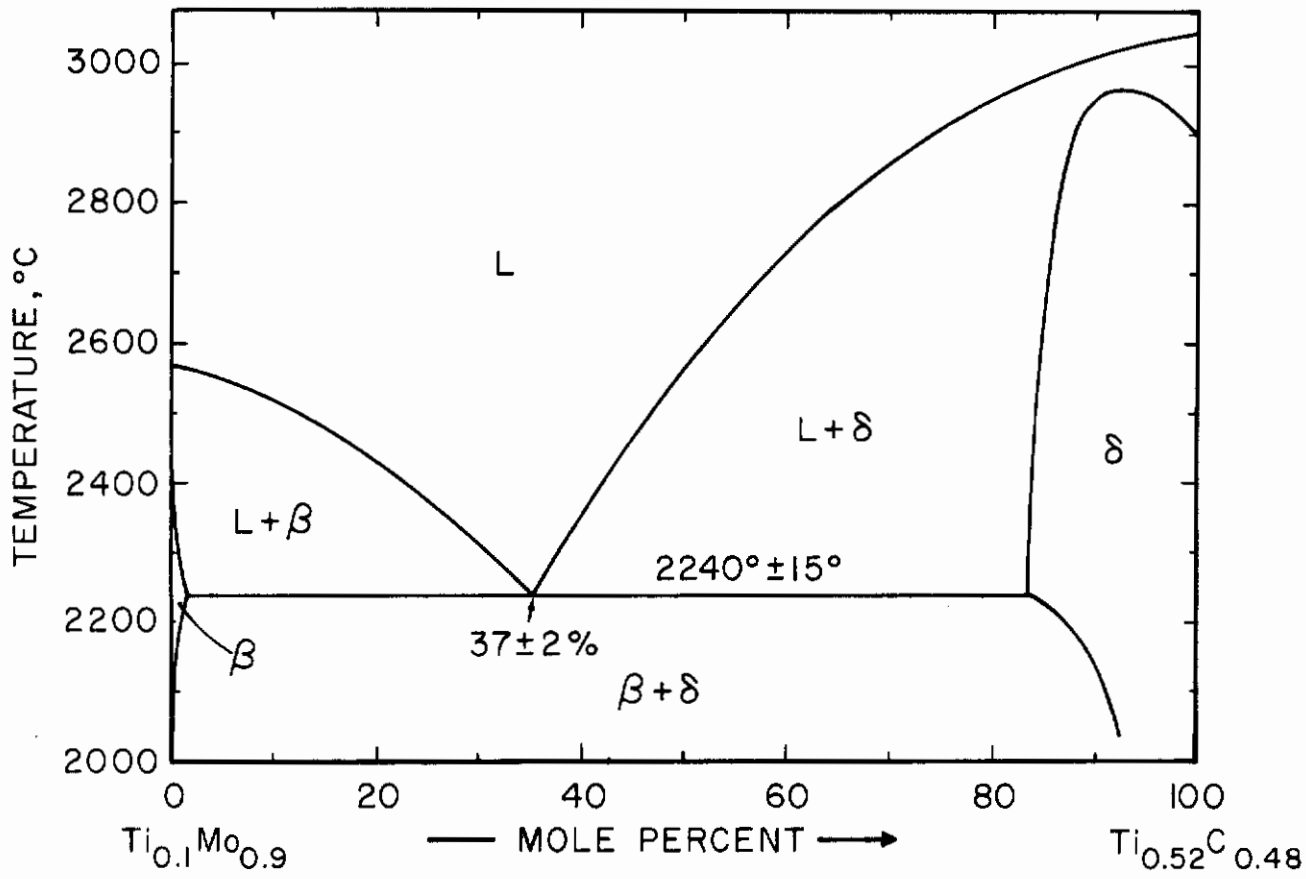

Figure 111. Isopleth at the Pseudobinary Section $Ti_{0.1}Mo_{0.9}Ti_{0.52}C_{0.48}$.

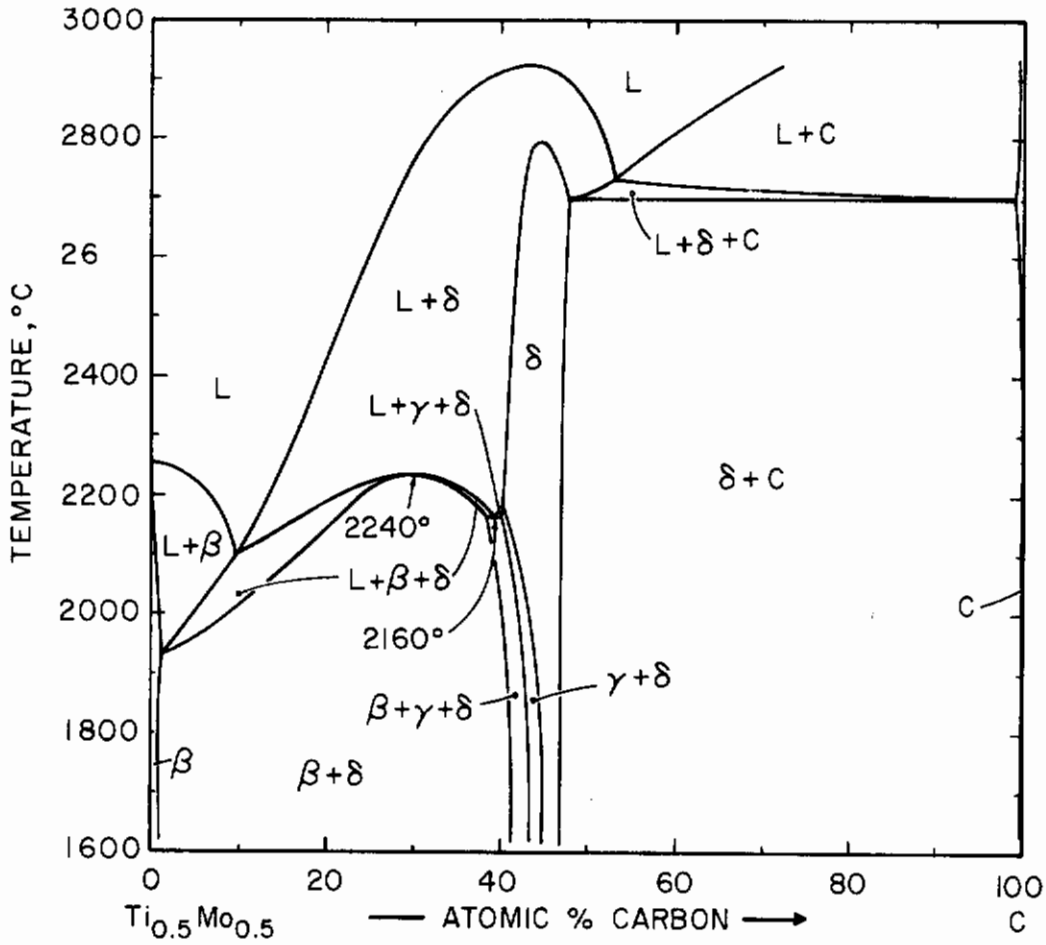

Figure 112. Isopleth $Ti_{0.5}Mo_{0.5}$-C.

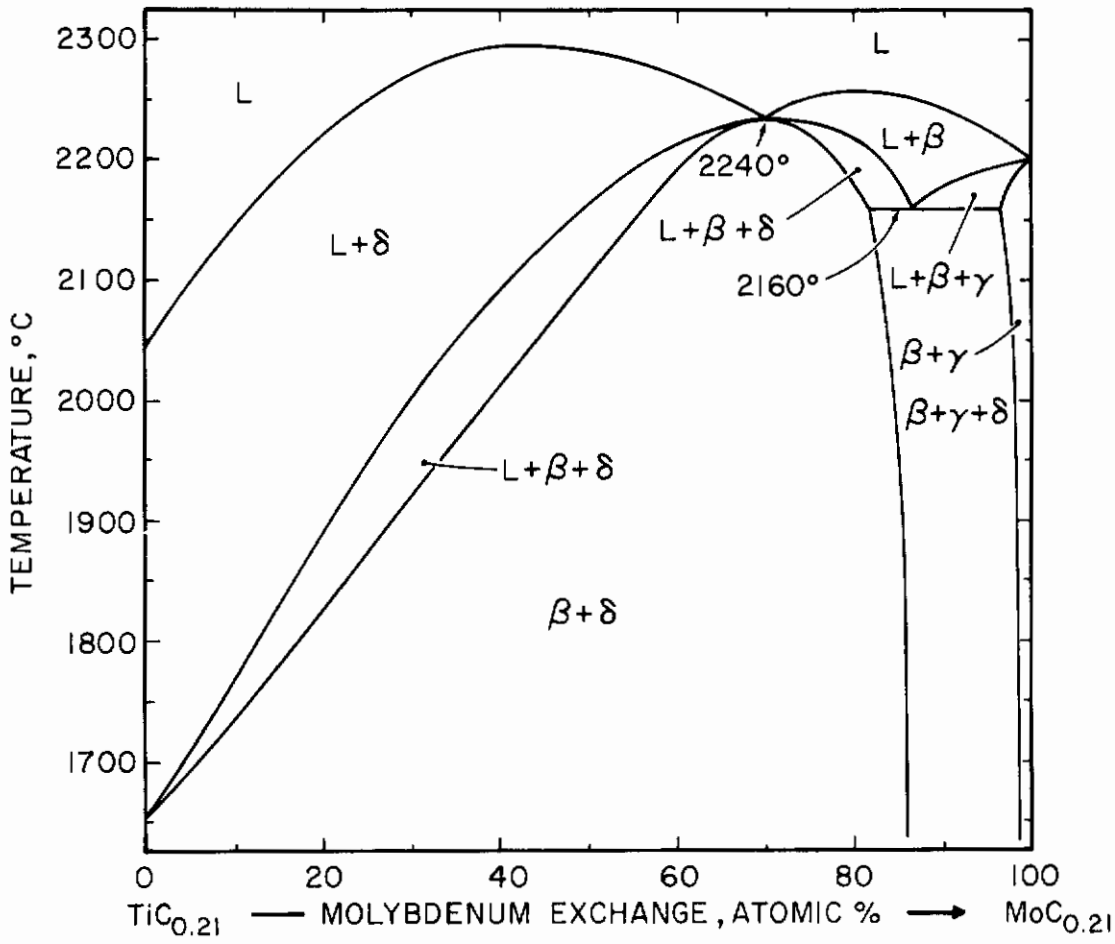

Figure 113. Isopleth $TiC_{0.21}$-$MoC_{0.21}$.

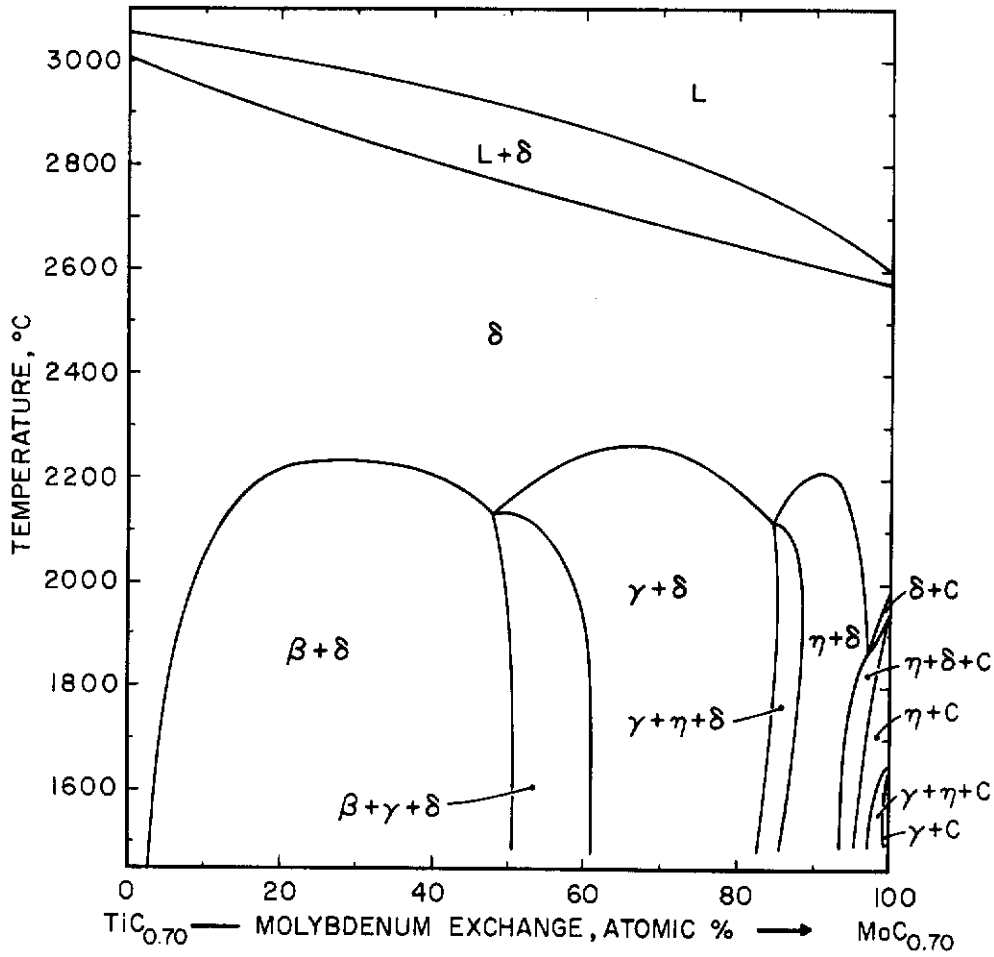

Figure 114. Isopleth $TiC_{0.70}$-$MoC_{0.70}$

V. DISCUSSION

The principal solid state phase relationships are the same in all three systems. The cubic monocarbides form complete series of solid solutions, while the subcarbides substitute only limited amounts of titanium and are terminated by three-phase equilibria of the type metal + subcarbide + monocarbide in the ternary.

The large difference in the titanium exchanges in Nb_2C ($\leq$ 12 At.%) and Ta_2C ($\leq$ 44 At.%) appear at a first glance somewhat peculiar, since the high temperature structures of Nb_2C and Ta_2C are identical and, furthermore, both phases have nearly identical unit cell volumes; the causes for the observed solubility differences are therefore not attributable to a grossly different thermodynamic behavior of the subcarbide, but rather must be sought in differences in the thermodynamic properties of the binary phases themselves.

A calculation of the free enthalpies of disproportionation ($\Delta G_{Z_1 MeC_{1/2}}$) of Ta_2C and Nb_2C according to methods developed earlier[39] yields for the reaction

$$MeC_{\sim 1/2} \rightarrow 2/3\ MeC_{\sim 0.75} + 1/3\ Me \ldots\ldots \Delta G_{Z, MeC_{1/2}},$$

and

$$\Delta G_{Z, TaC_{1/2}} = +2300 \text{ cal/gr.At Ta} \qquad (T = 2000^\circ K)$$

$$\Delta G_{Z, NbC_{1/2}} = +1240 \text{ cal/gr.At Nb}$$

The relative stability of Ta_2C is therefore nearly twice as high as that of Nb_2C, and a considerably higher titanium concentration in the subcarbide and the neighboring metal and monocarbide phases are therefore necessary in the tantalum system in order to counterbalance the higher stability of the

respective subcarbides. The higher stability of the tantalum carbides causes the swing of tie lines in the three two-phase equilibria adjoining the three-phase region Me + Me_2C + MeC_{1-x} to tend more towards equidistribution in the tantalum system. Thus an evaluation of the tie line distribution in the equilibrium (Ti, Ta) + $(Ti, Ta)_2C$ yields

$$\Delta G_{TiC_{1/2}} - \Delta G_{TaC_{1/2}} \approx 0 \qquad (2000^\circ K),$$

indicating, that the hypothetical 'Ti_2C' has about the same stability (free enthalpy of formation) as Ta_2C, but higher stability than Nb_2C. It is further interesting to note that the relative stability of the hypothetical Ti_2C-phase, which in this particular case coincides with the free enthalpy of transformation of the carbon-deficient, cubic monocarbide $TiC_{\sim 0.5}$ into the homotectic Ti_2C-phase, is only -1600 cal/gr.At Ti; i.e. the stability of the hypothetical Ti_2C-phase comes very close to that of the carbon-deficient monocarbide and accounts for the relatively large titanium solubilities in some other metal subcarbides.

The binary Mo_2C has about the same relative stability as Ta_2C, but the molybdenum carbides have much lower free enthalpies of formations than the carbides of the heavier group V metals. As a consequence, the tie lines in the two-phase fields adjoining the three-phase equilibrium (Ti,Mo) + Mo_2C-ss + $(Ti,Mo)C_{1-x}$ assume extreme inclinations such, that monocarbide alloys with titanium exchanges up to ~90 At.% are in equilibrium with very molybdenum-rich (> 95 At.%) metal and subcarbide alloys. The only free energy term of significance in counterbalancing the free enthalpy of disproportionation of the Mo_2C and which thus determines the location of the three-phase equilibrium Me + Me_2C + MeC_{1-x}, stems from the formation of the monocarbide solution. In view of the extreme inclination of the tie lines in this

system, sufficiently high titanium concentrations in the monocarbide phase to cut off the Mo_2C-phase are reached before the coexisting Mo_2C-phase would show any appreciable titanium concentration.

REFERENCES

1. C.E. Brukl and D.P. Harmon: U.S. Air Force Contract AF 33 (615)-1249, Tech. Doc. Report AFML-TR-65-2, Part II, Vol. II (Sept. 1965)

2. M. Hansen: "Constitution of Binary Alloys" (McGraw-Hill, 1958).

3. R.P. Elliott: "Constitution of Binary Alloys, First Supplement" (McGraw-Hill, 1965).

4. F.A. Shunk: "Constitution of Binary Alloys, Second Supplement" (McGraw-Hill, 1969).

5. E. Rudy, D.P. Harmon, and C.E. Brukl: U.S. Air Force Tech. Doc. Report AFML-TR-65-2, Part I, Vol. II (August 1965).

6. Compare the Compilation of earlier work in E.K. Storms: "The Refractory Carbides" (Academic Press, 1967).

7. J.T. Norton and R.K. Lewis: NASA-CR-321 (1963).

8. E. Rudy: US Air Force Tech. Doc. Report AFML-TR-69-117, Part VII (Jan 1970).

9. H. Goretzki: Max Planck Inst. Research Report BMwF-FB-K68-62 (Dec. 1968).

10. E.K. Storms and N.H. Krikorian: J.Phys.Chem., 64 (1960), 1471.

11. H. Kimura and Y. Sasaki: Trans. Jap. Inst. Met., 2 (1961), 98.

12. E. Rudy, St. Windisch, and C.E. Brukl: U.S. Air Force Tech. Doc. Report AFML-TR-65-2, Part I, Vol. XII (Sept. 1967); Planseeber. Pulvermet., 16 (1968), 3.

13. E. Rudy and C.E. Brukl: J.Amer.Ceram.Soc., 50 (1967), 265.

14. N. Terao: Jap. J. Appl. Phys., 3 (1964), 104.

15. N.M. Volkova and P.V. Gel'd: Izvest. Vysh. Uchebnik Zaved. Tsvetnaya Metallurgiya, 3 (1965), 77.

16. S.I. Alyamovskii, G.P. Sheikin, and P.V. Gel'd: J. Neorg. Chim. 8 (1963), 2000.

17. K. Yvon, H. Nowotny, and R. Kieffer: Mh.Chem., 98 (1967), 34.

18. E. Rudy: U.S. Air Force Tech. Doc. Report AFML-TR-65-2, Part II, Vol. VIII (March 1966), p.105.

19. K. Yvon, W. Rieger, and H. Nowotny: Mh.Chem., 97 (1966), 659.

20. K. Yvon and E. Parthe: Private Communication, 1969.

21. G. Brauer and R. Lesser: Z. Metallkde. 50 (1959), 8.

22. A.L. Bowman, T.C. Wallace, J.L. Yavnell, R.G. Wenzel, and E.K. Storms: Acta Cryst. 19 (1965), 6.

23. E. Rudy and D.P. Harmon: U.S. Air Force Tech. Doc. Report, AFML-TR-65-2, Part I, Vol. V (Jan 1966).

24. R. Lesser and G. Brauer: Z. Metallkde 49 (1958), 622.

25. E. Rudy, St. Windisch, A.J. Stosick, and J.R. Hoffman: Trans. AIME, 239 (1967), 1247.

26. E. Parthe and V. Sadagopan: Acta Cryst. 16 (1963), 202.

27. H. Nowotny, E. Parthe, R. Kieffer, and F. Benesovsky: Mh.Chem. 85 (1954), 255.

28. P. Stecher, F. Benesovsky, A. Neckel, and H. Nowotny: Mh.Chem. 95 (1964), 1630.

29. T.F. Fedorov, N.M. Popova, and E.I. Gladyshevskiy: Izvest. Akad. Nauk SSSR Metall. 3 (1965), 158.

30. Compare the Compilation of earlier work in R. Kieffer and F. Benesovsky: "Hartstoffe" (Wien, Springer, 1963).

31. J.G. McMullin and J.T. Norton: J. Metals, 5 (1953), 1205.

32. H.J. Albert and J.T. Norton: Planseeber. Pulvermet, 4 (1956), 2.

REFERENCES (Cont'd)

33. W.B. Pearson: "Handbook of Lattice Spacings and Structures of Metals and Alloys" (Pergamon Press, 1958).

34. E. Rudy and J. Progulski: Planseeber. Pulvermet., 15 (1967), 13.

35. M. Hansen, E.L. Kamen, H.D. Kessler, and D.J. McPherson: AIME, 191 (1951), 881.

36. D. Summers-Smith: J. Inst. Met., 81 (1952/1953), 73.

37. D.I. Maykuth, H.R. Ogden, and R.I. Jaffee: Trans. AIME 197 (1953), 231.

38. A.G. Metcalfe: J. Inst. Met., 73 (1947), 591.

39. E. Rudy: Z. Metallkde 54 (1963), 112-122; ibid. 213-223.

Unclassified
Security Classification

DOCUMENT CONTROL DATA - R & D
(Security classification of title, body of abstract and indexing annotation must be entered when the overall report is classified)

1. ORIGINATING ACTIVITY (Corporate author) Aerojet-General Corporation Materials Research Laboratory Sacramento, California	2a. REPORT SECURITY CLASSIFICATION Unclassified 2b. GROUP

3. REPORT TITLE
Phase Equilibria Investigation of Binary, Ternary, and Higher Order Systems.

Part I. The Phase Diagrams of the Systems Ti-Nb-C, Ti-Ta-C, and Ti-Mo-C.

4. DESCRIPTIVE NOTES (Type of report and inclusive dates)

5. AUTHOR(S) (First name, middle initial, last name)

E. Rudy

6. REPORT DATE August 1970	7a. TOTAL NO. OF PAGES 132	7b. NO. OF REFS 39
8a. CONTRACT OR GRANT NO. F 33 615-67-C-1513 b. PROJECT NO. 7350 Task No. 735001 c. d.	9a. ORIGINATOR'S REPORT NUMBER(S) 9b. OTHER REPORT NO(S) (Any other numbers that may be assigned this report) AFML-TR-69-117, Part I	

10. DISTRIBUTION STATEMENT
This document has been approved for public release and sale; its distribution is unlimited.

11. SUPPLEMENTARY NOTES	12. SPONSORING MILITARY ACTIVITY Air Force Materials Laboratory Wright-Patterson AFB, Ohio 45433

13. ABSTRACT

The ternary alloy systems Ti-Nb-C, Ti-Ta-C, and Ti-Mo-C were investigated by means of X-ray, melting point, DTA, and metallographic techniques techniques and phase diagrams for all three systems from 1500° C through the melting range were established.

The solid state phase relationships in all three systems are similar. The cubic monocarbides are completely miscible, whereas the subcarbides, $Nb(Ta,Mo)C_2$ show limited solubility and are terminated by three-phase equilibria $Me + Me_2C +$ $+ MeC_{1-x}$ in the ternary. The sublattice order-disorder transition in the subcarbides are lowered by titanium substitutions. The monocarbide solutions in all three systems show a regular melting behavior. The phase relationships of the three systems are discussed and the differences in particular equilibria related to the thermodynamic properties of the phases in the boundary systems.

DD FORM 1 NOV 65 1473

Unclassified
Security Classification

14. KEY WORDS	LINK A		LINK B		LINK C	
	ROLE	WT	ROLE	WT	ROLE	WT
Phase Equilibria						
Ternary Carbides						
Thermodynamics						